

# Numerical Simulation of Dislocation Reduction in InGaN and InGaAs Heteroepitaxy with Step-graded Interlayers

By

**Md. Arafat Hossain**

A thesis submitted in partial fulfillment of the requirements for the degree of  
Master of Science in Electrical & Electronic Engineering

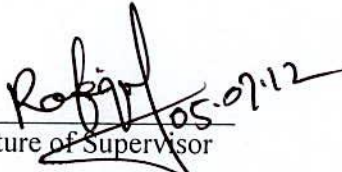


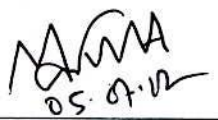
Department of Electrical and Electronic Engineering  
Khulna University of Engineering & Technology  
Khulna 9203, Bangladesh

July 2012

## Declaration

This is to certify that the thesis work entitled "*Numerical Simulation of Dislocation Reduction in InGaN and InGaAs Heteroepitaxy with Step-graded Interlayers*" has been carried out by *Md. Arafat Hossain* in the Department of *Electrical and Electronic Engineering*, Khulna University of Engineering & Technology, Khulna-9203, Bangladesh. The above thesis or any part of this has not been submitted anywhere for the award of any degree or diploma.


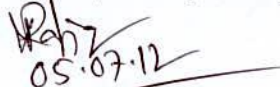
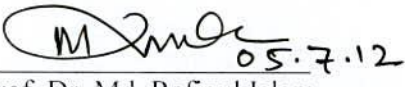
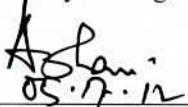

  
Signature of Supervisor

  
Signature of Student

## Approval

This is to certify that the thesis submitted by Md. Arafat Hossain entitled "*Numerical Simulation of Dislocation Reduction in InGaN and InGaAs Heteroepitaxy with Step-graded Interlayers*" has been approved by the board of examiners for the partial fulfillment of the requirements for the degree of M. Sc. Engineering in the Department of *Electrical and Electronic Engineering*, Khulna University of Engineering & Technology, Khulna-9203, Bangladesh on July 5, 2012.

### BOARD OF EXAMINERS

1.   
Dr. Md. Rafiqul Islam  
Associate Professor  
Dept. Electrical and Electronic Engineering  
Khulna University of Engineering & Technology  
Chairman  
(Supervisor)
2.   
Prof. Dr. Md. Abdur Rafiq  
Head, Dept. of Electrical and Electronic Engineering  
Khulna University of Engineering & Technology  
Member
3.   
Prof. Dr. Md. Rafiqul Islam  
Dept. of Electrical and Electronic Engineering  
Khulna University of Engineering & Technology  
Member
4.   
Prof. Dr. Ashraful Ghani Bhuiyan  
Dean  
Faculty of Electrical and Electronic Engineering  
Khulna University of Engineering & Technology  
Member
5.   
Prof. Dr. Md. Anwarul Abedin  
Dept. of Electrical and Electronic Engineering  
Dhaka University of Engineering & Technology  
Member  
(External)

## Acknowledgement

I would like to gratefully acknowledge my inspiring, enthusiastic and very supportive supervisor Dr. Md. Rafiqul Islam. His understanding, encouragement, motivation and expert guidance have provided a good basis for my entire research work. I offer my sincerest thanks to him for his patience, guidance, illustrious advices, useful suggestions, kind and dynamic supervision throughout the research work. His personal interest, valuable suggestions, most co-operative, constructive thoughtful and affectionate behavior resulted in completion of this thesis. He could not even realize how much I have learned from him.

My appreciation also extends to Prof. Dr. Md. Rafiqul Islam and Prof. Dr. Ashraful G. Bhuiyan, for their excellent research interest in semiconductor technologies over the time and creates a new era of research in KUET. Their efforts have been brought me into the fantastic world of semiconductor electronics since the undergraduate thesis work, and always inspired me to strive from the highest level of professionalism. I learned that a qualified researcher should keep open mind and pay persistent effort from him.

I would like to thank Prof. Dr. Md. Abdur Rafiq, Head, Department of EEE, KUET, for supporting and to be on the jury of this dissertation.

I am also thankful to Md. Mahbub Hasan, for his valuable suggestion and supports for mathematics during this work. Md. Rezaur Raihan and Naruttam Kumar Roy were very much helpful in providing the supporting documents from the abroad. I am also very much thankful to Md. Rejvi Kaysir and Md. Jahirul Islam.

Lastly but not least, I want to thank my parents for their love, their endless support, and all the sacrifices they have made over the years to provide me with the opportunities to pursue my interest.



## Abstract

### Numerical Simulation of Dislocation Reduction in InGaN and InGaAs Heteroepitaxy with Step-Graded Interlayers

In the recent years, the InGaN and InGaAs heteroepitaxy with low dislocation density have become crucial important for high performance electronic and optoelectronic devices, especially for multi junction solar cell. Theoretical efforts on dislocation reduction have become a potential issue to realize the future novel device using these materials. In this dissertation, a numerical simulation has been carried out for the reduction of dislocation density in wuzrite InGaN as well as cubic InGaAs heteroepitaxy with step-graded interlayers. An energy balance model has been developed for evaluating the misfit dislocation (MD) density in the step-graded structure of these heteroepitaxy. The residual strain from previous interlayer has been taken into account with misfit strain to calculate the MD density in each interlayer. To obtain a detail understanding of dislocation interactions and their propagation through the material, a reaction model has been developed considering the geometrical parameters of the step-graded heteroepitaxy. The reaction equations in each model are developed considering the possible annihilation and fusion reactions between each pair of threading dislocations (TDs) and blocking of TDs by MDs on their gliding paths. The evaluations of TD densities have been done using the numerical simulation of the reaction model by Euler method.

The simulation results confirm a significant improvement of epilayer quality due to the use of step-graded interlayers for the heteroepitaxy. The calculations have been done for 3 step-graded interlayers each containing 10% composition difference. Each interlayer and the total thickness of the film are 0.2  $\mu\text{m}$  and 1.5  $\mu\text{m}$  respectively. The edge, screw and mixed type MDs are found to be  $1.14 \times 10^{11}$ ,  $1.4 \times 10^{10}$  and  $9.9 \times 10^{11} \text{ cm}^{-2}$  respectively on the  $1/3\langle 11-23 \rangle(11-22)$  slip of the  $\text{In}_{0.4}\text{Ga}_{0.6}\text{N}$  epilayer. The MDs are also estimated in  $1/3\langle 11-23 \rangle(1-101)$  and  $1/3\langle 11-20 \rangle(0001)$  slip systems. Significant decreases in MD densities from first interlayer to second interlayer, second interlayer to third interlayer and third interlayer to final epilayer have been evaluated. The edge, screw and mixed MDs are found to be decreased from  $1.6 \times 10^{11}$  to  $1.14 \times 10^{11} \text{ cm}^{-2}$ ,  $2.0 \times 10^{10}$  to  $1.4 \times 10^{10} \text{ cm}^{-2}$  and  $1.4 \times 10^{12}$  to  $9.9 \times 10^{11} \text{ cm}^{-2}$  in the  $1/3\langle 11-23 \rangle(11-22)$  slip system from first interlayer to final InGaN epilayer. On the other hand, due to use of 3 interlayers for  $\text{In}_{0.4}\text{Ga}_{0.6}\text{As}$  the total edge and mixed type MDs are found to be decreased from  $1.1 \times 10^{11}$  to  $8.8 \times 10^8 \text{ cm}^{-2}$  and  $9.2 \times 10^{11}$  to  $7.6 \times 10^9 \text{ cm}^{-2}$  respectively. These step wise decrease in dislocation densities at each interlayer and final epilayer have good agreement with experimentally observed results. The numerical solutions of TD densities also confirm the improved epilayer

quality using step-graded interlayer. Due to more relative motion and step inclination at each interlayer a higher rate of reduction with film thickness have been reported for mixed type TDs. The average edge, screw and mixed type TDs densities for the step graded structures are found to be  $1.48 \times 10^{10}$ ,  $3.7 \times 10^{10}$  and  $1.1 \times 10^9 \text{ cm}^{-2}$  respectively at the top surface of the  $\text{In}_{0.4}\text{Ga}_{0.6}\text{N}$  epilayer. In contrast, these values are  $7.6 \times 10^{10}$ ,  $1.89 \times 10^{11}$  and  $6.26 \times 10^9 \text{ cm}^{-2}$  respectively for the without graded structure. In the same way, the average edge and mixed type TD densities decreased from  $4.9 \times 10^9$  to  $2.05 \times 10^9 \text{ cm}^{-2}$  and  $2.1 \times 10^{10}$  to  $2.28 \times 10^9 \text{ cm}^{-2}$  respectively for step grading in InGaAs heteroepitaxy.

The above performance analysis of the proposed step-graded technique suggests that it will be very promising and superior for improving the material quality in case of heteroepitaxial film.

*This work is dedicated to my beloved Parents, for guiding me with love and patience*

# Table of Contents

	Page
Declaration.....	i
Approval.....	ii
Acknowledgement.....	iii
Abstract.....	iv
Contents.....	vii
List of Figures.....	x
List of Table.....	xiii
Nomenclature.....	xiv
<b>Chapter I Introduction</b>	<b>1-10</b>
1.1 Research Background.....	01
1.1.1 Dislocations and Their Impact on Devices Performance.....	02
1.2 Dislocations Reduction and Thesis Motivation.....	03
1.3 Objectives of the Thesis.....	04
1.4 Synopsis of the Thesis.....	05
References.....	06
<b>Chapter II Fundamentals of Dislocation in III-V Semiconductors</b>	<b>11-30</b>
2.1 Introduction .....	11
2.2 Homo and Hetero-epitaxy.....	11
2.3 Strained Film and Critical Thickness .....	12
2.4 Different Models of Critical Thickness.....	12
2.4.1 Matthews and Blakeslee .....	13
2.4.2 People and Bean .....	14
2.4.3 Energy Balance Model .....	15
2.5 Elementary of Dislocations Engineering .....	17
2.6 Nucleation of Dislocations.....	18
2.6.1 Homogeneous .....	18
2.6.2 Heterogeneous .....	19
2.6.3 Dislocations Multiplication .....	19
2.6.3.1 Frank–Read Source .....	19
2.6.3.2 Spiral Source .....	20
2.7 Concept of Dislocations Reduction .....	21



2.7.1 Constant Composition Layer .....	21
2.7.2 Graded Layer .....	22
2.7.2.1 Linear and Nonlinear Grading.....	22
2.7.2.2 Step Grading .....	23
2.8 Slip Systems in Different Material Structure .....	24
2.8.1 Wuzrite InGaN.....	24
2.8.2 Cubic InGaAs .....	25
References.....	27
<b>Chapter III Methods of Dislocations Reduction</b>	<b>31-51</b>
3.1 Introduction.....	31
3.2 Critical Thickness for Step-graded Structure .....	31
3.3 MDs with Step-graded Interlayers .....	33
3.3.1 Wuzrite InGaN Heteroepitaxy .....	33
3.3.2 Cubic InGaAs Heteroepitaxy .....	36
3.4 TDs with Step-graded Interlayers .....	37
3.4.1 Reaction Model for InGaN Heteroepitaxy .....	42
3.4.2 Reaction Model for InGaAs Heteroepitaxy .....	45
References.....	50
<b>Chapter IV Simulation Results and Discussion</b>	<b>52-72</b>
4.1 Introduction .....	52
4.2 Critical Thickness of InGaN/GaN and InGaAs/GaAs System .....	52
4.2.1 Critical Thickness at Different Slips .....	54
4.3 Dislocation Sources in Step-graded Heteroepitaxy.....	55
4.4 MDs in Step-graded InGaN and InGaAs.....	56
4.4.1 MDs Generation in Wuzrite InGaN.....	56
4.4.2 MDs Generation in Cubic InGaAs .....	60
4.5 TDs Reduction Using Step-graded Interlayer.....	62
4.5.1 TDs in Wuzrite InGaN .....	62
4.5.2 TDs in Cubic InGaAs .....	67
4.6 Effect of Annihilation Radius .....	70
References.....	71
<b>Chapter V Conclusions and Future Work</b>	<b>73-75</b>
7.1 Conclusions.....	73
7.2 Future Work.....	74

**Appendix A: Values of Different Parameters of InGaN and InGaAs heteroepitaxy..... 76**  
**Related Publications List.....77**

## List of Figures

Figure No	Captions	Page
1.1	The effect of dislocation density in InGaN single junction solar cell performance	02
2.1	Schematic representation of homo and hetero-epitaxial growth and relation of lattice mismatch with critical thickness	12
2.2	Different forces acting on a dislocation in a strained heteroepitaxial layer	14
2.3	The straight misfit dislocation in the film–substrate interface. The thickness of the film is $h$ , the slip plane is tilted by the angle $\varphi$ from the normal to the interface.	16
2.4	Changing dislocation type along a single dislocation line: A-screw type, B-mixed type and C-edge type	17
2.5	Schematic cross-sectional representation of a Frank-Read dislocation source	20
2.6	Dislocation multiplication from spiral source	21
2.7	Schematic diagrams of linearly graded and step-graded layers, assuming compressive overgrowth to lattice constants larger than that of the substrate	22
2.8	Schematic representation of (a) low dislocation density step-graded layer and (b) high dislocation density without graded layer	23
2.9	Slip systems in a hexagonal lattice. Slip planes and directions are as indicated	25
2.10	Dislocation geometry in cubic heteroepitaxy. (a) TD gliding on a (111) slip plane with trailing MD, which appears at film/substrate interface as a result of TD motion (b) The geometry for TD motion in a strained film with fcc crystal structure and (c) Dislocation Burgers vector decomposition into the edge and screw components	26
3.1	Structure of the heteroepitaxy having step-graded interlayers with different In composition where $x_1 < x_2 < x_3$ .	32

3.2	(a) The three coordinate system for dislocation in wuzrite structure where the z-axis is perpendicular to the c-plane and the dislocation line lies along the y-axis and (b) geometrical representation of equally distributed dislocation array	34
3.3	Threading dislocation reduction mechanism in step-graded heteroepitaxy	38
3.4	Threading dislocation motion in growing film (a) dislocation geometry and their relative motion, (b) the interaction area swept by moving TD in plain view and (c) perspective view	39
3.5	Probable interactions between threading dislocations due to step-graded interlayers. Dislocations (a) may not or (b) may bend without being removed from the top layer. (c) A mixed dislocation may bend over and glide all the way to the edge, resulting in the elimination threading dislocation in the top layer, (d) Dislocation may participate in an annihilation reaction, and eliminate from the top layer, (e) two dislocation may coalesce to form a third dislocation. This process removes one dislocation from the upper layer and (f) scattering reaction between two dislocations to form two new dislocations	41
4.1	Comparison of critical thickness from various models for (a) $\text{In}_x\text{Ga}_{1-x}\text{N}/\text{GaN}$ and (b) $\text{In}_x\text{Ga}_{1-x}\text{As}/\text{GaAs}$ systems.	53
4.2	The critical thickness in different slip systems of $\text{In}_x\text{Ga}_{1-x}\text{N}/\text{GaN}$ heteroepitaxy	54
4.3	The critical thicknesses for different sources of dislocations in $\text{InGaN}$ heteroepitaxy	55
4.4	The critical thicknesses for different sources of dislocations in $\text{InGaAs}$ heteroepitaxy	55
4.5	The different types of misfit dislocations on $1/3\langle 11-23 \rangle (11-22)$ slip of a step-graded $\text{InGaN}$ ( $\text{In}_{0.4}\text{Ga}_{0.6}\text{N}/\text{In}_{0.3}\text{Ga}_{0.7}\text{N} / \text{In}_{0.2}\text{Ga}_{0.8}\text{N} / \text{In}_{0.1}\text{Ga}_{0.9}\text{N}/\text{GaN}$ heteroepitaxy) layer	57
4.6	The different types of misfit dislocations of a step-graded $\text{InGaN}$ ( $\text{In}_{0.4}\text{Ga}_{0.6}\text{N}/\text{In}_{0.3}\text{Ga}_{0.7}\text{N} / \text{In}_{0.2}\text{Ga}_{0.8}\text{N} / \text{In}_{0.1}\text{Ga}_{0.9}\text{N}/\text{GaN}$ heteroepitaxy) layer -	58



	(a) on $1/3\langle 11-23 \rangle$ (1-101) slip and (b) on $1/3\langle 1120 \rangle$ (0001) slip	
4.7	Comparison of total edge type misfit dislocations in step-graded and without graded InGaN/GaN heteroepitaxy using 3 interlayers	59
4.8	Comparison of total mixed type misfit dislocations in step-graded and without graded InGaN/GaN heteroepitaxy using 3 interlayers	59
4.9	The different types of misfit dislocations in step-graded InGaAs ( $\text{In}_{0.4}\text{Ga}_{0.6}\text{As}/\text{In}_{0.3}\text{Ga}_{0.7}\text{As} / \text{In}_{0.2}\text{Ga}_{0.8}\text{As} / \text{In}_{0.1}\text{Ga}_{0.9}\text{As}/\text{GaAs}$ heteroepitaxy) layer	60
4.10	Comparison of total edge type misfit dislocations in step-graded and without graded $\text{In}_x\text{Ga}_{1-x}\text{As}/\text{GaAs}$ heteroepitaxy using 3 interlayers	61
4.11	Total mixed type MD generated in step-graded and without graded $\text{In}_x\text{Ga}_{1-x}\text{As}/\text{GaAs}$ heteroepitaxy using 3 interlayers	61
4.12	The variation of edge type TD density with specific number in step-graded $\text{In}_x\text{Ga}_{1-x}\text{N}/\text{GaN}$ system	63
4.13	The variation of – (a) mixed type and (b) screw type TD density with specific number in step-graded $\text{In}_x\text{Ga}_{1-x}\text{N}/\text{GaN}$ system	64
4.14	The average edge, screw and mixed type TDs for- (a) step-graded and (b) without graded $\text{In}_x\text{Ga}_{1-x}\text{N}/\text{GaN}$ system	65
4.15	The variation of overall TD density with step-graded InGaN thickness	66
4.16	The variation of average TD density in step-graded $\text{In}_x\text{Ga}_{1-x}\text{As}/\text{GaAs}$ system	67
4.17	The total edge and mixed type TD density in - (a) step-graded and (b) without graded $\text{In}_x\text{Ga}_{1-x}\text{As}/\text{GaAs}$ system	68
4.18	The variation of overall TD density with step-graded $\text{In}_x\text{Ga}_{1-x}\text{As}$ thickness	69
4.19	The effects of annihilation radius on total TD density of InGaN/GaN heteroepitaxy	70
4.20	The effects of annihilation radius on total TD density of InGaAs/GaAs	70

## List of Tables

Table No	Title	Page
2.1	Parameters for favored slip systems in wuzrite crystal structure showing $b$ , $\varphi$ and $\theta$	25
2.2	Active slip systems for (001) heteroepitaxy of cubic semiconductors	26
3.1	Reaction table for threading dislocation in growing InGaN heteroepitaxy	45
3.2	Reaction table for TDs in growing InGaAs heteroepitaxy. Reactions that are not possible due to $b^2$ -criterion or for geometric reasons are indicated with a “-” while reactions that are possible are indicated with their designated number. Annihilation reactions are denoted with “0”	49

## Nomenclature

$C_{13}$	Elastic constants
$C_{33}$	Elastic constants
$F_a$	Misfit force
$F_l$	Line tension force
$G$	Share modulus
$b$	Burger vector
$h$	Layer thickness
$\varepsilon_m$	Misfit strain
$c$	A strain constant
$y_b$	Uniform strain component
$R$	Radius of curvature of bending strain
$\varepsilon$	Residual strain
$\lambda$	Angle between burger vector and direction of interfacial plane perpendicular to dislocation line
$\nu$	Poisson's ratio
$\theta$	Angle between dislocation line and burger vector
$\varphi$	Angle between slip plane and normal to the film substrate interface
$h_c$	Critical thickness
$\sigma_{xx}$	Misfit stress along the x-axis
$\sigma_{yy}$	Misfit stress along the y-axis
$\sigma_{zz}$	Misfit stress along the z-axis
$\sigma_m$	Non-zero component of uniform misfit stress
$E_m$	Strain energy
$E_d$	Dislocation energy
$E_t$	Total energy
$w$	Dislocation width
$a$	Lattice constant
$c$	Lattice constant
$r_0$	Dislocation core radius

$R_c$	Half-loop critical radius
$h_p$	Critical thickness of Frank-Read source
$h_s$	Critical thickness of spiral source
$x$	Indium mole fraction
$i$	Number of interlayer
$b_c$	Edge component of burger vector
$l$	Distance between two neighbor dislocation
$\gamma$	Angle of misfit dislocation array with x-axis
$\rho_{MD}$	Misfit dislocation density
$\rho_{TD}$	Threading dislocation density
$\rho_x$	Threading dislocation density of x type
$\rho_y$	Threading dislocation density of y type
$r_A$	Annihilation reaction radius
$r_F$	Fission reaction radius
$r_S$	Scattering reaction radius
$r$	Relative motion between dislocation
$N$	Number of threading dislocation
$\psi$	Angle between dislocation line and normal to film-substrate interface
$m$	Unit vector
$V_{xy}$	Relative velocity between dislocation x and y
$K_{xy}$	Reaction kinetic coefficient between dislocation x and y



# Chapter I

## Introduction

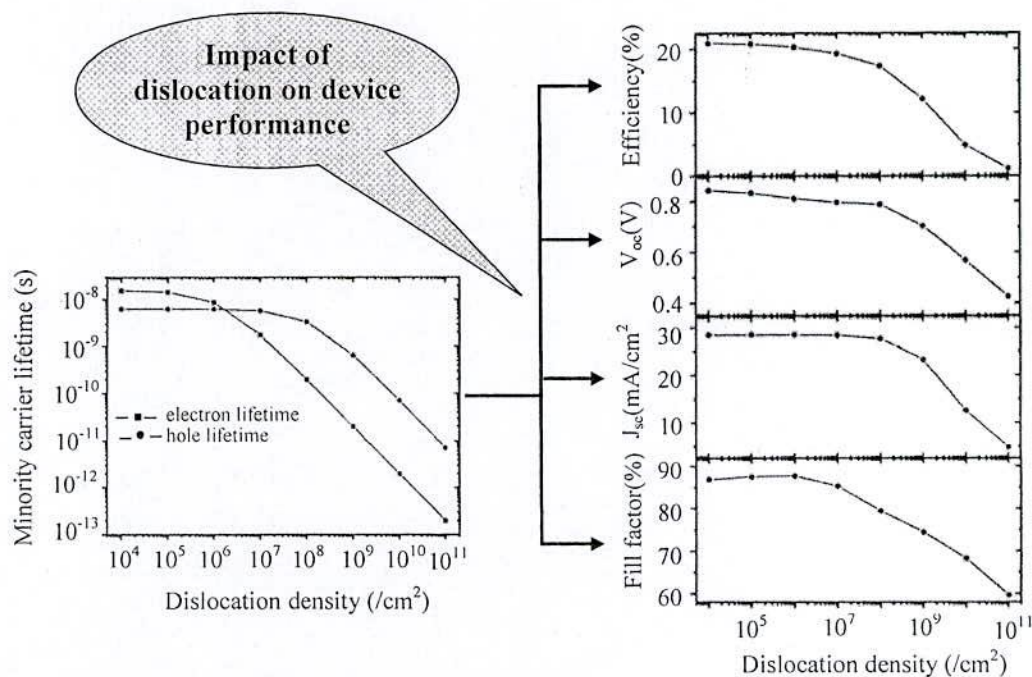
### 1.1 Research Background

The advanced III-V compound semiconductor single crystals such as GaN, InN, AlN and GaAs are key materials for future progresses in the emerging high speed electronic technologies. Their diverse applications include the optoelectronic as well as high power and high-frequency microelectronic devices [1-4]. Consequently, group-III nitride and arsenide with their related alloys have been intensively studied with remarkable breakthrough in the growth of multilayer structures for device applications in recent years. Among them InN-based alloys are predicted to show high mobility, high absorption coefficient, long lifetime of charge carriers, low effective mass of electrons and holes and superior resistance against ingredient damages [5-6]. Ternary nitride alloy such as InGaN is currently a major topic of research due to its widespread uses in high electron mobility transistors (HEMTs), light-emitting diodes (LEDs) and laser diodes (LDs) [7-8]. Especially, this material is a promising candidate for multi-junction (MJ) tandem solar cells with high conversion efficiency [9-10]. The wide band gap range of InGaN material has provided a possibility to fabricate a full spectrum solar cell ranging from deep ultraviolet to near infrared based on the material system. On the other hand, the efficient optoelectronic and photon emission properties of the ternary arsenide, InGaAs, alloys are also essential in the field of the modern optoelectronic and microelectronic technologies [11-12]. Various high performance devices based on this material are already fabricated and approaching in the markets. Particularly, due to excellent current matching, InGaAs has been recognized their dominance for the choice of three junction  $\text{In}_{0.5}\text{Ga}_{0.5}\text{P}(1.8\text{eV})/\text{GaAs}(1.4\text{eV})/\text{In}_{0.3}\text{Ga}_{0.7}\text{As}(1.0\text{eV})$  tandem solar cell [13-15]. In order to realize a tandem solar cell based on InGaN or InGaAs, it is essential to grow InGaN and InGaAs alloys with high indium (In) content [9,13]. As a result of increasing the In composition, during growth of InGaN or InGaAs, poses many challenges in controlling defect densities due to large difference in lattice constant between InN and GaN (11%) or InAs and GaAs (7.2%). Therefore, despite the tremendous success, these technologies still suffer mostly from the lack of perfect substrates and have to cope with strongly mismatched heteroepitaxial growth. Though the wafer size and electrical property requirements of GaAs can be met by the present state of the art, cost-effective high volume production of low dislocation density single crystal still desired. In addition, unavailability of device quality GaN substrate remains a key problem. Since the performance of devices are greatly depends on dislocation

density, it is a potential issue to improve the film quality during the growth of InGaN and InGaAs heteroepitaxy.

### 1.1.1 Dislocations and Their Impact on Device Performance

In order to fabricate a high performance device, the epitaxial layer must have a low defect density. The major problem that needs to be resolved is the ability to produce a high quality crystalline layer, which is greatly determined by the substrate on which the epitaxial layer is grown [16-17]. Since there has been no successful technique devised for the bulk growth of InGaN and InGaAs, they are usually grown epitaxially. Due to the lack of suitable lattice matched substrate currently these materials are grown hetero-epitaxially [18-19]. Therefore, the large lattice as well as thermal expansion coefficient mismatches between the epilayer and substrate introduces dislocation which leads to degrade the material quality and consequently the performance of their constituent devices [20-22]. In order to fabricate high performance devices, the InGaN and InGaAs epitaxial layer must have low dislocation density. These dislocations act as scattering centers and midband gap states, which function as recombination centers and reducing minority carrier lifetime. Therefore, in the case of minority carrier devices, such as solar cells, threading dislocation density beyond a certain value will have a deleterious impact on carrier lifetime. As a result, efficiency, open circuit voltage ( $V_{oc}$ ), short circuit current density



**Figure 1.1:** The effect of dislocation density in InGaN single junction solar cell performance [23]



( $J_{sc}$ ) and fill factor decreases gradually with the increase of dislocation density. These effects have been observed in a InGaN solar cell using n on p (n-p) device structure as shown in Fig. 1.1 [23]. Further reports confirmed that the edge dislocations are the origin of most yellow luminescence typically observed in Si-doped GaN [25-26]. These defects serve as nonradiative carrier recombination sites, which affect the light emission efficiency. Similarly, another challenge to low threshold current and high efficiency InGaAs/GaAs(111) heterostructures laser for industrial applications is defect formation due to misfit [24]. The external quantum efficiency also reduces due to high dislocation density. Besides their influence on optical performance, dislocations can act as acceptor-like centers, which can capture electrons. Some defects can lead to the formation of space charge region along the dislocation lines [27]. This results in the reduction in carriers' mobility and affecting the performance of electronic devices, like MOSFETs and HEMTs structure [28]. Hence the reduction of dislocation density is a budding issue for InGaN and InGaAs heteroepitaxial devices.

## 1.2 Dislocations Reduction and Thesis Motivation

In the development of semiconductor devices utilizing InGaN and InGaAs heteroepitaxy there is an increasing effort of finding the way to decrease the dislocation density. The concept of dislocation reduction during the heteroepitaxial growth of InGaN and InGaAs requires an understanding of misfit strain caused by lattice mismatch. The very common mode of strain relaxation is by the formation of misfit dislocations (MDs) from different homogeneous and heterogeneous sources and dislocation multiplication during the growth [29]. The experimental results also confirmed the strain relaxation mechanism by the formation of MD at the layer substrate interface in case of InGaN thin film grown on GaN and InGaAs on GaAs substrate [20,30]. The misfit dislocations generate due to biaxial lattice mismatch and the threading dislocations (TDs) which threaded the multilayer may be initiated from MDs or any other sources [20]. Due to the adverse effects of dislocation, the researchers are highly interested to find a suitable growth technique which will reduce the dislocations density of future high performance devices fabrication.

The heteroepitaxial layers may be grown on substrate directly or with an intermediate buffer layer. Due to the large lattice mismatch it introduces a high density of MDs which is the main source of TDs in the upper layers [20, 22]. Therefore, efforts have been carried out in several ways to reduce the MDs as well as TDs [31]. The compositional grading is one of the most effective techniques which can be very effective to reduce both MDs and TDs [32-37]. In a properly designed graded layer, misfit strain as well as dislocation is greatly reduced due to spreading the strain profile throughout the entire layer thickness instead being concentrated to a



single interface. This grading of epitaxial layer may be done in several approaches such as step grading, linear or nonlinear grading, grading with overshoot interfaces and reverse grading [32-37]. Most of the experimental and theoretical studies with graded heteroepitaxial layer have been carried out on linear and nonlinear grading [34, 38-39]. However, the efficient strategy to reduce dislocation density is to initiate annihilation and fusion reaction among them during their glide process. In this process, the inclinations of TDs at layer-substrate or layer-layer interface are responsible for interaction between them and hence results in reduction by reaction [40]. Consequently, linear or nonlinear grading shows poor performance for reducing the TDs in the epilayer due to the less interaction probability.

All these objections are a driving force for further investigations of a technique which is best suitable for MDs as well as TDs reduction. In heteroepitaxy growth of InGaN and InGaAs using step graded interlayer, the step increase of In composition in the epitaxial layers, a multiple step inclination of TDs at each interface will occur. This promotes the reaction among the TDs at each interlayer. Few experimental works have been carried out on step-graded interlayer used for different material system such as InGaN/GaN, SiGe/Si, InGaAs/GaAs [32-33, 41-43]. The results confirmed that, this technology will be a promising solution for dislocation reduction during growth of heteroepitaxy. In addition, different dislocation multiplication source could not be generated in the interlayers, if their thicknesses are properly controlled while step-grading. As a result less MDs as well as TDs could be generated in step-graded interlayers. The step-graded interlayers will relax the misfit strain mostly through the glide motion of existing threading dislocations from previous interlayer instead of the large MDs nucleation. Therefore, the reuse of dislocations is achieved by controlling the magnitude and rate of strain. Theoretically, well-designed step-graded interlayers have higher performance compared to non-graded even of the linear graded layers in strain relaxation and dislocation reduction. Although available theoretical works have been developed for without grading or linear and nonlinear grading, there is no such work on step-graded interlayers for wuzrite as well as cubic materials. In order to realize future high performance devices, a detail analysis of dislocation reduction using step-graded interlayer is urgently required.

### **1.3 Objectives of the Thesis**

The numerical simulation for dislocation reduction in wuzrite as well as cubic material using step-graded interlayer will be very promising for the future high performance devices. The primary objective of this research work is to understand the mechanism of dislocation formation in the compositionally step-graded wuzrite InGaN and cubic InGaAs heteroepitaxy which can be employed for other material systems. Then efforts will subsequently be placed on the reduction



of dislocations in these heteroepitaxy using the step-graded interlayer technique. The development of a successful numerical simulation requires the following series of tasks to investigate MD and TD densities.

An analytical energy balance model has been developed for the step-graded structure in order to calculate the MDs generation with increasing film thickness. For this purpose, the total energy contained in each interlayer and final epilayer have been calculated from the misfit strain energy and energy released by MDs considering the elastic constants. The critical thicknesses which are the key issue for MD formation have been calculated numerically in different possible slips at each interlayer. The generation of different types of MDs such as edge, screw and mixed dislocations on different slips has been calculated from their geometrical parameters, in plane misfit and residual strain for multilayer structure.

Since TDs are concomitantly generated with MDs, another main objective of this research is to develop a reaction model for TDs in step-graded structures of both material systems. The reaction tables have been developed considering the crystal geometry and all possible burger vectors. A couple of ordinary differential equations have been developed considering the possible annihilation and fusion reaction between TDs and TDs blocking by MDs. The system of equations has been solved using the Euler numerical method. The reaction kinetic coefficients at each interlayer are calculated considering the effective strain and lateral differential motion of TDs with increasing thickness.

Finally, the results obtained from these simulations have been compared to the available experimental data.

### **1.3 Synopsis of the Thesis**

This dissertation consists of five chapters and is mainly focused on the dislocation reduction using step-graded interlayers (in chapter 3) in InGa<sub>N</sub> and InGaAs heteroepitaxy. The results are analyzed from different point of view in these heteroepitaxy (in chapter 4). An extensive literature survey was carried out during this period of research work to relate the observations with other published results and to identify new frontiers. References are made to acknowledge the work by other authors at the end of each chapter. The brief summary for each chapter is as given below;

**Chapter 1** introduces the potential of group III-nitride and arsenide materials with a brief review of impacts of dislocations in their devices. After analyzing the conventional approaches of dislocation reduction, motivation and objectives for carrying out this thesis work are highlighted.

**Chapter 2** reviews the theory and fundamentals of dislocation in group III-nitrides and arsenides. This includes the literature study of different critical thickness model and sources of dislocations. Conventional approaches of dislocation reduction have been discussed with possible slip systems in the wuzrite and cubic material systems.

**Chapter 3** presents the mathematical modeling of dislocation density in the step-graded structure in details. The first section covers the strain relaxation via MD generation in both heteroepitaxy and the last one presents a reaction models for all possible TDs considering annihilation and fusion reaction among them and blocking by MDs.

**Chapter 4** reports the expected results from the analytical and numerical simulation of the mathematical model developed in Chapter 3 for the proposed step-graded technique. This includes the different types of MD generation in different slips, effects of interlayer on them, variation of different types of TDs and effects of different parameters on them. Finally, some results are compared with experimental work for model verification.

**Chapter 5** concludes the thesis work and offers some suggestions which can serves as future problem areas for predecessors.

#### References:

- [1] U. K. Mishra, W. Yi-Feng, B. P. Keller, S. Keller, and S. P. Denbaars, "GaN microwave electronics," IEEE Transactions on Microwave Theory and Techniques, Vol. 46 Issue 6, pp. 756-761 (1998).
- [2] Y. C. Kong, Y. D. Zheng, C. H. Zhou, Y. Z. Deng, B. Shen, S. L. Gu, R. Zhang, P. Han, R. L. Jiang, and Y. Shi, "A novel  $\text{In}_x\text{Ga}_{1-x}\text{N}/\text{InN}$  heterostructure field effect transistor with extremely high two-dimensional electron-gas sheet," Solid State Electronics, Vol. 49, Issue 2, pp. 199-203 (2005).
- [3] L. Shen, S. Heikman, B. Moran, R. Coffie, N. Q. Zhang, D. Buttari, I. P. Smorchkova, S. Keller, S. P. DenBaars, and U. K. Mishra, "AlGaIn/AlN/GaN high-power microwave HEMT," IEEE Electron Device Letters, Vol. 22, Issue 10, pp. 457-459 (2001).
- [4] J. Wurfl, and B. Janke, "Technology towards GaAs MESFET-based IC for high temperature applications," Materials Science and Engineering: B, Vol. 46, Issues 1-3, pp. 52-56 (1997).
- [5] Y. Nanishi, Y. Saito, and T. Yamaguchi, "RF-Molecular beam epitaxy growth and properties of InN and related alloys," Jpn J. Appl. Phys., Vol. 42, Issue 5A, p. 2549 (2003).



- [6] J. Wu, W. Walukiewicz, K. M. Yu, W. Shan, J. W. Ager III, E. E. Haller, H. Lu, W. J. Schaff, W. K. Metzger, and S. Kurtz, "Superior radiation resistance of  $\text{In}_{1-x}\text{Ga}_x\text{N}$  alloys: Full-solar-spectrum photovoltaic material system," *Journal of Applied Physics*, Vol. 94, Issue 10, pp. 6477-6482 (2003).
- [7] M. T. Hasan, M. R. Kaysir, M. S. Islam, A. G. Bhuiyan, M. R. Islam, A. Hashimoto, and A. Yamamoto, "2DEG properties in InGaN/InN/InGaN-based double channel HEMTs," *Phys. Stat. Sol. C* 7, No. 7-8, pp. 1997-2000 (2010).
- [8] C. F. Lin, J. H. Zheng, Z. J. Yang, J. J. Dai, D. Y. Lin, C. Y. Chang, Z. X. Lai, and C. S. Hong, "High-efficiency InGaN-based light-emitting diodes with nonporous GaN:Mg structure," *Applied Physics Letter*, Vol. 88, Issue 8, pp. 083121-3 (2006).
- [9] A. Yamamoto, M. R. Islam, T. T. Kang, and A. Hashimoto, "Recent advances in InN-based solar cells: status and challenges in InGaN and InAlN solar cells," *Phys. Stat. Sol. C* 7, No. 5, pp. 1309-1316 (2010).
- [10] C. J. Neufeld, N. G. Toledo, S. C. Cruz, M. Lza, S. P. DenBaars, U. K. Mishra, "High quantum efficiency InGaN/GaN solar cells with 2.95 eV band gap," *Applied Physics Letter*, Vol. 93, pp. 143502-3 (2008).
- [11] E. I. Davydova, M. V. Zverkov, V. P. Konyaev, V. V. Krichevskii, M. A. Ladugin, A. A. Marmalyuk, A. A. Padalitsa, V. A. Simakov, A. V. Sukharev, and M. B. Uspenskii, "High-power laser diodes based on triple integrated InGaAs/AlGaAs/GaAs structures emitting at 0.9  $\mu\text{m}$ ," *Quantum Electronics*, Vol. 39, No. 8, p. 723 (2009).
- [12] I. Kimukin, N. Biyikli, B. Butum, O. Aytur, S. M. Unlu, and E. Ozbay "InGaAs-based high-performance p-i-n photodiodes," *IEEE Photonics Technology Letters*, Vol. 14, Issue: 3 pp. 366-368 (2002).
- [13] J. F. Geisz, S. R. Kurtz, M. W. Wanlas, J. S. Ward, A. Duda, D. J. Friedman, M. Olson, W. E. MeMhan, J. T. Kiehl, M. J. Romero, A. G. Norman, and K. M. Jones, "Inverted GaInP/(In)GaAs / InGaAs Triple-Junction Solar Cells With low-stress metamorphic bottom junctions," *Proc. of 33<sup>rd</sup> IEEE Photovoltaic Specialist Conference*, San Diego, May 11-16 (2008).
- [14] P. Ribas, V. Krishnomoorthy, and R. M. Park, "Device quality InGaAs grown on GaAs by molecular beam epitaxy," *Applied Physics Letter*, Vol. 57, Issue 10, pp. 1040-1042 (1990).
- [15] N. Dharmarasu, M. Yamaguchi, A. Khan, T. Yamada, T. Tanaba, S. Takagishi, T. Takamoto, T. Ohshima, H. Itoh, M. Imaizumi, and S. Matsuda, "High-radiation-resistant InGaP, InGaAsP, and InGaAs solar cells for multijunction solar cells," *Applied Physics Letters*, Vol. 79, issue 15, pp. 2399-2401 (2001).

- [16] T. Matsuoka, "Lattice-matching growth of InGaAlN systems," in Proc. Fall Meeting of Material Research Symp., 395, pp. 39-50 (1996).
- [17] K. Vanhollebeke, I. Moerman, P. V. Daele, and P. Demeester, "Lattice-mismatched InGaAs layers grown by OMVPE on GaAs based compliant substrates," Journal of Electronic Materials, Vol. 29, No. 7, pp. 933-939 (2000).
- [18] Y. Liu, "Heteroepitaxial growth of InN and InGaN alloys on GaN(0001) by molecular beam epitaxy" Postgraduate thesis, The University of Hong Kong, (2005).
- [19] T. P. Chin, and C. W. Tu, "Heteroepitaxial growth of InP/In<sub>0.52</sub>Ga<sub>0.48</sub>As structures on GaAs (100) by gas-source molecular beam epitaxy," Applied Physics Letter, Vol. 62, Issue 21, pp. 2708-2710 (1993).
- [20] J. W. Matthews, and A. E. Blakeslee, "Defects in epitaxial multilayer: 1. Misfit dislocation," Journal of Crystal Growth, Vol. 27, pp. 118-125 (1974).
- [21] J. Kaitcki, J. Ratajczak, J. Adamczewska, F. Phillipp, N.Y. J. Phillipp, K. R. Ski, and M. Bugajski, "Formation of dislocations in InGaAs/GaAs heterostructure," Phys. Stat. Sol. (a) 171, pp. 275-282 (1999).
- [22] H. Nishino, I. Sugiyama, and Y. Nishijima, "Misfit stress relaxation mechanism in CdTe(100) and CdTe/ZnTe(100) on a GaAs(100) highly mismatched heteroepitaxial layer," Journal of Applied Physics, Vol. 80, Issue 6, pp. 3238-3243 (1996).
- [23] M. Song, Z. Wu, Y. Fang, R. Xiang, Y. Sun, H. Wang, C. Yu, H. Xiong, J. Dai, and C. Chen, "Improved photovoltaic performance of InGaN single junction solar cells by using n-on-p type device structure," Journal of Optoelectronics and Advanced Materials, Vol. 12, No. 7, pp 1452-1456 (2010).
- [24] M. Gutierrez, D. Gonzalez, G. Aragon, M. Hopkinson, and R. Garcia, "Effect of graded buffer design on the defect structure in InGaAs:GaAs (111) B heterostructures," Materials Science and Engineering, B 80, pp. 27-31 (2001).
- [25] W. Grieshaber, E. F. Schubert, I. D. Goepfert, R. F. Karlicek, J. M. J. Schurman, and C. Tran, "Competition between band gap and yellow luminescence in GaN and its relevance for optoelectronic device," Journal of Applied Physics, Vol. 80, pp. 4615-4620 (1996).
- [26] E. F. Schubert, I. D. Goepfert, W. Grieshaber, and J. M. Redwing, "Optical properties of Si-doped GaN," Applied Physics Letter, Vol. 71, pp. 921-923 (1997).
- [27] D. C. Look, and J. R. Sizelove, "Dislocation scattering in GaN," Phys. Rev. Lett. Vol. 82, pp. 1237-1240 (1999).



- [28] C. Sasaoka, H. Sunakawa, A. Kimura, M. Nido, A. Usui, and A. Sakai, "High-quality InGaN MQW on low-dislocation-density GaN substrate grown by hydride vapor-phase epitaxy," *Journal of Crystal Growth*, Vol. 189/190, pp. 61-66 (1998).
- [29] J. E. Ayers, "Heteroepitaxy of semiconductors theory, growth, and characterization," © 2007 by Taylor & Francis Group, LLC, pp 180-189, ISBN 0-8493-7195-3.
- [30] T. Hanada, T. Shimada, S. Y. Ji, K. Hobo, Y. Liu, and T. Matsuoka, "Strain relaxation mechanism of InGaN thin film grown on m-GaN," *Phys. Stat. Sol. C* 8, No. 2, pp. 444-446 (2011).
- [31] E. Kasper, and K. Lyutovich, "Strain adjustment with thin virtual substrates," *Solid-State Electronics* Vol. 48, Issue 8, pp. 1257-1263 (2004).
- [32] M. R. Islam, Y. Ohmura, A. Hashimoto, A. Yamamoto, K. Kinoshita, and Y. Koji, "Step-graded interlayers for the improvement of MOVPE  $\text{In}_x\text{Ga}_{1-x}\text{N}$  ( $x \sim 0.4$ ) epi-layer quality," *Phys. Stat. Sol. C* 7, No. 7-8, pp. 2097-2100 (2010).
- [33] S. Nakamura, P. Jayavel, T. Koyama, and Y. Hayakawa, "Investigations on the effect of InSb and InAsSb step-graded buffer layers in  $\text{InAs}_{0.5}\text{Sb}_{0.5}$  epilayers grown on GaAs (001)," *Journal of Crystal Growth*, Vol. 300, pp. 497-502 (2007).
- [34] B. Bertoli, D. Sidoti, S. Xhurxhi, T. Kujofsa, S. Cheruku, J. P. Correa, P. B. Rago, E. N. Suarez, F. C. Jain, and J. E. Ayers, "Equilibrium strain and dislocation density in exponentially graded  $\text{Si}_{1-x}\text{Ge}_x/\text{Si}$  (001)," *Journal of Applied Physics*, Vol. 108, Issue 11, pp. 113525-5 (2010).
- [35] J. F. Ocampo, E. Suarez, F. C. Jain, and A. E. Ayers, "Overshoot graded layers for mismatched heteroepitaxial devices," *Journal of Electronic Materials*, Vol. 37, p. 1035 (2008).
- [36] J. E. Ayers, "Multiple critical layer thicknesses in retro-graded heterostructures," *Applied Physics Letters*, Vol. 92, pp. 102104-3 (2008).
- [37] E. A. Fitzgerald, "Dislocations in strained-layer epitaxy: Theory, Experiment, and Applications," *Mats. Sci. Reports* Vol. 7, pp. 87 (1991).
- [38] E. A. Fitzgerald, A. Y. Kim, M. T. Currie, T. A. Langdo, G. Taraschi, and M. T. Bulsara, "Dislocation dynamics in relaxed graded composition semiconductor," *Material Science and engineering B67*, pp. 53-61 (1999).
- [39] B. Bertoli, N. Suarez, J. E. Ayers, and F. C. Jain, "Misfit dislocation density and strain relaxation in graded semiconductors with arbitrary composition profiles," *Journal of Applied Physics*, Vol. 106, pp. 073519-7 (2009).

- [40] A. E. Romanov, W. Pompe, S. Mathis, G. E. Beltz, and J. S. Speck, "Threading dislocation reduction in strained layers," *Journal of Applied Physics* Vol. 85, pp.182-192 (1999).
- [41] P. M. Mooney, J. L. Jordan-Sweet, J. O. Chu, and F. K. LeGoues, "Evolution of strain relaxation in step-graded SiGe/Si structures," *Applied Physics Letter*, Vol. 66, pp. 3642-3644 (1995).
- [42] V. Krishnamoorthy, Y. W. Lin, and R. M. Park, "Application of 'critical compositional difference concept to growth of low dislocation density ( $<10^4/\text{cm}^2$ )  $\text{In}_x\text{Ga}_{1-x}\text{As}$  ( $x \leq 0.5$ ) on GaAs," *Journal of Applied Physics*, Vol. 72, pp. 1752-1757 (1992).
- [43] G. Macpherson, R. Beanland, and J. P. Goodhew, "A novel design method for the suppression of edge dislocation formation in step-graded InGaAs/GaAs layers," *Philosophical Magazine A*, Vol. 73, No. 05, pp. 1439-1450 (1996).



## Chapter II

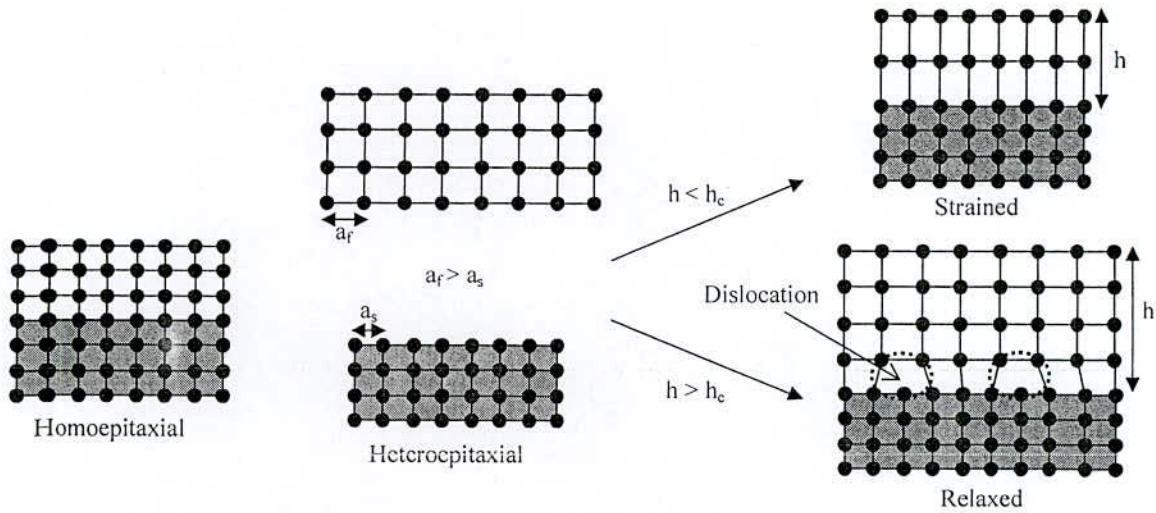
### Fundamentals of Dislocations in III-V Semiconductor

#### 2.1 Introduction

The improvement of III-V heteroepitaxial device structures requires an understanding of dislocation formation mechanism and their propagation through the material because these influence the device performance strongly. They propagate up towards the active region of electronic and optoelectronics devices and severely degrade device performance and reliability, particularly for minority carrier devices like light emitting diodes (LEDs), heterojunction bipolar transistors (HBT) and specially the photovoltaics [1-2]. Efforts have subsequently been done to reduce the dislocation density with the course of time. In this chapter different types of compositionally grading technique have been discussed leading to the idea of step grading. The potential issues such as the ideas of critical thickness and the sources of dislocation, thickness for their multiplication have been analyzed for further optimization. Besides these, the geometrical analysis of wuzrite InGaN and cubic InGaAs extends the knowledge of different types of dislocation and their propagation through a material.

#### 2.2 Homo- and Heteroepitaxy

An epitaxial growth technique is one in which a film is grown layer by layer onto a preexisting substrate. The crystalline semiconductor thin films may be grown on a crystalline substrate homoepitaxially, meaning that atoms absorbing onto the growing surface find a suitable preexisting lattice site on which to incorporate. It is therefore critical that the crystal structure and the lattice constant of the crystalline material attempting to be grown very nearly the same as those of the substrate. If two materials are dissimilar in crystal lattice parameter and the film is very thin, the in-plane lattice parameter of the film will strain in order to incorporate coherently onto the substrate, as illustrated in the schematic of Fig. 2.1. However, after a certain thickness, the film will build up enough strain energy that it will become energetically favorable for the film to relax through the formation of crystal defects, namely misfit dislocations (MDs) that relieve the strain [3]. In order to grow high quality thick films on lattice-mismatched substrates such as wuzrite InGaN on GaN or cubic InGaAs on GaAs substrate, there have been several suitable engineering solution which then introduces low dislocation density.



**Figure 2.1:** Schematic representation of homo- and heteroepitaxial growth and relation of lattice mismatch with critical thickness

### 2.3 Strained Films and Critical Thickness

The semiconductor thin film where the film is of different lattice constant than the substrate introduces strain. The strain energy containing in the film increases with the increase of thickness. If the film is thin enough to remain coherent to the substrate, then in the plane parallel to the growth surface, the thin film will adopt the in-plane lattice constant of the substrate. Fig. 2.1 shows a substrate and a film with an equal and unequal lattice constant. The film is taken to be of larger lattice constant than the substrate e.g. InGaAs on GaAs or InGaN on GaN, and the top right illustration represents a thin coherent compressively strained film. The strain applied to the film by the substrate in the plane of the interface between the two is the result of biaxial compression. The lattice constant of the film in the direction perpendicular to the growth direction will likewise be strained according to the elastic properties of the film. It will either be smaller or larger than the unstrained value depending on whether the biaxial strain is tensile or compressive. However, if the film is thicker than the critical thickness, there will be sufficient strain energy in the film to create misfit dislocations to relieve the excess strain [4].

### 2.4 Different Models of Critical Thickness

The concept of critical thickness (CT) discovered a new era for dislocation engineering and there have been many progresses in the course of time. In 1963 van der Merwe proposed a theory for the calculation of stresses at an interface between two adjacent crystals that have



different lattice and/or elastic constants followed by his earlier work with Frank [5-7] and subsequent work for isotropic material [8]. Matthews and Blakeslee introduced a force balance model (MB model) in 1974 [4]. They investigated alternating layers of GaAs and GaAs<sub>0.5</sub>P<sub>0.5</sub> and revealed that, some threading dislocations (TDs) experienced by misfit force and tension of dislocation line, bent back and forth in the layers interfaces, which gave rise to misfit dislocations. Though they have good agreement with experimental observation, some objections were raised. These were the driving force for further investigations and People-Bean published an article on the CT calculation based purely on an energy balance of the dislocation self-energy and the elastic energy which was compared with experimental results [9]. However, some drawbacks and uncertainties of their model were pointed out by Hu [10]. The story then continued with a semi-empirical model by Dodson and Tsao and studies of the excess stress for glide of a dislocation in a strained epitaxial layer by Freund-Hull and Fischer-Richter [11-13]. They proposed a model which has been recently revised [14]. It is one of the “force models” and it was again discussed in detail by Holec [15].

Almost at the same time, calculations done by Willis et al., Jain et al. and Freund and Suresh based on the minimization of the overall energy appeared in the literature (energy balanced model) [16-18]. One of the advantages of the energy balanced (EB) model is that additional considerations of hexagonal symmetry such as GaN or more complex geometry can be incorporated in a straight forward manner. Therefore, mainly the EB model is used in this work. A brief summary of some commonly used model have been discussed in the subsequent sections.

#### 2.4.1 Matthews and Blakeslee

The basis of this model is about two main forces, misfit force,  $F_a$  and the line tension,  $F_l$  acting on a preexisting dislocation in a strained film [4]. These have been illustrated in Fig. 2.2 where the first one is due to lattice mismatch, whose stress field is on the interfacial plane and expressed as

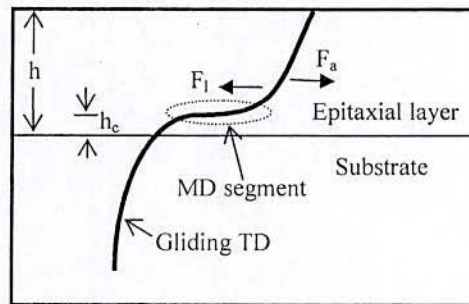
$$F_a = 2Gb h \epsilon_m \frac{1+\nu}{1-\nu} \cos \lambda \quad (2.1)$$

Where  $G$  is the shear modulus of the film,  $b$  is the magnitude of the burger vector of the misfit dislocation,  $h$  is the film thickness,  $\nu$  is the Poisson's ratio,  $\lambda$  is the angle between the burgers vector and the direction on the interfacial plane that is perpendicular to the dislocation line,  $\epsilon_m$  is the lattice mismatch strain, whose value is  $(a_f - a_s)/a_s$ , where  $a_s$  and  $a_f$  are the lattice parameters

of the substrate and the film, respectively. The second force on the misfit dislocation is due to the line tension, which acts like a restoring force, resisting the motion of the dislocation. This force ( $F_l$ ) is given by

$$F_l = \frac{Gb^2(1-\nu\cos^2\theta)}{4\pi(1-\nu)} \left[ \ln\left(\frac{h}{b}\right) + 1 \right] \quad (2.2)$$

Here  $\theta$  is the angle between the misfit dislocation line and its burgers vector. Therefore, total force acting on the dislocation, is  $F_{total} = F_a + F_l$ . For very small film thicknesses  $h$ , the total force  $F_{total}$  is negative and therefore acts against the extension (and possibly also against the creation)



**Figure 2.2:** Different forces acting on a dislocation in a strained heteroepitaxial layer

of the misfit dislocation. On the contrary, for sufficiently thick layers  $F_{total}$  is positive and thus the dislocation bends and create misfit segment. The CT is therefore determined by the equation  $F_{total}(h_c) = 0$ , and in this equation  $\varphi$  is the angle between slip plane and normal to the film-substrate interface and  $r_0$  is dislocation cut-off parameter. Eqs. (2.1) and (2.2) yield the CT value as

$$h_c = \frac{b(1-\nu\cos^2\theta)}{8\pi(1+\nu)|\epsilon|\sin\theta\sin\varphi} \ln\left(\frac{h_c}{r_0}\right) \quad (2.3)$$

#### 2.4.2 People and Bean

On the contrary to the force balance model by Matthews and Blakeslee, People and Bean have approached the problem by balancing the overall energy. The stress field caused by misfit of the lattice parameters of the thin film and the substrate is generally a biaxial stress with the only



non-zero components,  $\sigma_{xx} = \sigma_{yy} = \sigma_m$ , where  $\sigma_m$  is the misfit stress [9]. This is true for isotropic materials as well as for wurtzite materials where the interface is the  $c$ -plane (in which all directions are equivalent). According to this model, the strain energy per unit area of the film-substrate interface is

$$E_m = 2G \frac{1+\nu}{1-\nu} \varepsilon_m^2 h \quad (2.4)$$

Taking the dislocation energy in the simplest possible case the “areal” energy of the dislocation with some characteristic width  $w$  is

$$E_d = \frac{1}{w} \frac{dE_d}{d\ell} = \frac{Gb^2(1-\nu\cos^2\theta)}{4\pi(1-\nu)w} \ln\left(\frac{h}{r_0}\right) \quad (2.5)$$

People and Bean suggested that when  $E_d$  is exceeded by  $E_m$ , the misfit strain in the film will be replaced by misfit dislocations. By equating  $E_m$  and  $E_d$  one obtains the equation for the critical thickness  $h_c$  can be obtained as [13].

$$h_c = \frac{(1-\nu)}{(1+\nu)} \frac{b^2}{16\sqrt{2\pi a(x)}\varepsilon_m^2} \ln\left(\frac{h_c}{r_0}\right) \quad (2.6)$$

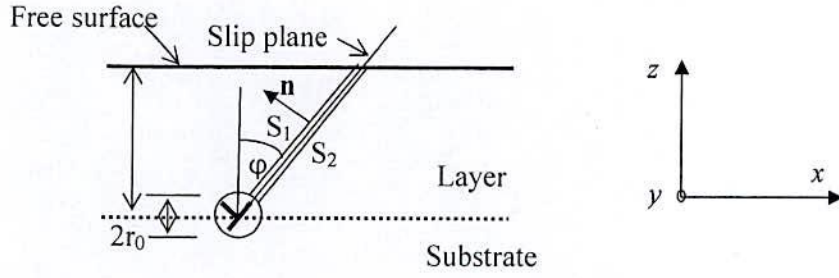
The most remarkable feature of Eq. (2.6) is that there is a quadratic dependence on the misfit strain  $\varepsilon_m$  in contrast to Eq. (2.3) for the CT using the force balance model. This is a qualitatively different feature and thus one may expect very different curves of the CT against composition for these two models.

### 2.4.3 Energy Balance Model

The critical thickness criterion presented below is based on the balance of total elastic energy in the system [18]. Assume a specimen with the geometry given in Fig. 2.3. The top surface of the specimen is stress free and therefore  $\sigma_{zz} = 0$ . The only non-zero components of the uniform misfit stress are  $\sigma_{xx} = \sigma_{yy} = \sigma_m$  within the thin layer. All directions within the  $xy$ -plane (the hexagonal  $c$ -plane) are equivalent and thus the mismatch strain components are  $\sigma_{xx} = \sigma_{yy} = \varepsilon_m$ .

Hooke's law gives

$$0 = \sigma_{zz} = c_{13}\varepsilon_{xx} + c_{13}\varepsilon_{yy} + c_{33}\varepsilon_{zz} \quad (2.7)$$



**Figure 2.3:** The straight misfit dislocation in the film–substrate interface. The thickness of the film is  $h$ , the slip plane is tilted by the angle  $\phi$  from the normal to the interface.

which results in

$$\varepsilon_{zz} = -2 \frac{c_{13}}{c_{33}} \varepsilon_m \quad (2.8)$$

Then, using Hooke's law again, the mismatch stress is

$$\sigma_m = \sigma_{xx} = \frac{(c_{11} + c_{12})c_{33} - 2c_{13}^2}{c_{33}} \varepsilon_m \quad (2.9)$$

The work  $dW/d\ell$  done by the mismatch stress while bringing the unit length of the dislocation from the free surface into its position on the interface is [18]

$$\frac{dW}{d\ell} = -\frac{dE_m}{d\ell} = \int_{\frac{h}{\cos\phi}}^0 \sum_{i,j} b_i \sigma_{i,j} n_j d\ell \quad (2.10)$$

where  $\ell$  is the coordinate along the slip plane and perpendicular to the dislocation line (the dislocation is brought from the surface to its actual position on the interface and this results in the order of integral boundaries). The integrand is constant along the integration path and with

$$\mathbf{b} = \begin{pmatrix} -b \sin\phi \sin\theta \\ b \cos\theta \\ b \cos\phi \sin\theta \end{pmatrix}, \quad \boldsymbol{\sigma} = \begin{pmatrix} \sigma_m & 0 & 0 \\ 0 & \sigma_m & 0 \\ 0 & 0 & 0 \end{pmatrix}, \quad \mathbf{n} = \begin{pmatrix} -\cos\phi \\ 0 \\ \sin\phi \end{pmatrix}$$

Eq. (2.10) yields

$$\frac{dE_m}{d\ell} = b \sigma_m h \sin\phi \sin\theta \quad (2.11)$$

According to the energy balance model, the critical thickness criterion is

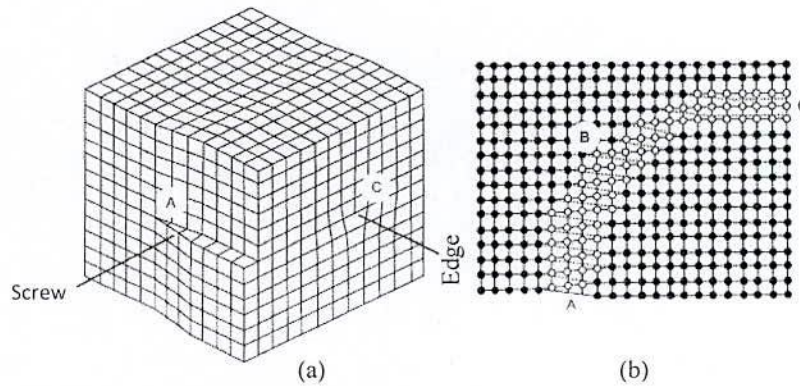


$$\frac{dE_d}{dl}(h_c) = \frac{dE_m}{dl}(h_c) \quad (2.12)$$

Freund and Suresh have shown that this approach gives the same results as the force balance model [8]. The significant difference is that in the original work of Matthews and Blakeslee pre-existing threading dislocations were needed whereas the infinite long straight misfit dislocations glide down from the free surface here (and thus this model is more similar to the propagation of the dislocation loops).

## 2.5 Elementary of Dislocations Engineering

The dislocations formed during mismatched strain relaxation, after reaching the critical thickness, consist of two different segments: the misfit dislocation (MD) segment, which lies in the plane of the mismatched interface, and the threading dislocation (TD) segment, which propagates up through the film and threaded the multilayer [4, 19]. The MD segment relieves the misfit strain, while the TD segments exist in order to complete the full dislocation loop at the epilayer surface (it is energetically unfavorable for dislocations to terminate within the crystal lattice). The MDs are considered as the main source of TDs in the upper layers. However, these MDs and TDs are usually represented by an oriented dislocation line,  $l$  and characterized by its burger vector,  $b$ , describing displacements introduced in the crystal by the dislocation. Based on the relationship of  $l$  and  $b$ , three dislocation types are distinguished as shown in Fig. 2.4: an edge-type dislocations, where  $l \perp b$ , corresponding to an extra half plane in the crystal, a screw-type dislocation with  $l \parallel b$ , and a mixed-type dislocations ( $b \perp l \nparallel b$ ). The dislocation type can



**Figure 2.4:** Changing dislocation type along a single dislocation line: A-screw type, B-mixed type and C-edge type

change as the dislocation line changes its direction in the crystal, since the burgers vector  $b$  is a constant characteristic of a dislocation which remains unchanged along the whole single dislocation line. A dislocation can only make either a closed loop or end at the crystal surfaces. The burgers vector of a perfect dislocation is a lattice vector. As such, there are three basic types of dislocations in GaN according to the burgers vector:  $a$ -type dislocations with  $\mathbf{b} = 1/3\langle 1120 \rangle$ ,  $c$ -type dislocations with  $\mathbf{b} = \langle 0001 \rangle$ , and  $(a+c)$ -type dislocations with  $\mathbf{b} = 1/3\langle 1123 \rangle$ . It is important to distinguish between these two nomenclatures: an  $a$ -type dislocation can be either, an edge, screw or mixed dislocation depending on the actual dislocation line direction and so for  $c$ - and  $(a+c)$ -type dislocations. On the other hand the dislocations in cubic InGaAs are mostly  $60^\circ$  type on inclined  $\{111\}$  planes with few edge types and are quite simple as all these materials have a cubic symmetry.

## 2.6 Nucleation of Dislocations

Despite the fact that Matthews and Blakeslee assumed substrate dislocations bend over to produce misfit dislocations after  $h_c$ , heteroepitaxial layers may contain much more dislocations density than their substrates; thus substrate dislocations are usually not the sole source. Instead, other dislocation nucleation must take place during mismatched heteroepitaxy. The mechanisms for dislocation nucleation could be placed into three broad categories, *homogeneous*, *heterogeneous* and *multiplication* [20-21]. Heterogeneous nucleation and multiplication are important for selecting the thickness of epitaxial layer. The following sections will review the mechanism of their generation and critical thickness of these sources of dislocations.

### 2.6.1 Homogeneous

Homogeneous nucleation is the spontaneous creation of dislocations at a free surface due to intrinsic epilayer strain. A possible mechanism for the introduction of misfit dislocations is the homogeneous nucleation of half-loops at the surface. The glide of such a half-loop to the interface results in a misfit dislocation segment with two associated threading dislocations is shown in Fig. 2.5. The critical radius for MD formation and the associated half-loop energy were calculated by Matthews. The formation of dislocation half-loop with a radius  $R$  considering the line energy, strain energy, stacking fault energy, energy of the surface step and expressed as [3, 22]



$$R_c = \frac{(Gb^2/8)(2-\nu)[\ln(R_c/b)+2]+2\sigma(1-\nu)b\sin\alpha}{2\pi G(1+\nu\epsilon_m b\cos\lambda\cos\phi)} \quad (2.13)$$

Activation energy of 40 eV is calculated for dislocation formation of this type, and is only likely to occur under conditions of significant epilayer strain and high material quality where no other mechanisms are available or at very high temperature [23].

### 2.6.2 Heterogeneous

Heterogeneous nucleation can occur through the inclusion of particulates or impurity precipitates that result in a local lattice strain that is significantly higher than in the bulk. As such the rate of heterogeneous nucleation is likely to be very dependent on the cleanliness of the epitaxial growth chamber, and could contribute significantly to dislocation nucleation in an epilayer of low strain.

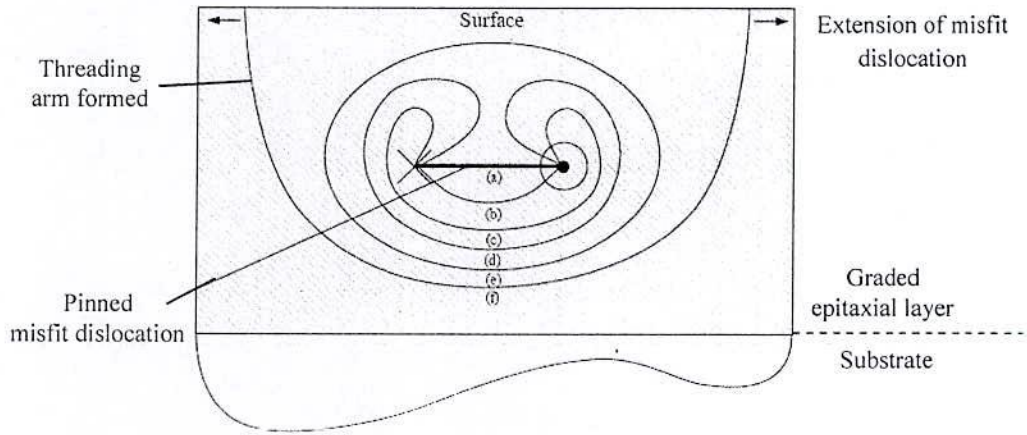
### 2.6.3 Dislocations Multiplication

Multiplication mechanisms allow for a rapid increase in dislocation nucleation, whereby a small number of initial dislocations could repeatedly act to generate many additional dislocations. There is strong evidence to suggest that the dominant mechanism for dislocation generation in a thick, low strained epilayer is multiplication [24]. The critical thickness for Frank-Read multiplication, spiral mechanism has been specifically calculated to design the optimum thickness of the graded layer.

#### 2.6.3.1 Frank-Read Source

Frank-Read multiplication sources could result when a section of dislocation becomes pinned at either end by the climb or jog (step moving dislocation from one atomic slip plane to another) of the dislocation between different glide planes, represented schematically in Fig. 2.5(a) [25]. The influence of a shear stress on the pinned segment can cause it to bow out toward the substrate along a single glide plane, Fig. 2.5(b-d), eventually closing upon itself to form a complete dislocation loop as well as reforming the initial dislocation. The loop then continues to expand until it intersects the surface at which point the formed threading arms glide away from one to another, Fig. 2.5(f). This process can be repeated as long as sufficient stress remains available to





**Figure 2.5:** Schematic cross-sectional representation of a Frank-Read dislocation source

drive bowing of the initial dislocation. However, the critical thickness for the operation of such a Frank-Read source has been calculated by Beanland [26]. The minimum thickness,  $h_f$  for which the Frank-Read source may operate can be expressed as below, where  $h_c$  is the Matthews and Blakeslee critical layer thickness.

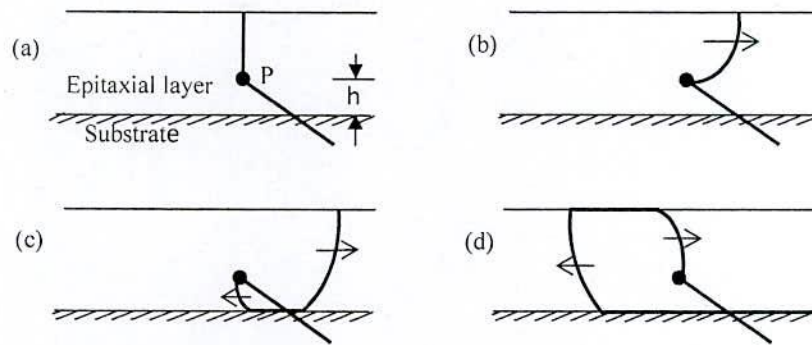
$$h_f = h_c + 2h_p \quad (2.14)$$

$$h_p = \frac{(2+\nu)b}{4\pi|\epsilon_m|(1-\nu)} \left[ \ln \left( \frac{4\sqrt{6}h_p}{b} \right) + \frac{(\nu-2)}{(\nu+2)} \right] \quad (2.15)$$

### 2.6.3.2 Spiral Source

A possible configuration for the spiral source in a heteroepitaxial layer was described by Beanland and is shown in Fig. 2.6 [26]. It is assumed that a threading dislocation is anchored at a single point P, as shown in Fig. 2.6(a). With an applied stress, the dislocation may bow out above the pinning point, as in Fig. 2.6(b). The bowed section will continue to expand and may glide to the interface to relieve mismatch strain, as in Fig. 2.6(c). Further expansion of the bowed portion may lead to production of a half-loop if the bow reaches the surface and splits in two, as in Fig. 2.6(d). The original dislocation is then available to produce more dislocations by the same process. The critical thickness for the operation of such a spiral source has also been calculated by Beanland as

$$h_s = h_c + h_p \quad (2.16)$$



**Figure 2.6:** Dislocation multiplication from spiral source

## 2.7 Concept of Dislocations Reduction

There have been many approaches explored in the production of high quality heteroepitaxial layers involving compositional variation, temperature variation and even the intentional introduction of defects [27]. Among them composition variation is the most suitable approach for incorporation of low dislocation density. The compositional grading technique is based on the elongation and recycling of the low density of dislocations either already presents within a film or produced early on in the growth at each subsequent interface, thereby relaxing the film without nucleating additional dislocations. The following is a brief summary of the evolution of available compositional grading technique leading to the idea of step grading that forms the main focus of this work.

### 2.7.1 Constant Composition Layer

The most basic form of heteroepitaxial growth consists of a layer with uniform composition that greatly exceeds the critical thickness for relaxation. Such structures undergo sudden relaxation with a large network of misfit dislocations forming at the epilayer growth interface [4, 28-29]. Since the large numbers of MD network is confined to a single plane a significant number of interactions occur. Numerous MDs become pinned and large interaction force among them makes unable to glide, hence further contribution to the relaxation process, resulting in the need to introduce greater numbers of dislocations. As a consequence the epilayer contains extremely high numbers of surface threading dislocations [30].

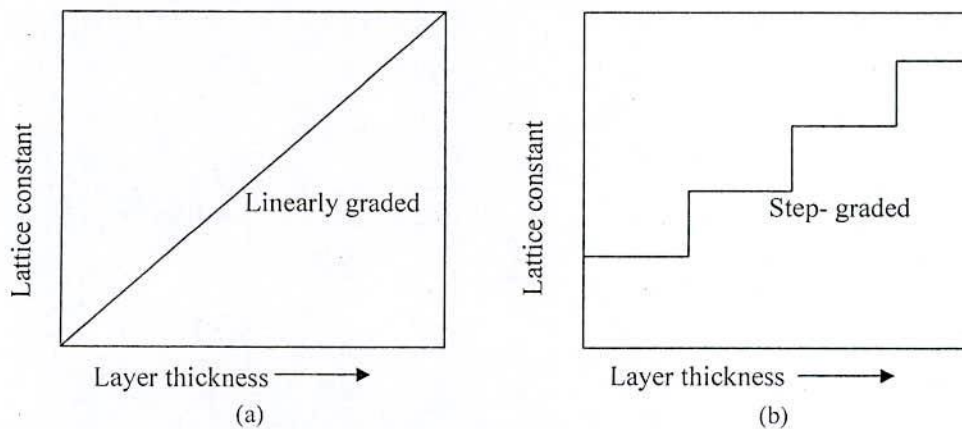


## 2.7.2 Graded Layer

Compared to the direct growth on lattice-mismatched substrates, metamorphic compositionally graded layer have some advantages that help to reduce the misfit dislocation as well as density of threading dislocations in upper layers. First, in the growth of graded layer, dislocations are distributed throughout the entire layer instead of a single interface. Thus, the probability of pinning by intersecting dislocations, which impedes the glide of the TDs, is decreased in graded layers. Second, the strain in the graded layer is greatly reduced due to spreading the strain profile across the layer thickness; therefore, the nucleation of dislocation loops is inhibited. The existing TDs are able to glide more easily and relieve the strain. However, in the technique of compositionally graded buffers, there are mainly two kinds of graded layer designs, one is linear or nonlinear-graded layers and the other is step-graded layers. The schematic diagrams of both graded buffers are shown in Fig. 2.7 (a) and (b).

### 2.7.2.1 Linear and Nonlinear Grading

During the growth, the misfit and the lattice constant of the layer change continuously with the same or different rate in the linear and nonlinear-graded layer structure [31-34]. The misfit dislocation network is no longer confined to either a single or small number of layers but can instead form anywhere throughout the layer. Such a layer allows strain to build slowly with dislocations introduced a few at a time, promoting the expansion of existing dislocations with a reduced likelihood of interaction. Once the initial MDs after critical thicknesses at each infinitely small stepped layer have formed either homogeneously or heterogeneously the gradual



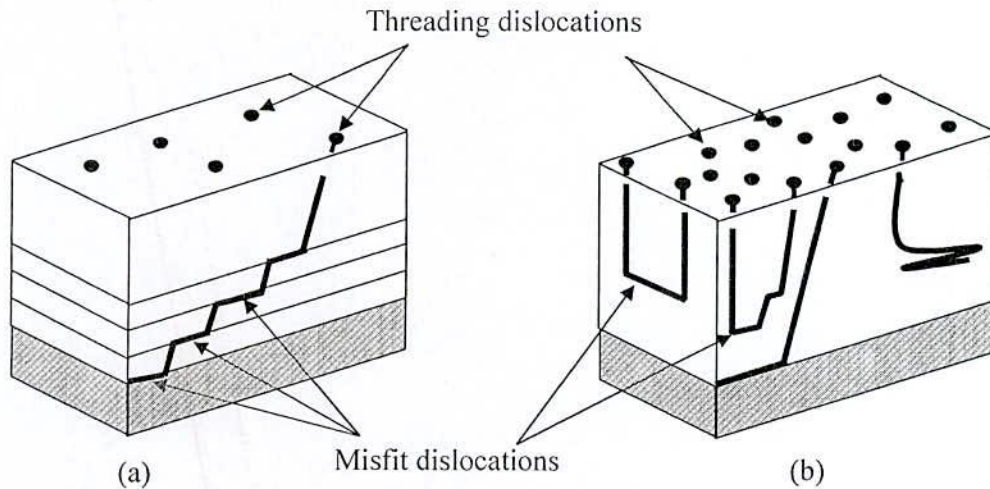
**Figure 2.7:** Schematic diagrams of- (a) linearly graded and (b) step-graded layers, assuming compressive overgrowth to lattice constants larger than that of the substrate



application of strain is conducive to further nucleation. This could be happen by means of dislocation multiplication (MFR) as a consequence of the low nucleation energy barrier. However, due to slowly increase of misfit strain, the inclination of TDs during the gliding process are very small in these types of layers. Therefore less interaction among the TDs happens in this case, results poor performance of TDs reduction with heteroepitaxial growth [35].

### 2.7.2.2 Step Grading

On the other hand, the misfit and the lattice constant of the epitaxial layer change in a stepwise manner for the step-graded layers [36-38]. The most significant difference between linear-graded and step-graded layers is that linear-graded layers have no abrupt interfaces while step-graded layers provide multiple low mismatch interfaces. These low-mismatch interfaces are able to facilitate the glide of existing threading dislocations to relieve the strain and reduce the nucleation rate of new dislocations. In lattice-mismatched step-graded epitaxy, when the thin film exceeds the critical thickness, misfit dislocation nucleation accompanies with the glide motion of TDs. During the motion of TDs, their density can be reduced through reactions between each other [35, 39]. Since the strain inside the thin film drives the TDs to move and react with each other, the introduction of an intentionally step-graded strained layer can be used to facilitate the TDs reaction and subsequent reduction process. This is the basic TDs reduction mechanism of step-graded layers. The amount of strain relieved by a MD is directly proportional



**Figure 2.8:** Schematic representation of (a) low dislocation density step-graded layer and (b) high dislocation density without graded layer

to its length; the greater the average MD length, the fewer the total number of dislocations needed to relax the strain. This process can be seen in Fig. 2.8, where (a) represents the case of a TD already present in the film, or created at the first misfit interface, being reused multiple times (i.e. dislocation recycling), thereby resulting in a lower dislocation density, and (b) is for the nucleation of new dislocations with limited 'reuse', thereby resulting in a higher dislocation density. Practically, the reuse of dislocations is achieved by controlling the magnitude and rate of introduction of strain in order to allow sufficient time and energy for MD glide to occur. A step-graded layer should relax the misfit strain mostly through the glide motion of existing threading dislocations instead of the misfit dislocation nucleation. Theoretically, well-designed step-graded layers have higher efficiency compared to linear-graded buffers in strain relaxation and threading dislocation reduction. However, in order to realize an optimal graded layer design, a much theoretical and experimental effort is still needed in further understanding of misfit and threading dislocation behaviors in step-graded layers.

## 2.8 Slip Systems in Different Material Structure

Since a periodic array of dislocations are not observed at  $\text{In}_x\text{Ga}_{1-x}\text{N}/\text{GaN}$  interfaces, unlike in well known alloys such as  $\text{Si}_x\text{Ge}_{1-x}/\text{Si}$  and  $\text{In}_x\text{Ga}_{1-x}\text{As}/\text{GaAs}$  there must have some specific slip system in wuzrite InGaN. In the following section the appropriate slip system for InGaN and InGaAs material systems are discussed in brief which have been considered during calculation of dislocation in graded layer.

### 2.8.1 Wuzrite InGaN

It has been estimated theoretically the appropriate slip systems for the misfit dislocations in wuzrite InGaN crystal as  $1/3\langle 11-23 \rangle(11-22)$  and  $1/3\langle 11-23 \rangle(1-101)$  [40]. However, there is also report of pure a-type MDs which are theoretically the most efficient MD types for relieving the misfit strain [41]. Therefore, the basal plane slip system  $1/3\langle 1120 \rangle(0001)$  is also included for theoretical considerations in this work. Possible slip systems were derived in a similar manner for the m-plane and the a-plane material. The possible slip systems for wuzrite InGaN are shown in Fig. 2.8 and the Table 2.1 contains their geometrical properties the three favored slip systems as mentioned above on which the MDs can be generated [42].



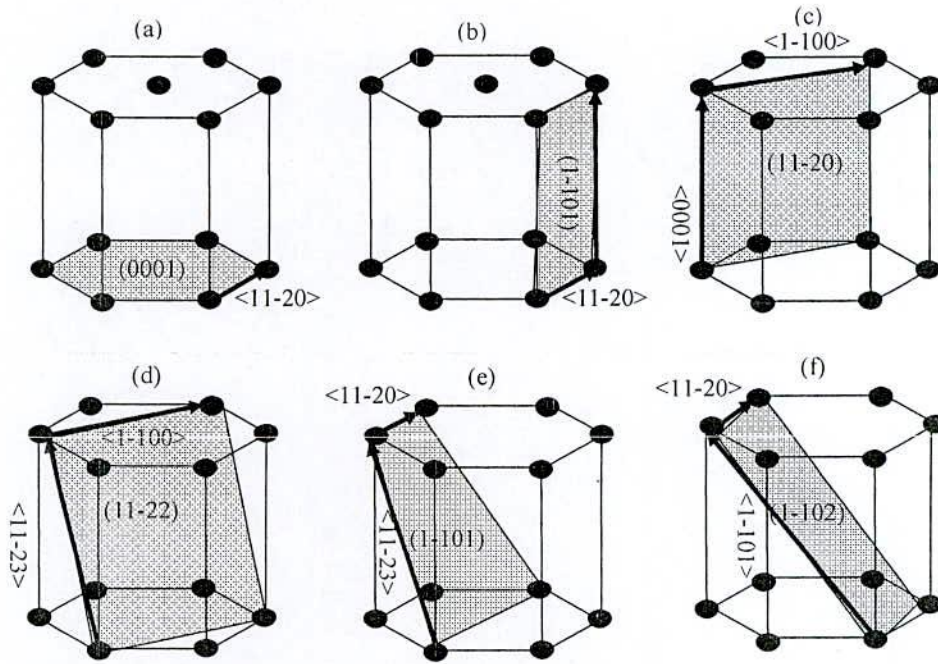


Figure 2.9: Slip systems in a hexagonal lattice. Slip planes and directions are as indicated

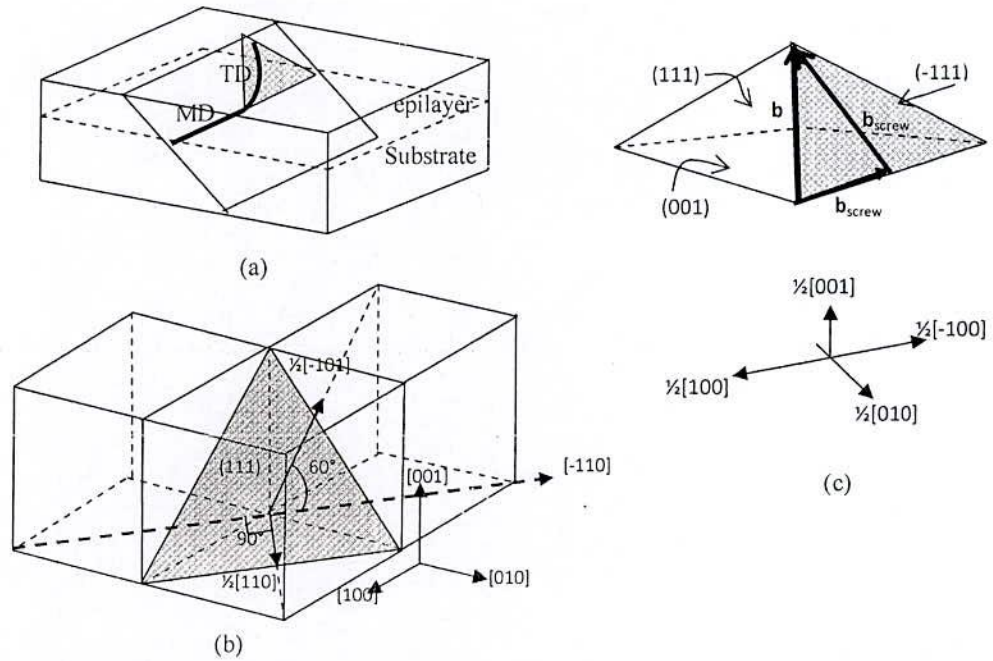
Table 2.1: Parameters for favored slip systems in wuzrite crystal structure showing  $b$ ,  $\varphi$  and  $\theta$

Possible Slip	$b$	$\varphi$
$1/3\langle 11-23 \rangle (11-22)$	$\sqrt{a^2(x) + c^2(x)}$	$\arctan \frac{a(x)}{c(x)}$
$1/3\langle 11-23 \rangle (1-101)$	$\sqrt{a^2(x) + c^2(x)}$	$\arctan \frac{\sqrt{3}a(x)}{2c(x)}$
$1/3\langle 1120 \rangle (0001)$	$\sqrt{3}a(x)$	$90^\circ$

### 2.8.2 Cubic InGaAs

For cubic semiconductor materials, such as  $\text{In}_x\text{Ga}_{1-x}\text{As}$ , the most common slip system is  $a/2 \langle 110 \rangle \{111\}$ , where  $a$  is the film lattice parameter. The burgers vectors for this system are of the type  $a/2 \langle 110 \rangle$  [43]. They are directed along the face diagonals of the cubic cell and are the shortest possible primitive translation vectors. The set of possible burgers vectors can be constructed by considering the edges of a half-octahedron, as shown in Fig. 7.10(c). The half-octahedron is oriented such that its square base is parallel to the (001) plane. For instance, if the dislocation glide plane is (-111), which is inclined with respect to the film/substrate interface by





**Figure 2.10:** Dislocation geometry in cubic heteroepitaxy. (a) TD gliding on a (111) slip plane with trailing MD, which appears at film/substrate interface as a result of TD motion (b) The geometry for TD motion in a strained film with f.c.c. crystal structure and (c) Dislocation Burgers vector decomposition into the edge and screw components

**Table 2.2:** Active slip systems for (001) heteroepitaxy of cubic semiconductors

Slip Systems	MD Line Vector	Glide Plane	Burger Vector, b
S <sub>1</sub>	[1-10]	(111)	$a/2[10-1]$
S <sub>2</sub>	[1-10]	(111)	$a/2[01-1]$
S <sub>3</sub>	[1-10]	(-1-11)	$a/2[101]$
S <sub>4</sub>	[1-10]	(-1-11)	$a/2[011]$
S <sub>5</sub>	[110]	(-111)	$a/2[101]$
S <sub>6</sub>	[110]	(-111)	$a/2[01-1]$
S <sub>7</sub>	[110]	(1-11)	$a/2[10-1]$
S <sub>8</sub>	[110]	(1-11)	$a/2[011]$

the angle  $\alpha = \cos^{-1}(1/\sqrt{3}) = 54.7^\circ$ , then the MD will have a [110] line direction. For this example, if the Burgers vector  $b = \frac{1}{2}[0-11]$  with  $b = \frac{1}{2}a/\sqrt{2}$ , the MD is a mixed  $60^\circ$  dislocation. Such mixed misfit dislocations with their lines laying at (001) film/substrate interface are typical for

heteroepitaxy of semiconductors with f.c.c. crystal lattice. All possible slip system with MD and TD line vectors and the burger vectors are listed in Table 2.2. The dislocation burger vectors can be decomposed into edge  $b_{\text{edge}}$  and screw  $b_{\text{screw}}$  components as illustrated in Fig. 2.10(c).

### References:

- [1] M. C. Tseng, R. H. Horng, D. S. Wu, and M. D. Yang, "Effect of crystalline quality on photovoltaic performance for  $\text{In}_{0.17}\text{Ga}_{0.83}\text{As}$  solar cell using X-Ray reciprocal space mapping," *IEEE Journal of Quantum Electronics*, Vol. 47, No. 11, pp. 1434-1440 (2011).
- [2] M. Song, Z. Wu, Y. Fang, R. Xiang, Y. Sun, H. Wang, C. Yu, H. Xiong, J. Dai, and C. Chen, "Improved photovoltaic performance of InGaN single junction solar cells by using *n-on-p* type device structure," *Journal of Optoelectronics and Advanced Materials*, Vol. 12, No. 7, pp. 1452-1456 (2010).
- [3] J. W. Matthews, "Defects associated with the accommodation of misfit between crystals," *J. Vac. Sci. Technol.*, Vol. 12, No. 1, pp. 126-132 (1975).
- [4] J. W. Matthews, and A. E. Blakeslee, "Defects in epitaxial multilayer: 1. Misfit dislocation," *Journal of Crystal Growth* 27, pp. 118-125 (1974).
- [5] F. C. Frank, and J. H. van der Merwe, "One-dimensional dislocations. I. Static theory," *Proc. R. Soc. London, Ser. A, Mathematical and Physical Science*, Vol. 198, No.1053, pp. 205-216 (1949).
- [6] F. C. Frank, and J. H. van der Merwe, "One-dimensional dislocations. II. Misfitting monolayers and oriented overgrowth," *Proc. R. Soc. London, Ser. A, Mathematical and Physical Science*, Vol. 198, No.1053, pp. 216-225 (1949).
- [7] J. H. van der Merwe, "Crystal interfaces. Part I. Semi-infinite crystals," *Journal of Applied Physics*, Vol. 34, Issue 1, pp. 117-122 (1963).
- [8] J. H. van der Merwe, "Crystal interfaces. Part II. Finite overgrowths," *Journal of Applied Physics*, Vol. 34, Issue 1, pp. 123-127 (1963).
- [9] R. People, and J.C. Bean, "Calculation of critical layer thickness versus lattice mismatch for  $\text{Ge}_x\text{Si}_{1-x}/\text{Si}$  strained-layer heterostructures," *Applied Physics Letter*, Vol. 47, Issue 3, pp. 322-324 (1985).
- [10] S. M. Hu, "Misfit dislocations and critical thickness of heteroepitaxy," *Journal of Applied Physics*, Vol. 69, Issue 11, pp. 7901-7903 (1991).



- [11] B. W. Dodson, and J. Y. Tsao, "Relaxation of strained-layer semiconductor structures via plastic-flow," *Applied Physics Letter*, Vol. 51, Issue 17, pp. 1325-1327 (1987).
- [12] L. B. Freund, and R. Hull, "On the Dodson-Tsao excess stress for glide of a threading dislocation in a strained epitaxial layer," *Applied Physics Letter*, Vol. 71, Issue 4, pp. 2054-2056 (1992).
- [13] A. Fischer, and H. Richter, "On plastic flow and work hardening in strained layer heterostructures," *Applied Physics Letter*, Vol. 64, Issue 10, pp. 1218-1220 (1994).
- [14] A. Fischer, "Stability constraints in SiGe epitaxy" In J. D. Cressler, editor, *Silicon Heterostructures Handbook – Materials, Fabrication, Devices, Circuits, and Applications of SiGe and Si Strained-Layer Epitaxy*, chapter 2.7, pp. 127-143. CRC Press, Taylor & Francis Group, Boca Raton (2006).
- [15] D. Holec, "Critical thickness calculations for  $\text{In}_x\text{Ga}_{1-x}\text{N}/\text{GaN}$  systems," CPGS thesis, University of Cambridge/Selwyn College (2006).
- [16] J. R. Willis, S. C. Jain, and R. Bullough, "The energy of an array of dislocations implications for strain relaxation in semiconductor heterostructures," *Phil. Mag. A*, Vol. 62, Issue 1, pp. 115-129 (1990).
- [17] S. C. Jain, A. H. Harker, and R. A. Cowley, "Misfit strain and misfit dislocations in lattice mismatched epitaxial layers and other systems," *Phil. Mag. A*, Vol. 75, pp. 1461-1515 (1997).
- [18] L. B. Freund, and S. Suresh, "Thin film materials: stress, defect formation, and surface evolution," Cambridge University Press, Cambridge, (2003).
- [19] J. W. Matthews, and A. E. Blakeslee, "Defects in epitaxial multilayers: II. Dislocation pile-ups, threading dislocations, slip lines and cracks," *Journal of Crystal Growth*, Vol. 29, pp. 273-280 (1975).
- [20] J. E. Ayers, "Heteroepitaxy of semiconductors theory, growth, and characterization," © 2007 by Taylor & Francis Group, LLC, pp. 180-189, ISBN 0-8493-7195-3.
- [21] E. Kasper, "Properties of strained and relaxed Silicon Germanium," London, INSPEC. (1995).
- [22] J. W. Matthews, A. E. Blakeslee, and S. Mader, "Use of misfit strain to remove dislocations from epitaxial thin films," *Thin Solid Films*, Vol. 33, pp. 253-266 (1976).



- [23] R. Hull, and J. C. Bean, "Nucleation of misfit dislocations in strained-layer epitaxy in the  $\text{Ge}_x\text{Si}_{1-x}/\text{Si}$  system," *Journal of Vacuum Science & Technology A-Vacuum Surfaces and Films*, Vol. 7, Issue 4, pp. 2580-2585 (1989).
- [24] F. K. LeGoues, and B. S. Meyerson, "Mechanism and conditions for anomalous strain relaxation in graded thin-films and superlattices," *Journal of Applied Physics*, Vol. 71, Issue 9, pp. 4230-4243 (1992).
- [25] F.C. Frank, and W. T. Read, "Multiplication processes for slow moving dislocations," *Phys. Rev.*, 79, pp. 722-723 (1950).
- [26] R. Beanland, "Multiplication of misfit dislocations in epitaxial layers," *Journal of Applied Physics*, Vol. 72, p. 4031 (1992).
- [27] E. Kasper, and K. Lyutovich, "Strain adjustment with thin virtual substrates," *Solid-State Electronics*, Vol. 48, Issue 8, pp. 1257-1263 (2004).
- [28] H. Nishino, I. Sugiyama, and Y. Nishijima, "Misfit stress relaxation mechanism in  $\text{CdTe}(100)$  and  $\text{CdTe}/\text{ZnTe}(100)$  on a  $\text{GaAs}(100)$  highly mismatched heteroepitaxial layer," *Journal of Applied Physics*, Vol. 80, Issue 6, pp. 3238-3243 (1996).
- [29] J. Kaltcki, J. Ratajczak, J. Adamczewska, F. Phillipp, N. Y. Jin-Phillipp, K. R. Ski, and M. Bugajski, "Formation of dislocations in  $\text{InGaAs}/\text{GaAs}$  heterostructure," *Phys. Stat. Sol. (a)* Vol. 171, pp. 275-282 (1999).
- [30] A. N. Larsen, "Defects in epitaxial  $\text{SiGe}$ -alloy layers." *Materials Science and Engineering B-Solid State Materials for Advanced Technology*, Vol. 71, pp. 6-13 (2000).
- [31] B. Bertoli, E. N. Suarez, J. E. Ayers, and F. C. Jain, "Misfit dislocation density and strain relaxation in graded semiconductor heterostructures with arbitrary composition profile," *Journal of Applied Physics*, Vol. 106, pp. 073519-7 (2009).
- [32] D. Sidoti, S. Xhurxhi, T. Kujofsa, S. Cheruku, J. Reed, B. Bertoli, P. B. Rago, E. N. Suarez, F. C. Jain, and J. E. Ayers, "Critical layer thickness in exponentially graded heteroepitaxial layers," *Journal of Electronic Materials*, Vol. 39, No. 8, pp. 1140-1145 (2010).
- [33] B. Bertoli, D. Sidoti, S. Xhurxhi, T. Kujofsa, S. Cheruku, J. P. Correa, P. B. Rago, E. N. Suarez, F. C. Jain, and J. E. Ayers, "Equilibrium strain and dislocation density in exponentially graded  $\text{Si}_{1-x}\text{Ge}_x/\text{Si}$  (001)," *Journal of Applied Physics*, Vol. 108, pp. 113525-5 (2010).

- [34] E. A. Fitzgerald, A. Y. Kim, M. T. Currie, T. A. Langdo, G. Taraschi, and M. T. Bulsara, "Dislocation dynamics in relaxed graded composition semiconductor," *Material Science and engineering*, Vol. B67, pp. 53-61 (1999).
- [35] M. Haerberlen, D. Zhu, C. McAleese, M. J. Kappers, and C. J. Humphreys, "Dislocation reduction in MOVPE grown GaN layers on (111) Si using SiNx and AlGaIn layers," *16th International Conference on Microscopy of Semiconducting Materials, Journal of Physics: Conference Series 209*, pp. 012017 (2010).
- [36] P. M. Mooney, J. L. Jordan-Sweet, J. O. Chu, and F. K. LeGoues, "Evolution of strain relaxation in step-graded SiGe/Si structures," *Applied Physics Letter*, Vol. 66, pp. 3642-3644 (1995).
- [37] G. Macpherson, R. Beanland, and J. P. Goodhew, "A novel design method for the suppression of edge dislocation formation in step-graded InGaAs/GaAs layers," *Philosophical Magazine A*, Vol. 73, No 05, pp. 1439-1450 (1996).
- [38] V. Krishnamoorthy, Y. W. Lin, and R. M. Park, "Application of 'critical compositional difference concept to growth of low dislocation density ( $<10^4/\text{cm}^2$ )  $\text{In}_x\text{Ga}_{1-x}\text{As}$  ( $x \leq 0.5$ ) on GaAs," *Journal of Applied Physics*, Vol. 72, pp. 1752-1757 (1992).
- [39] A. E. Romanov, W. Pompe, S. Mathis, G. E. Beltz, and J. S. Speck, "Threading dislocation reduction in strained layers," *Journal of Applied Physics*, Vol. 85, pp. 182-192 (1999).
- [40] S. Srinivasan, L. Geng, F. A. Ponce, Y. Narukawa, and S. Tanaka, "Slip systems and misfit dislocations in InGaN epilayers," *Applied Physics Letters*, Vol. 83, Issue 25, pp. 5187-5189 (2003).
- [41] P. Vennegues, Z. Bougrioua, J. M. Bethoux, M. Azize, and O. Tottereau, "Relaxation mechanisms in metal-organic vapor phase epitaxy grown Al-rich (Al,Ga)N/GaN heterostructures," *Journal of Applied Physics*, Vol. 97, Issue 2, pp. 024912-6 (2005).
- [42] D. Holec, "Multi-scale modeling of III-nitrides: from dislocations to the electronic structure", PhD Dissertation, University of Cambridge, July (2008)
- [43] A. M. Andrews, R. Lesar, M. A. Kerner, J. S. Speck, A. E. Romanov, A. L. Kolesnikova, M. Bobeth, and W. Pompe, "Modeling crosshatch surface morphology in growing mismatched layers. Part II: Periodic boundary conditions and dislocations group," *Journal of Applied Physics*, Vol. 95, Issue 11, pp. 6032-6046 (2004).



## Chapter III

### Methods of Dislocations Reduction

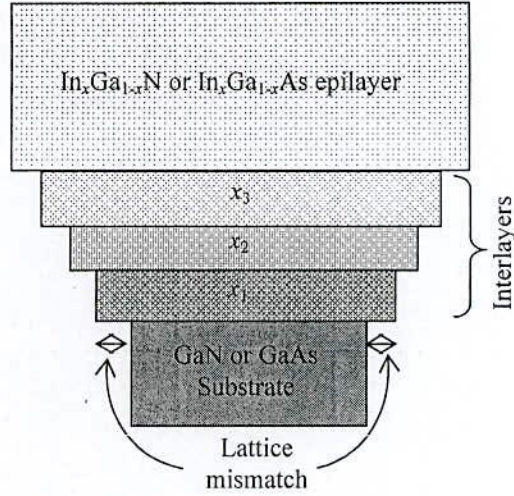
#### 3.1 Introduction

The large lattice and thermal expansion coefficient mismatch between epitaxial layer and substrate of InGaN and InGaAs heteroepitaxy introduce large number of dislocations which is the main challenge of these materials growth [1-2]. In this fact, the step-graded interlayer technique is expected to be a very superior for improving the material quality with reduced dislocation densities. Although available theoretical works have been developed for without grading or linear and nonlinear grading, there is no such work on step-graded interlayers for wuzrite as well as cubic materials [3-5]. A mathematical modeling for dislocation reduction using step-graded interlayer will be very hopeful for the future high performance devices. In the first section of this chapter, a mathematical modeling of misfit dislocation (MD) generation has been developed for wuzrite InGaN and cubic InGaAs heteroepitaxy by using the energy balance model of dislocation. The objective of the modeling is to identify the behavior of different type of MDs in both heteroepitaxy using step-graded interlayers. Another main part of this modeling is the development of threading dislocations (TDs) reaction models and numerical simulations to increase the understanding of the basic physics associated with TD. The ultimate long term goal is to introduce a model with predictive capabilities so much fewer experimental works would be needed.

#### 3.2 Critical Thickness for Step-graded Structure

The critical thickness ( $h_c$ ) of MDs formation and strain relaxation is very essential issue for designing the lattice mismatched heteroepitaxy such as  $\text{In}_x\text{Ga}_{1-x}\text{N}/\text{GaN}$  or  $\text{In}_x\text{Ga}_{1-x}\text{As}/\text{GaAs}$ . Different expressions of critical thickness have been depicted from the ideas of some well developed models in sections 2.4. All of these models predicted an inverse dependence of  $h_c$  on misfit strain of epitaxial layer with respect to substrate. In case of step-graded structure of these heteroepitaxy as shown schematically in Fig. 3.1,  $In$  composition ( $x_1, x_2, x_3$ ) increase step wise with thickness. The variation of in plane strain in multilayer is completely different to that of the





**Figure 3.1:** Structure of the heteroepitaxy having step-graded interlayers with different  $In$  composition where  $x_1 < x_2 < x_n$ .

single layer case. It has been shown that the in plane strain in multilayer decreases with thickness [6]. Consequently, in step-graded structure multiple interfaces between the interlayers and layer-substrate introduce multiple critical thicknesses. These thicknesses are comparatively larger than that of the single without graded layer for all possible slip systems. The expression for critical layer thicknesses, for each step increase of  $In$  at each  $InGaN$  or  $InGaAs$  interlayer and final epilayer can be written using the MB model as [1]

$$h_{ci} = \frac{b_i(1 - \nu_i \cos^2 \theta)}{8\pi(1 + \nu_i)\epsilon_{mi}|\sin\theta \sin\phi} \ln\left(\frac{h_{ci}}{r_{0i}}\right) \quad (3.1)$$

$$\epsilon_{mi} = c + \frac{y_i - y_b}{R} \quad (3.2)$$

The subscript  $i$  used in Eq. (3.1) and (3.2) for indicating the step number of epitaxy. The other parameters have been defined in section 2.4.1 and used their appropriate values at different slips for these materials given in Appendix A. The in plane lattice misfit strain for  $i^{\text{th}}$  layer can be calculated by Eq. (3.2) which has been developed for multilayer structure and the expressions of  $c$ ,  $y_b$  and  $R$  have been published elsewhere [6].

### 3.3 MDs with Step-graded Interlayers

#### 3.3.1 Wuzrite InGaN Heteroepitaxy

According to the energy balance model discussed in section 2.4.3, the material with hexagonal symmetry, such as in InGaN, the only non-zero component of biaxial misfit stress tensor takes the form [7]

$$\sigma_{xx} = \sigma_{yy} = \left( c_{11} + c_{12} - \frac{2c_{13}^2}{c_{33}} \right) \epsilon \quad (3.3)$$

Where  $c_{ij}$  are elastic constant and therefore the elastic energy density will become

$$w = \frac{1}{2} \sum_{i,j} \sigma_{ij} \epsilon_{ij} = \left( c_{11} + c_{12} - \frac{2c_{13}^2}{c_{33}} \right) \epsilon^2 \quad (3.4)$$

Then the energy per unit area of the interface will be

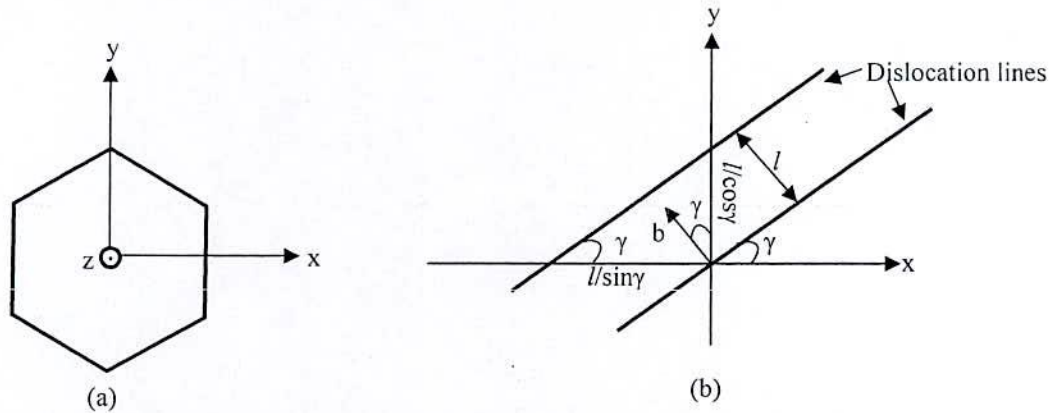
$$W = \left( c_{11} + c_{12} - \frac{2c_{13}^2}{c_{33}} \right) \epsilon^2 h \quad (3.5)$$

In the above equation,  $h$  is the thickness of the epitaxial layer grown on the GaN substrate. Fig. 3.2(a) shows the three coordinate representation of hexagonal cell where the dislocation line lies along the  $y$ -axis and  $z$ -axis is perpendicular to the  $c$ -plane. In order to calculate the partially relaxed misfit strain let us consider an array of MDs be inclined by an angle  $\gamma$  from the  $x$ -axis as shown in Fig. 3.2(b). The  $c$ -plane edge component burger vector,  $b_c = b \cos \phi \sin \theta$ . Let  $l$  is the distance between two neighbor dislocations. In such a system the average strain produced for a layer with thickness  $h$  are

$$\epsilon_{xx}(\gamma) = \frac{b_c \sin \gamma}{l / \sin \gamma} = \frac{b_c}{l} \sin^2 \gamma \quad (3.6)$$

$$\epsilon_{yy}(\gamma) = \frac{b_c \cos \gamma}{l / \cos \gamma} = \frac{b_c}{l} \cos^2 \gamma \quad (3.7)$$

The  $\langle 11\bar{2}3 \rangle(11\bar{2}2)$  slip system has been identified as the active one thus the three arrays of misfit dislocations are simultaneously rotated by  $60^\circ$ . The total average strain as a result of these arrays are



**Figure 3.2:** (a) The three coordinate system for dislocation in wuzrite structure where the z-axis is perpendicular to the c-plane and the dislocation line lies along the y-axis and (b) geometrical representation of equally distributed dislocation array

$$\varepsilon_{xx}^y = \varepsilon_{xx}(\gamma) + \varepsilon_{xx}(\gamma + \pi/3) + \varepsilon_{xx}(\gamma + 2\pi/3) = \frac{3b_c}{2l} \quad (3.8)$$

$$\varepsilon_{yy}^y = \varepsilon_{yy}(\gamma) + \varepsilon_{yy}(\gamma + \pi/3) + \varepsilon_{yy}(\gamma + 2\pi/3) = \frac{3b_c}{2l} \quad (3.9)$$

Now the strain in the epitaxial layer is partially relaxed by the MDs after reaching the critical thickness. Therefore the residual strain after a thickness of  $h > h_c$  is

$$|\varepsilon_i| = \left| \varepsilon_{mi} - \frac{3b_{ci}}{2l_i} \right| = \left| \varepsilon_{mi} - \frac{3}{2} b_{ci} \rho_{MDi} \right| \quad (3.10)$$

Therefore the strain energy per unit area of the interface becomes

$$\frac{dW_i}{dA} = \left( c_{11} + c_{12} - \frac{2c_{13}^2}{c_{33}} \right) \left( \left| \varepsilon_{mi} - \frac{3}{2} b_{ci} \rho_{MDi} \right| \right)^2 h_i \quad (3.11)$$



Where,  $i = 1, 2, 3 \dots$  for residual strain of the first, second, third interlayer respectively and so on. The energy per unit length of a dislocation lying in the layer-substrate or interlayer-interlayer interface of a material with hexagonal symmetry has been derived as [8, 9]

$$\frac{dE_{d(i)}}{dl} = b_{ci} \left( c_{11} + c_{12} - \frac{2c_{13}^2}{c_{33}} \right) \epsilon_{mi} h_{ci} \left[ \ln \left( \frac{h_i}{r_{0i}} \right) / \ln \left( \frac{h_{ci}}{r_{0i}} \right) \right] \quad (3.12)$$

The energy per unit interface area of an array of evenly distributed dislocations with spacing,  $l$  is then  $(1/l)(dE_{d(i)}/dl)$ . As all three arrays of non-interacting MDs are assumed to be independent, the total energy per unit area may be expressed as

$$\frac{dE_i}{dA} = \frac{3}{1} \frac{dE_{d(i)}}{dl} = \frac{3}{1} b_{ci} \left( c_{11} + c_{12} - \frac{2c_{13}^2}{c_{33}} \right) \epsilon_{mi} h_{ci} \left[ \ln \left( \frac{h_i}{r_{0i}} \right) / \ln \left( \frac{h_{ci}}{r_{0i}} \right) \right] h_i \quad (3.13)$$

The total energy stored by the array of misfit dislocation in the  $i^{\text{th}}$  layer with partially relaxed misfit strain

$$E_{ti} = \left( c_{11} + c_{12} - \frac{2c_{13}^2}{c_{33}} \right) \left( |\epsilon_{mi}| - \left| \frac{3}{2} b_{ci} \rho_{MDi} \right| \right)^2 + \frac{3}{1} b_{ci} \left( c_{11} + c_{12} - \frac{2c_{13}^2}{c_{33}} \right) \epsilon_{mi} h_{ci} \left[ \ln \left( \frac{h_i}{r_{0i}} \right) / \ln \left( \frac{h_{ci}}{r_{0i}} \right) \right] h_i \quad (3.14)$$

It is assumed that the dislocation spacing  $l$  is such that it minimizes the total energy  $E_{ti}$  within the interlayer. So the misfit dislocation density within the  $i^{\text{th}}$  interlayer is found from  $dE_{ti}/dl=0$  as

$$\rho_{MDi} = \frac{1}{l_i} = \frac{2|\epsilon_{mi}|}{3b_i \sin \theta \cos \varphi} \left( 1 - \frac{h_{ci} \ln(h_i/r_{0i})}{h_i \ln(h_{ci}/r_{0i})} \right) \quad \left. \begin{array}{l} \text{for } h_i > h_{ci} \\ \\ \text{for } h_i \leq h_{ci} \end{array} \right\} \quad (3.15)$$

$$= 0$$

The layer grown upon the partially relaxed interlayer of thickness  $h_i$ , will experience a misfit strain,  $\epsilon_{m(i+1)}$  reduced by the residual strain  $\epsilon_i$  of the previous layer from Eq. (3.10). Therefore  $\epsilon_{m(i+1)}$  becomes

$$|\epsilon_{m(i+1)}| = \left| \frac{a_{l(i)} - a_{l(i+1)}}{a_{l(i)}} \right| - |\epsilon_i| \quad (3.16)$$

The misfit dislocation density for the next  $(i+1)^{\text{th}}$  layer,  $\rho_{MD(i+1)}$  will be updated using the Eq. (3.15) and (3.16) and corresponding residual strain  $\varepsilon_{(i+1)}$  from Eq. (3.10). The subsequent results takes the form as

$$\rho_{MD(i+1)} = \frac{2|\varepsilon_{m(i+1)}|}{3b_{(i+1)} \sin \theta \cos \varphi} \left( 1 - \frac{h_{c(i+1)} \ln(h_{(i+1)}/r_{0(i+1)})}{h_{(i+1)} \ln(h_{c(i+1)}/r_{0(i+1)})} \right) \quad \left. \begin{array}{l} \text{for } h_i > h_{ci} \\ \text{for } h_i \leq h_{ci} \end{array} \right\} \quad (3.17)$$

$$= 0$$

$$|\varepsilon_{i+1}| = \left| |\varepsilon_{m(i+1)}| - \left| \frac{3}{2} b_{c(i+1)} \rho_{MD(i+1)} \right| \right| \quad (3.18)$$

The parameters used for calculating the edge, screw and mixed MDs in different favored slip system of InGaN have been mentioned in Appendix A.

### 3.3.2 Cubic InGaAs Heteroepitaxy

The misfit dislocations are generally formed on  $\{111\}$  planes in  $\text{In}_x\text{Ga}_{1-x}\text{As}/\text{GaAs}$  heteroepitaxy [5, 9]. The crystallography for dislocation assisted strain relaxation in the InGaAs film growth on (001) oriented substrates has been illustrated in Fig. 2.10. The relaxation occurs by MD formation on the inclined glide planes. In order to find MD density the misfit strain energy of the film and energy released by misfit dislocations in cubic heteroepitaxy have been evaluated [1, 10-13]. The expressions proposed by Hu are used to calculate MD generation for each interlayer.

Assume the misfit dislocation generated after the critical thickness have burgers vector that tilts from the dislocation line by an angle  $\theta$ , and a glide plane that tilts from the film plane by an angle  $\varphi$ . The energy stored by the dislocation due to the misfit strain of the  $i^{\text{th}}$  interlayer can be written as

$$E_{di} = \frac{Gb_i^2}{4\pi} \left[ \frac{\sin^2 \theta}{1-\nu_i} + \cos^2 \theta \right] \left( \ln \frac{h_i}{r_{0i}} - 1 \right) \quad (3.19)$$

Where the first term in the bracket is due to the edge component of the dislocation and the second term is for the screw component. The core radius of the dislocation is  $r_0$ , which taken approximately to equal  $b$ . The in-plane stress from the misfit bringing a misfit dislocation from the surface to the epitaxial interface causes a net displacement in the film by a distance,  $(\delta u) =$



$b \sin \theta \cos \varphi$ . This displacement is uniform in the direction perpendicular to the vertical film cross section containing the dislocation line. The strain energy dissipated by this displacement per unit length of the MD introduced by

$$E_{si} = \frac{2G(1+\nu_i)}{1-\nu_i} \varepsilon_{mi} h_i b_i \sin \theta \cos \varphi \quad (3.20)$$

Where the subscript  $i$  used for indicating the energy values at different interlayers. The occurrence of the first misfit dislocation becomes feasible when this energy exceeds the dislocation energy given in Eq. (3.19) and the total energy stored by the system will be lowest. Assume these misfit dislocations have a density  $\rho_i$  within the  $i^{\text{th}}$  interlayer. The in-plane strain, after the first dislocation appears, starts to decrease as more MDs are introduced, and can be expressed as a function of dislocation density:

$$\varepsilon_i = \varepsilon_{mi} - \rho_i b_i \sin \theta \cos \varphi \quad (3.21)$$

The density of MDs as a function of film thickness is obtained by minimizing, with respect to  $\rho_i$  within the interlayer. Therefore we have

$$\left. \begin{aligned} \rho_i &= \frac{\varepsilon_{mi}}{b_i \sin \theta \cos \varphi} \left( 1 - \frac{h_{ci}}{h_i} \right) && \text{for } h_i > h_{ci} \\ &= 0 && \text{for } h_i \leq h_{ci} \end{aligned} \right\} \quad (3.22)$$

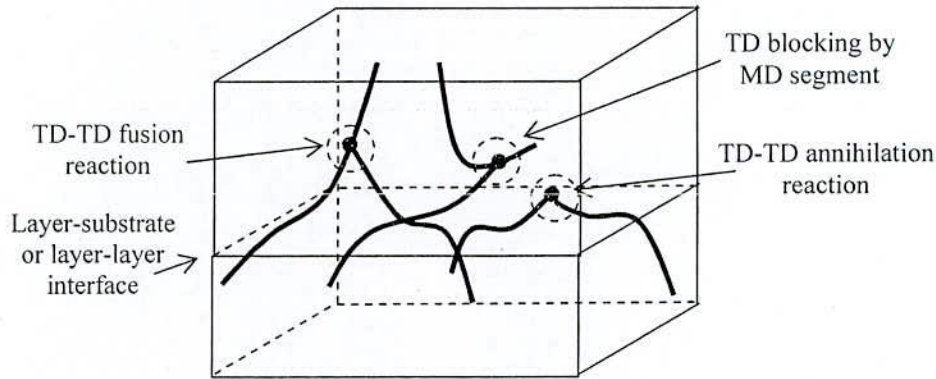
The process for updating the equations for MDs density and misfit strain with increasing the interlayer are assumed to be similar of InGaN heteroepitaxy as mentioned in Eq. (3.17) and (3.18). The layer grown upon the partially relaxed layer of thickness  $h_i$ , will experience a misfit strain less by the residual strain  $\varepsilon_i$  of the previous layer as expressed in Eq. (3.21).

### 3.4 TDs with Step-graded Interlayers

As we have mentioned above, in the growth of lattice-mismatched heteroepitaxy, TDs are concomitantly generated with MDs. These TDs are non-equilibrium defects that always raise the internal energy of the film/substrate system [14]. Thus, there is a natural driving force to reduce the internal energy and TD density, subsequently. This reduction may occur due to reactions between pairs of inclined TDs and blocking by interaction between gliding TD with a MD line



on its gliding plane as shown schematically in Fig. 3.3 [14-15]. For reduction of the total TD density, fusion and annihilation reactions are considered as primary reason. A fusion reaction happens when two TD ( $b_1$  and  $b_2$ ) lines becomes one TD with new burger vector,  $b_3=b_1+b_2$ . Annihilation reaction happens when two TD lines with equal and opposite burger vectors ( $b_1=-$

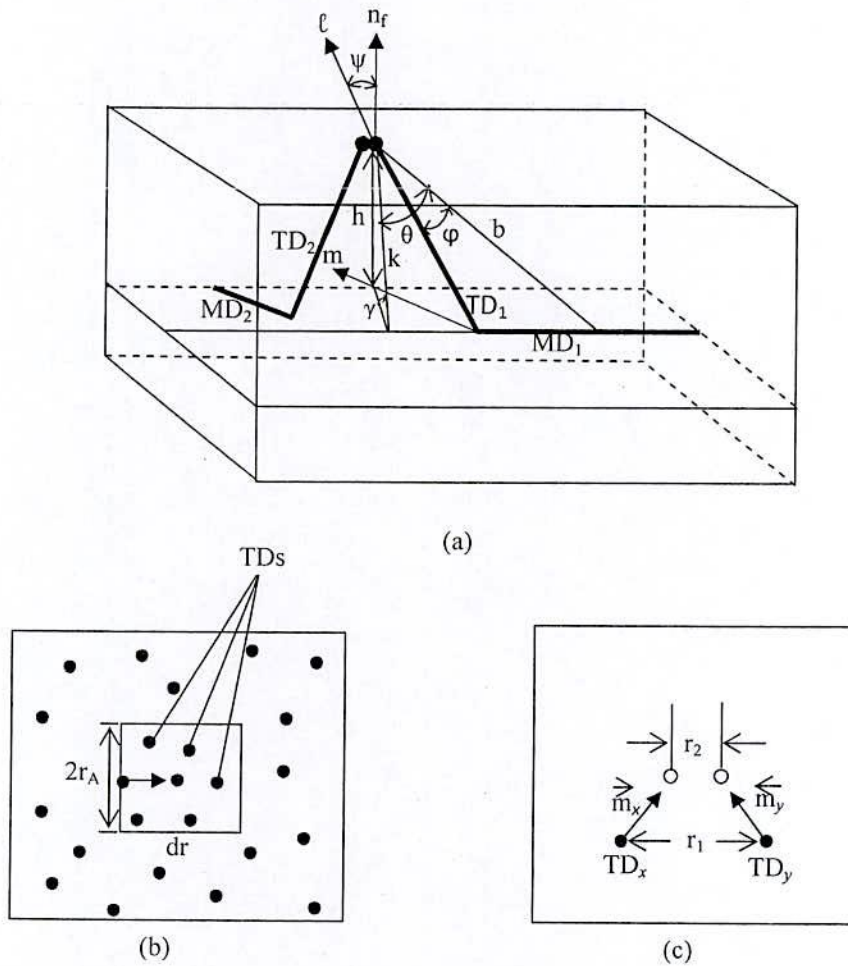


**Figure 3.3:** Threading dislocation reduction mechanism in step-graded heteroepitaxy

$b_2$ ) undergo the reaction  $b_1+b_2=0$ , removing the dislocations entirely. Another type of reaction may take place with producing two new TDs with different burger vectors from two TDs and known as scattering reaction,  $b_1+b_2=b_3+b_4$ . We have neglected the effect of scattering reactions because of no reduction of TDs are made with it. However all of these reactions can take place when the distance between interacting dislocations becomes smaller than the characteristic cross-section of a specific reaction: annihilation radius,  $r_A$  for annihilation and fusion radius,  $r_F$  for fusion reactions [15-16]. After two TDs or a TD and a MD have fallen within the interaction distance, they glide or climb together under the action of internal forces. So there must be an initial relative motion for TDs to come within an interaction distance and hence their inclinations with respect to the film normal are responsible to increase the probability of reaction. This can be enhanced by step change of mismatch strain with increasing film thickness. In order to derive the governing equation for TDs reduction at each interlayer of the step-graded structure, only annihilation and fusion reactions are considered [17]. The geometry of two TDs connected with MD segments and their relative motion with film thickness in a particular interlayer is shown in Fig. 3.4(a). Assuming that the points of TD intersections with the film surface may experience relative motion with increasing film thickness, each TD will sweep [see Fig. 3.6(b)] an

interaction area  $dS = 2r_A dr$ , where  $dr$  is the differential value of the TDs relative motion. Each TD will encounter  $dN = \rho \delta S$  other TDs where  $\rho$  is the density of TDs. Therefore, the change of TD density due to annihilation reactions will be

$$d\rho = -\rho dN = -2r_A \rho^2 dr = -2r_A \tan \psi \rho^2 \Delta h \quad (3.23)$$



**Figure 3.4:** Threading dislocation motion in growing film (a) dislocation geometry and their relative motion, (b) the interaction area swept by moving TD in plain view and (c) perspective view

which could be simplified as

$$d\rho = -K\rho^2 dh \quad (3.24)$$



Where,  $K=r_A M$ , is average reaction kinetic coefficient between all pair of TDs and  $M$  represents the average value of the net relative motion of TDs with changing film thickness. The TDs that will interact must have net relative motion, which can be characterized by the factor  $M = |\tan \psi_x m_x - \tan \psi_y m_y|$  [17]. Where  $\mathbf{m}$  is a unit vector that gives the lateral motion of TDs of  $x$  and  $y$  on the film surface with changing film thickness, shown in Fig. 3.4(c). In order to make analogy to simple chemical reaction kinetics, consider TDs of the  $x^{\text{th}}$  and  $y^{\text{th}}$  types with corresponding densities  $\rho_x$  and  $\rho_y$ . We suppose that due to the effective motion of inclined TDs at each interlayer, the reactions occur with uniform probability at any point on the surface. Then for diminishing dislocation densities  $\rho_x$  or  $\rho_y$  as a result of the direct reaction of TDs of the  $x^{\text{th}}$  and  $y^{\text{th}}$  types Eq. (3.24) can be written as

$$\frac{d\rho_{x(y)}}{dt} = -V_{xy} \rho_x \rho_y \quad (3.25)$$

The reaction velocity can be expressed with relative dislocation motion and interaction cross-section in the following form:

$$V_{xy} = 2r_l |V_x - V_y|, \quad I = A, F, \text{ or } S \text{ indicate annihilation, fusion and scattering reaction}$$

The velocity can be written for  $y$  type TD as

$$V_y = \frac{dr}{dt} = \dot{h} \tan(\psi) m_y \quad (3.26)$$

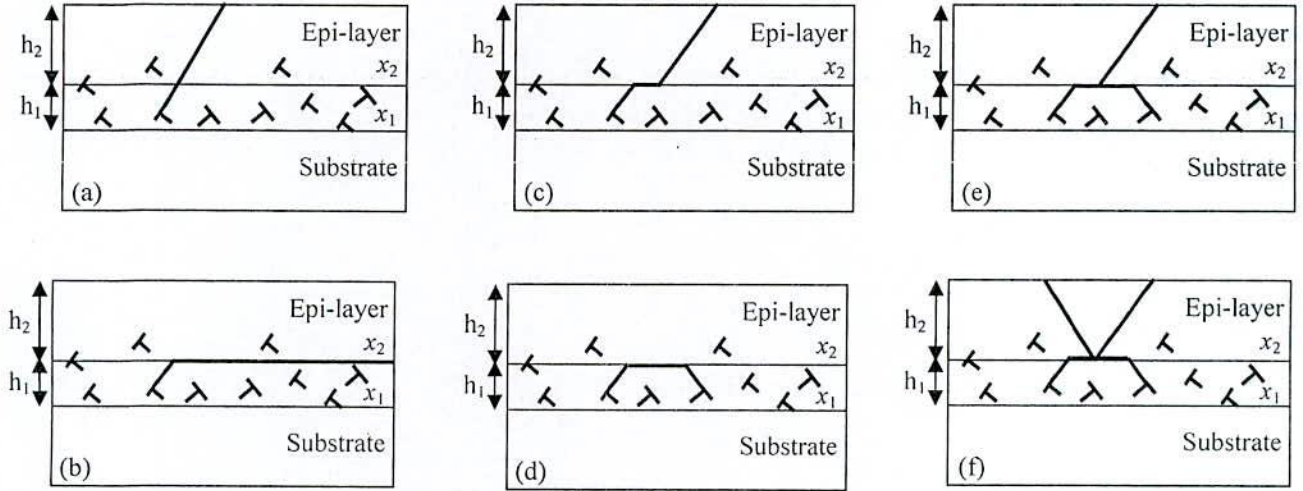
Therefore Eq. (3.25) becomes

$$\frac{d\rho_{x(y)}}{dt} = -K_{xy} \rho_x \rho_y \quad (3.27)$$

The reaction kinetic coefficient  $K_{xy}$  in Eq. (3.27) presents the extent to participate in reaction of TDs type  $x$  and  $y$  which depends on the average differential motion with increasing interlayer thickness. To understand the effects internal and external stress, layer thickness the average differential motion  $dr$  for a particular interlayer has been analyzed from another report on intentionally introduced strained layers [14, 18]. The effects of mismatch strain on differential motion with respect to layer thickness have been considered in step-graded interlayer for calculating the reaction kinetic coefficients between each pair of TDs. Though the mismatches strain in without graded layer is higher, the lateral motion of TDs with respect to interlayer



thickness is larger for step-graded layer due to comparatively lower stepped increase of thickness. Therefore, a multiple inclination of TDs at each interface enables them to increase the probability of interaction in step-graded structure. All the possible reactions between two TD in a step-graded interlayer are shown schematically in Fig. 3.5 [19]. They should be summarized mathematically for developing the governing equation of TD density with increasing film



**Figure 3.5:** Probable interactions between threading dislocations due to step-graded interlayers. Dislocations (a) may not or (b) may bend without being removed from the top layer. (c) A mixed dislocation may bend over and glide all the way to the edge, resulting in the elimination threading dislocation in the top layer, (d) Dislocation may participate in an annihilation reaction, and eliminate from the top layer, (e) two dislocation may coalesce to form a third dislocation. This process removes one dislocation from the upper layer and (f) scattering reaction between two dislocations to form two new dislocations

thickness. This needs the values of  $K_{xy}$  between all pair of TDs for each interlayer which have been calculated considering the stress at each interlayer [14, 18]. A reaction table can be developed for the whole step-graded heteroepitaxy which contains all possible reaction according to the possible burger vector arranged in column and row. From the reaction table developed for a specific material a couple of differential equations can be written [14, 18, 20]. They are summarized in a generalized form as

$$\frac{d\rho_x}{dh} = -\sum_y K_{xy}\rho_x\rho_y + \sum_l \sum_n K_{ln}\rho_l\rho_n - \sum_m \rho_x\rho_m \quad (3.28)$$

Here  $\rho_x$  represents the density of specific TD family, with number  $x$  designated in reaction table. The first summation is for the annihilation and fusion reactions which reduce the TDs density of  $x^{\text{th}}$  family one per reaction. The second summation is for fusion reactions between the other families ' $l$ ' and ' $m$ ' that produce the dislocation in the  $x^{\text{th}}$  family and the last term is for TD of  $x^{\text{th}}$  family reduction by MD blocking on its gliding path.

### 3.4.1 Reaction Model for InGaN Heteroepitaxy

The possible annihilation, fusion reactions between each pair of TDs in each step-graded InGaN interlayer, with characteristic radii  $r_A$  and  $r_F$  have been considered. There are 20 unique families of dislocations in InGaN according to their burger vector and line directions [20]. Among them, two for screw dislocation ( $+c$  and  $-c$ ), six different edge dislocations ( $+a_1, -a_1, +a_2, -a_2, +a_3$  and  $-a_3$ ) and twelve for different mixed character dislocations ( $+a_1+c, +a_1-c, -a_1+c, -a_1-c, +a_2+c, +a_2-c, -a_2+c, -a_2-c, +a_3+c, +a_3-c, -a_3+c, \text{ and } -a_3-c$ ). According to the reaction Table 3.1 developed for wuzrite InGaN, TDs from family 1 can only have annihilation and fusion reactions with TDs from family 9, 10, 11, 12, 15, and 16 that reduce the TDs. The first term of Eq. (3.28) can be expressed for the  $i^{\text{th}}$  InGaN interlayer as

$$\left(\frac{d\rho_1}{dh}\right)_{i^{\text{th}}\text{layer}} = \left(-K_{1,9}\rho_1\rho_9 - K_{1,10}\rho_1\rho_{10} - K_{1,11}\rho_1\rho_{11} - K_{1,12}\rho_1\rho_{12} - K_{1,15}\rho_1\rho_{15} - K_{1,16}\rho_1\rho_{16}\right)_{i^{\text{th}}\text{layer}} \quad (3.29)$$

On the other hand it follows from the analysis of the Table 3.1 that, TDs from family 1 may be generated within the interlayer only as the product of fusion reactions between TDs from the following pairs of families 7-8, 7-14, 7-18, 7-20, 8-13, 8-17, 8-19, 13-18 and 14-17. Therefore, for production of TDs from family 1 as a result of fusion, one can write

$$\left(\frac{d\rho_1}{dh}\right)_{i^{\text{th}}\text{layer}} = \left(+2K_{7,8}\rho_7\rho_8 + K_{7,14}\rho_7\rho_{14} + K_{7,18}\rho_7\rho_{18} + K_{7,20}\rho_7\rho_{20} + K_{8,13}\rho_8\rho_{13} + K_{8,17}\rho_8\rho_{17} + K_{8,19}\rho_8\rho_{19} + K_{13,18}\rho_{13}\rho_{18} + K_{14,17}\rho_{14}\rho_{17}\right)_{i^{\text{th}}\text{layer}} \quad (3.30)$$

Finally, the TD of family 1 could be blocked by MDs in InGaN on its gliding path. Therefore the TD reduction for type 1 within the interlayer due to this effect can be written as

$$\left(\frac{d\rho_1}{dh}\right)_{i^{\text{th}}\text{layer}} = \left(-\rho_1\rho_m\right)_{i^{\text{th}}\text{layer}} \quad (3.31)$$

Combining the decrease of TDs as a result of annihilation, fusion between TD and blocking by



MD we can arrive at the governing differential equation for the density of TD family 1 in the  $i^{\text{th}}$  interlayer of step-grade InGaN, in the absence of scattering reactions, as

$$\left(\frac{d\rho_1}{dh}\right)_{i^{\text{th}}\text{layer}} = \left( \begin{array}{l} -\rho_1(K_{1,9}\rho_9 + K_{1,10}\rho_{10} + K_{1,11}\rho_{11} + K_{1,12}\rho_{12} + K_{1,15}\rho_{15} + K_{1,16}\rho_{16}) \\ + 2K_{7,8}\rho_7\rho_8 + K_{7,14}\rho_7\rho_{14} + K_{7,18}\rho_7\rho_{18} + K_{7,20}\rho_7\rho_{20} + K_{8,13}\rho_8\rho_{13} \\ + K_{8,17}\rho_8\rho_{17} + K_{8,19}\rho_8\rho_{19} + K_{13,18}\rho_{13}\rho_{18} + K_{14,17}\rho_{14}\rho_{17} - \rho_1\rho_m \end{array} \right)_{i^{\text{th}}\text{layer}} \quad (3.32)$$

Similarly, reaction equations for six different edge TDs, twelve mixed and two screw character TDs *i. e.* a total of twenty equations could be developed for each interlayer of step-graded InGaN heteroepitaxy. These are summarized in Eq. (3.32) to (3.51). Each of the 20 possible TD families is listed in Table 3.1 with its designated number. Several of the reactions produce compound burger vector dislocations. Reactions that are not possible due to  $b^2$ -criterion [16] or for geometric reasons are indicated with a “-” while reactions that are possible are indicated with their designated number. Reactions that produce two dislocations are denoted with two numbers corresponding to their products.

$$\left(\frac{d\rho_2}{dh}\right)_{i^{\text{th}}\text{layer}} = \left( \begin{array}{l} -\rho_2(K_{2,7}\rho_7 + K_{2,8}\rho_8 + K_{2,13}\rho_{13} + K_{2,14}\rho_{14} + K_{2,17}\rho_{17} + K_{2,18}\rho_{18}) \\ + 2K_{9,10}\rho_9\rho_{10} + K_{9,12}\rho_9\rho_{12} + K_{9,16}\rho_9\rho_{16} + K_{9,20}\rho_9\rho_{20} + K_{10,11}\rho_{10}\rho_{11} \\ + K_{10,15}\rho_{10}\rho_{15} + K_{10,19}\rho_{10}\rho_{19} + K_{11,16}\rho_{11}\rho_{16} + K_{12,15}\rho_{12}\rho_{15} - \rho_2\rho_m \end{array} \right)_{i^{\text{th}}\text{layer}} \quad (3.33)$$

$$\left(\frac{d\rho_3}{dh}\right)_{i^{\text{th}}\text{layer}} = \left( \begin{array}{l} -\rho_3(K_{3,7}\rho_7 + K_{3,8}\rho_8 + K_{3,13}\rho_{13} + K_{3,14}\rho_{14} + K_{3,15}\rho_{15} + K_{3,16}\rho_{16}) \\ + K_{9,12}\rho_9\rho_{12} + K_{9,18}\rho_9\rho_{18} + K_{10,11}\rho_{10}\rho_{11} + K_{10,17}\rho_{10}\rho_{17} + 2K_{11,12}\rho_{11}\rho_{12} \\ + K_{11,18}\rho_{11}\rho_{18} + K_{11,20}\rho_{11}\rho_{20} + K_{12,17}\rho_{12}\rho_{17} + K_{12,19}\rho_{12}\rho_{19} - \rho_3\rho_m \end{array} \right)_{i^{\text{th}}\text{layer}} \quad (3.34)$$

$$\left(\frac{d\rho_4}{dh}\right)_{i^{\text{th}}\text{layer}} = \left( \begin{array}{l} -\rho_4(K_{4,9}\rho_9 + K_{4,10}\rho_{10} + K_{4,11}\rho_{11} + K_{4,12}\rho_{12} + K_{4,17}\rho_{17} + K_{4,18}\rho_{18}) \\ + K_{7,14}\rho_7\rho_{14} + K_{7,16}\rho_7\rho_{16} + K_{8,13}\rho_8\rho_{13} + K_{8,15}\rho_8\rho_{15} + 2K_{13,14}\rho_{13}\rho_{14} \\ + K_{13,16}\rho_{13}\rho_{16} + K_{13,20}\rho_{13}\rho_{20} + K_{14,15}\rho_{14}\rho_{15} + K_{14,19}\rho_{14}\rho_{19} - \rho_4\rho_m \end{array} \right)_{i^{\text{th}}\text{layer}} \quad (3.35)$$

$$\left(\frac{d\rho_5}{dh}\right)_{i^{\text{th}}\text{layer}} = \left( \begin{array}{l} -\rho_5(K_{5,7}\rho_7 + K_{5,8}\rho_8 + K_{5,11}\rho_{11} + K_{5,12}\rho_{12} + K_{5,17}\rho_{17} + K_{5,18}\rho_{18}) \\ + K_{9,14}\rho_9\rho_{14} + K_{9,16}\rho_9\rho_{16} + K_{10,13}\rho_{10}\rho_{13} + K_{10,15}\rho_{10}\rho_{15} + K_{13,16}\rho_{13}\rho_{16} \\ + K_{14,15}\rho_{14}\rho_{15} + 2K_{15,16}\rho_{15}\rho_{16} + K_{15,20}\rho_{15}\rho_{20} + K_{16,19}\rho_{16}\rho_{19} - \rho_5\rho_m \end{array} \right)_{i^{\text{th}}\text{layer}} \quad (3.36)$$

$$\left(\frac{d\rho_6}{dh}\right)_{i^{\text{th}}\text{layer}} = \left( \begin{array}{l} -\rho_6(K_{6,9}\rho_9 + K_{6,10}\rho_{10} + K_{6,13}\rho_{13} + K_{6,14}\rho_{14} + K_{6,15}\rho_{15} + K_{6,16}\rho_{16}) \\ + K_{7,12}\rho_7\rho_{12} + K_{7,18}\rho_7\rho_{18} + K_{8,11}\rho_8\rho_{11} + K_{8,17}\rho_8\rho_{17} + K_{11,18}\rho_{11}\rho_{18} \\ + K_{12,17}\rho_{12}\rho_{17} + 2K_{17,18}\rho_{17}\rho_{18} + K_{17,20}\rho_{17}\rho_{20} + K_{18,19}\rho_{18}\rho_{19} - \rho_6\rho_m \end{array} \right)_{i^{\text{th}}\text{layer}} \quad (3.37)$$

$$\left(\frac{dp_7}{dh}\right)_{i^{th}layer} = \left( \begin{array}{l} -K_{7,10}\rho_7\rho_{10} - \rho_7(K_{2,7}\rho_2 + K_{3,7}\rho_3 + K_{5,7}\rho_5 + K_{7,8}\rho_8 + K_{7,12}\rho_{12} + K_{7,14}\rho_{14}) \\ + K_{7,16}\rho_{16} + K_{7,18}\rho_{18} + K_{7,20}\rho_{20} \end{array} + K_{4,17}\rho_6\rho_{13} + K_{6,13}\rho_6\rho_{13} - \rho_6\rho_m \right)_{i^{th}layer} \quad (3.38)$$

$$\left(\frac{dp_8}{dh}\right)_{i^{th}layer} = \left( \begin{array}{l} -K_{8,9}\rho_8\rho_9 - \rho_8(K_{2,8}\rho_2 + K_{3,8}\rho_3 + K_{5,8}\rho_5 + K_{7,8}\rho_8 + K_{8,11}\rho_{11} + K_{8,13}\rho_{13}) \\ + K_{8,15}\rho_{15} + K_{8,17}\rho_{17} + K_{8,19}\rho_{19} \end{array} + K_{4,18}\rho_4\rho_{18} + K_{6,14}\rho_6\rho_{14} - \rho_8\rho_m \right)_{i^{th}layer} \quad (3.39)$$

$$\left(\frac{dp_9}{dh}\right)_{i^{th}layer} = \left( \begin{array}{l} -K_{8,9}\rho_8\rho_9 - \rho_9(K_{1,9}\rho_1 + K_{4,9}\rho_4 + K_{6,9}\rho_6 + K_{9,10}\rho_{10} + K_{9,12}\rho_{12} + K_{9,14}\rho_{14}) \\ + K_{9,16}\rho_{16} + K_{9,18}\rho_{18} + K_{9,20}\rho_{20} \end{array} + K_{3,15}\rho_3\rho_{15} + K_{5,11}\rho_5\rho_{11} - \rho_9\rho_m \right)_{i^{th}layer} \quad (3.40)$$

$$\left(\frac{dp_{10}}{dh}\right)_{i^{th}layer} = \left( \begin{array}{l} -K_{7,10}\rho_7\rho_{10} - \rho_{10}(K_{1,10}\rho_1 + K_{4,10}\rho_4 + K_{6,10}\rho_6 + K_{9,10}\rho_9 + K_{10,11}\rho_{11} + K_{10,13}\rho_{13}) \\ + K_{10,15}\rho_{15} + K_{10,17}\rho_{17} + K_{10,19}\rho_{19} \end{array} + K_{3,16}\rho_3\rho_{16} + K_{5,12}\rho_5\rho_{12} - \rho_{10}\rho_m \right)_{i^{th}layer} \quad (3.41)$$

$$\left(\frac{dp_{11}}{dh}\right)_{i^{th}layer} = \left( \begin{array}{l} -K_{1,14}\rho_1\rho_{14} - \rho_{11}(K_{1,11}\rho_1 + K_{4,11}\rho_4 + K_{5,11}\rho_5 + K_{8,11}\rho_8 + K_{10,11}\rho_{10} + K_{11,12}\rho_{12}) \\ + K_{1,16}\rho_{16} + K_{1,18}\rho_{18} + K_{1,20}\rho_{20} \end{array} + K_{2,17}\rho_2\rho_{17} + K_{6,9}\rho_6\rho_9 - \rho_{11}\rho_m \right)_{i^{th}layer} \quad (3.42)$$

$$\left(\frac{dp_{12}}{dh}\right)_{i^{th}layer} = \left( \begin{array}{l} -K_{12,13}\rho_{12}\rho_{13} - \rho_{12}(K_{1,12}\rho_1 + K_{4,12}\rho_4 + K_{5,12}\rho_5 + K_{7,12}\rho_7 + K_{9,12}\rho_9 + K_{11,12}\rho_{11}) \\ + K_{12,15}\rho_{15} + K_{12,17}\rho_{17} + K_{12,19}\rho_{19} \end{array} + K_{2,18}\rho_2\rho_{18} + K_{6,10}\rho_6\rho_{10} - \rho_{12}\rho_m \right)_{i^{th}layer} \quad (3.43)$$

$$\left(\frac{dp_{13}}{dh}\right)_{i^{th}layer} = \left( \begin{array}{l} -K_{12,13}\rho_{12}\rho_{13} - \rho_{13}(K_{2,13}\rho_2 + K_{3,13}\rho_3 + K_{6,13}\rho_6 + K_{8,13}\rho_8 + K_{10,13}\rho_{10} + K_{13,14}\rho_{14}) \\ + K_{13,16}\rho_{16} + K_{13,18}\rho_{18} + K_{13,20}\rho_{20} \end{array} + K_{1,15}\rho_1\rho_{15} + K_{5,7}\rho_5\rho_7 - \rho_{13}\rho_m \right)_{i^{th}layer} \quad (3.44)$$

$$\left(\frac{dp_{14}}{dh}\right)_{i^{th}layer} = \left( \begin{array}{l} -K_{1,14}\rho_1\rho_{14} - \rho_{14}(K_{2,14}\rho_2 + K_{3,14}\rho_3 + K_{6,14}\rho_6 + K_{7,14}\rho_7 + K_{9,14}\rho_9 + K_{13,14}\rho_{13}) \\ + K_{14,15}\rho_{15} + K_{14,17}\rho_{17} + K_{14,19}\rho_{19} \end{array} + K_{1,16}\rho_1\rho_{16} + K_{5,8}\rho_5\rho_8 - \rho_{14}\rho_m \right)_{i^{th}layer} \quad (3.45)$$

$$\left(\frac{dp_{15}}{dh}\right)_{i^{th}layer} = \left( \begin{array}{l} -K_{15,18}\rho_{15}\rho_{18} - \rho_{15}(K_{1,15}\rho_1 + K_{3,15}\rho_3 + K_{6,15}\rho_6 + K_{8,15}\rho_8 + K_{10,15}\rho_{10} + K_{12,15}\rho_{12}) \\ + K_{14,15}\rho_{14} + K_{15,16}\rho_{16} + K_{15,20}\rho_{20} \end{array} + K_{4,9}\rho_4\rho_9 + K_{2,13}\rho_2\rho_{13} - \rho_{15}\rho_m \right)_{i^{th}layer} \quad (3.46)$$

$$\left(\frac{dp_{16}}{dh}\right)_{i^{th}layer} = \left( \begin{array}{l} -K_{16,17}\rho_{16}\rho_{17} - \rho_{16}(K_{1,16}\rho_1 + K_{3,16}\rho_3 + K_{6,16}\rho_6 + K_{7,16}\rho_7 + K_{9,16}\rho_9 + K_{11,16}\rho_{11}) \\ + K_{13,16}\rho_{13} + K_{15,16}\rho_{15} + K_{16,19}\rho_{19} \end{array} + K_{4,10}\rho_4\rho_{10} + K_{2,14}\rho_2\rho_{14} - \rho_{16}\rho_m \right)_{i^{th}layer} \quad (3.47)$$

$$\left(\frac{dp_{17}}{dh}\right)_{i^{th}layer} = \left( \begin{array}{l} -K_{16,17}\rho_{16}\rho_{17} - \rho_{17}(K_{2,17}\rho_2 + K_{4,17}\rho_4 + K_{5,17}\rho_5 + K_{8,17}\rho_8 + K_{10,17}\rho_{10} + K_{12,17}\rho_{12}) \\ + K_{14,17}\rho_{14} + K_{17,18}\rho_{18} + K_{17,20}\rho_{20} \end{array} + K_{1,11}\rho_1\rho_{11} + K_{3,7}\rho_3\rho_7 - \rho_{17}\rho_m \right)_{i^{th}layer} \quad (3.48)$$

$$\left(\frac{dp_{18}}{dh}\right)_{i^{th}layer} = \left( \begin{array}{l} -K_{15,18}\rho_{15}\rho_{18} - \rho_{18}(K_{2,18}\rho_2 + K_{4,18}\rho_4 + K_{5,18}\rho_5 + K_{7,18}\rho_7 + K_{9,18}\rho_9 + K_{11,18}\rho_{11}) \\ + K_{13,18}\rho_{13} + K_{17,18}\rho_{17} + K_{18,19}\rho_{18} \end{array} + K_{1,12}\rho_1\rho_{12} + K_{3,8}\rho_3\rho_8 - \rho_{18}\rho_m \right)_{i^{th}layer} \quad (3.49)$$



$$\left(\frac{dp_{19}}{dh}\right)_{i^{\text{th}}\text{layer}} = \left( \begin{array}{l} -\rho_{19}(K_{8,19}\rho_8 + K_{10,19}\rho_{10} + K_{12,19}\rho_{12} + K_{14,19}\rho_{14} + K_{16,19}\rho_{16} + K_{18,19}\rho_{18}) \\ + K_{1,9}\rho_1\rho_9 + K_{2,7}\rho_2\rho_7 + K_{3,13}\rho_3\rho_{13} + K_{4,11}\rho_4\rho_{11} + K_{5,17}\rho_5\rho_{17} \\ + K_{6,15}\rho_6\rho_{15} - \rho_{19}\rho_m \end{array} \right)_{i^{\text{th}}\text{layer}} \quad (3.50)$$

$$\left(\frac{dp_{20}}{dh}\right)_{i^{\text{th}}\text{layer}} = \left( \begin{array}{l} -\rho_{20}(K_{7,20}\rho_7 + K_{9,20}\rho_9 + K_{11,20}\rho_{11} + K_{13,20}\rho_{13} + K_{15,20}\rho_{15} + K_{17,20}\rho_{17}) \\ + K_{1,10}\rho_1\rho_{10} + K_{2,8}\rho_2\rho_8 + K_{3,14}\rho_3\rho_{14} + K_{4,12}\rho_4\rho_{12} + K_{5,18}\rho_5\rho_{18} \\ + K_{6,16}\rho_6\rho_{16} - \rho_{20}\rho_m \end{array} \right)_{i^{\text{th}}\text{layer}} \quad (3.51)$$

**Table 3.1:** Reaction table for threading dislocation in growing InGaN heteroepitaxy

$\rho_x$	1	2	3	4	5	6	7	8	9	10	11	12	13	14	15	16	17	18	19	20	
$\rho_y$	b	a <sub>1</sub>	-a <sub>1</sub>	a <sub>2</sub>	-a <sub>2</sub>	a <sub>3</sub>	-a <sub>3</sub>	a <sub>1</sub> +c	a <sub>1</sub> -c	-a <sub>1</sub> -c	-a <sub>1</sub> -c	a <sub>2</sub> +c	a <sub>2</sub> -c	-a <sub>2</sub> +c	-a <sub>2</sub> -c	a <sub>3</sub> +c	a <sub>3</sub> -c	-a <sub>3</sub> +c	-a <sub>3</sub> -c	c	-c
1	a <sub>1</sub>	-	-	-	-	-	-	-	-	19	20	17	18	-	-	13	14	-	-	-	-
2	-a <sub>1</sub>	-	-	-	-	-	-	19	20	-	-	-	-	15	16	-	-	11	12	-	-
3	a <sub>2</sub>	-	-	-	-	-	-	17	18	-	-	-	-	19	20	9	10	-	-	-	-
4	-a <sub>2</sub>	-	-	-	-	-	-	-	-	15	16	19	20	-	-	-	-	7	8	-	-
5	a <sub>3</sub>	-	-	-	-	-	-	13	14	-	-	9	10	-	-	-	-	19	20	-	-
6	-a <sub>3</sub>	-	-	-	-	-	-	-	-	11	12	-	-	7	8	19	20	-	-	-	-
7	a <sub>1</sub> +c	-	19	17	-	13	-	-	1&1	-	A	-	6	-	1&4	-	4	-	1&6	-	1
8	a <sub>1</sub> -c	-	20	18	-	14	-	1&1	-	A	-	6	-	1&4	-	4	-	1&6	-	1	-
9	-a <sub>1</sub> +c	19	-	-	15	-	11	-	A	-	2&2	-	2&3	-	5	-	2&5	-	3	-	2
10	-a <sub>1</sub> -c	20	-	-	16	-	12	A	-	2&2	-	2&3	-	5	-	2&5	-	3	-	2	-
11	a <sub>2</sub> +c	17	-	-	19	9	-	-	6	-	2&3	-	3&3	-	A	-	2	-	3&6	-	3
12	a <sub>2</sub> -c	18	-	-	20	10	-	6	-	2&3	-	3&3	-	A	-	2	-	3&6	-	3	-
13	-a <sub>2</sub> +c	-	15	19	-	-	7	-	1&4	-	5	-	A	-	4&4	-	4&5	-	1	-	4
14	-a <sub>2</sub> -c	-	16	20	-	-	8	1&4	-	5	-	A	-	4&4	-	4&5	-	1	-	4	-
15	a <sub>3</sub> +c	13	-	9	-	-	19	-	4	-	2&5	-	2	-	4&5	-	5&5	-	A	-	5
16	a <sub>3</sub> -c	14	-	10	-	-	20	4	-	2&5	-	2	-	4&5	-	5&5	-	A	-	5	-
17	-a <sub>3</sub> +c	-	11	-	7	19	-	-	1&6	-	3	-	3&6	-	1	-	A	-	6&6	-	6
18	-a <sub>3</sub> -c	-	12	-	8	20	-	1&6	-	3	-	3&6	-	1	-	A	-	6&6	-	6	-
19	c	-	-	-	-	-	-	-	1	-	2	-	3	-	4	-	5	-	6	-	-
20	-c	-	-	-	-	-	-	-	1	-	2	-	3	-	4	-	5	-	6	-	-

### 3.4.2 Reaction Model for InGaAs Heteroepitaxy

The threading dislocations for InGaAs single layer are divided into two categories as 60° or mixed TDs gliding along the inclined {111} planes and edge TDs with burger vector parallel to the (001) plane. The TDs associated with surface nucleation of dislocation half-loop will form on inclined slip planes with burger vectors that are inclined with respect to film substrate interface are of 60° type [14]. For the (001) growth of f.c.c. semiconductors, this plane corresponds to one of the four inclined faces of the half-octahedron shown in Fig. 2.10(b) and the possible burgers

vector of the dislocations will be one of the following:  $\pm a/2[101]$ ,  $\pm a/2[011]$ ,  $\pm a/2[-101]$ ,  $\pm a/2[0-11]$ . For dislocation half-loop nucleation at the film surface, the burgers vectors of the half-loop, and eventually the pair of TDs and the MD, will be parallel to one of the inclined half-octahedron edges. This gives the set of possible burgers vectors for surface nucleation as  $\pm a/2[101]$ ,  $\pm a/2[011]$ ,  $\pm a/2[-101]$ ,  $\pm a/2[0-11]$ . For TDs associated with island growth generated MDs may have their burgers vectors lying in the film/substrate interface are of edge type. This set of burger vectors will be parallel to one of the edges of the square base of the half-octahedron and will be form the set  $\pm a/2[110]$ ,  $\pm a/2[-110]$ . Although there are 12 unique burgers vectors, a total of 24 burgers vectors/slip plane combinations exist for cubic material system. Thus, in considering the overall reactions between TDs, a  $24 \times 24$  matrix can be constructed to investigate all possible TD-TD interactions and these are listed in Table 3.2. A similar reaction model has been developed for step-graded cubic InGaAs interlayers with different crystal geometry of TDs.

According to Table 3.2 TDs from family 1 in the  $i^{\text{th}}$  interlayer can only have annihilation reactions with TDs from family 4 and fusion reactions with TDs from families 11, 12, 15, 16, 19, 20, 23, and 24. Therefore, only reactions with these families will contribute to the process of diminishing the density of TDs from family 1 in the  $i^{\text{th}}$  interlayer, i.e.

$$\left( \frac{d\rho_1}{dh} \right)_{i^{\text{th}}\text{layer}} = \left( \begin{array}{l} -K_{1,4}\rho_1\rho_4 - K_{1,11}\rho_1\rho_{11} - K_{1,12}\rho_1\rho_{12} - K_{1,15}\rho_1\rho_{15} - K_{1,16}\rho_1\rho_{16} - K_{1,19}\rho_1\rho_{19} \\ -K_{1,20}\rho_1\rho_{20} - K_{1,23}\rho_1\rho_{23} - K_{1,24}\rho_1\rho_{24} \end{array} \right)_{i^{\text{th}}\text{layer}} \quad (3.52)$$

It follows from the analysis of Table 3.2 that TDs of family 1 may be generated only as the product of fusion reactions between TDs from the following pairs of families:  $13\pm 17$ ,  $13\pm 18$ ,  $14\pm 17$ ,  $14\pm 18$ . Therefore, for production of TDs from family 1 as a result of fusion, we can write

$$\left( \frac{d\rho_1}{dh} \right)_{i^{\text{th}}\text{layer}} = \left( +K_{13,17}\rho_{13}\rho_{17} + K_{13,18}\rho_{13}\rho_{18} + K_{14,17}\rho_{14}\rho_{17} + K_{14,18}\rho_{14}\rho_{18} \right)_{i^{\text{th}}\text{layer}} \quad (3.53)$$

In case of cubic semiconductor all possible planes contains misfit dislocation with corresponding density. Therefore all 24 equations carry the term of TD blocking by MD and can be written for TD of family 1 as

$$\left( \frac{d\rho_1}{dh} \right)_{i^{\text{th}}\text{layer}} = \left( -\rho_1\rho_m \right)_{i^{\text{th}}\text{layer}} \quad (3.54)$$



Combining the reduction of TDs as a result of fusion, annihilation reaction and blocking by MDs, we can arrive at the governing differential equation for the density of TD of family 1, in the absence of scattering reactions as

$$\left(\frac{dp_1}{dh}\right)_{i^{\text{th}}\text{layer}} = \left( \begin{array}{l} -\rho_1 (K_{1,4}\rho_4 + K_{1,11}\rho_{11} + K_{1,12}\rho_{12} + K_{1,15}\rho_{15} + K_{1,16}\rho_{16} + K_{1,19}\rho_{19} + K_{1,20}\rho_{20} + K_{1,23}\rho_{23}) \\ + K_{1,24}\rho_{24} + K_{1,317}\rho_{13}\rho_{17} + K_{1,318}\rho_{13}\rho_{18} + K_{1,417}\rho_{14}\rho_{17} + K_{1,418}\rho_{14}\rho_{18} - \rho_1 \rho_{mi} \end{array} \right)_{i^{\text{th}}\text{layer}} \quad (3.55)$$

Similar equations can be readily derived for all twenty-four dislocation families. These 24 equations will include in the most general cases of 256 coefficients,  $K_{xy}$ . Due to the geometrical symmetry and the sake of simplicity, an identical values of coefficients  $K_{xy}=k$  for annihilation and fusion reaction are used for simulation in cubic InGaAs heteroepitaxy. Therefore Eq. (3.55) and other similar equations can be simplified as

$$\left(\frac{dp_1}{dh}\right)_{i^{\text{th}}\text{layer}} = \left( \begin{array}{l} -\rho_1 k(\rho_4 + \rho_{11} + \rho_{12} + \rho_{15} + \rho_{16} + \rho_{19} + \rho_{20} + \rho_{23} + \rho_{24}) + k\rho_{13}\rho_{17} + k\rho_{13}\rho_{18} \\ + k\rho_{14}\rho_{17} + k\rho_{14}\rho_{18} - \rho_1 \rho_m \end{array} \right)_{i^{\text{th}}\text{layer}} \quad (3.56)$$

$$\left(\frac{dp_2}{dh}\right)_{i^{\text{th}}\text{layer}} = \left( \begin{array}{l} -\rho_2 k(\rho_3 + \rho_{11} + \rho_{12} + \rho_{15} + \rho_{16} + \rho_{19} + \rho_{20} + \rho_{23} + \rho_{24}) + k\rho_9\rho_{21} + k\rho_9\rho_{22} \\ + k\rho_{10}\rho_{21} + k\rho_{10}\rho_{22} - \rho_2 \rho_m \end{array} \right)_{i^{\text{th}}\text{layer}} \quad (3.57)$$

$$\left(\frac{dp_3}{dh}\right)_{i^{\text{th}}\text{layer}} = \left( \begin{array}{l} -\rho_3 k(\rho_2 + \rho_9 + \rho_{10} + \rho_{13} + \rho_{14} + \rho_{17} + \rho_{18} + \rho_{21} + \rho_{22}) + k\rho_{15}\rho_{19} + k\rho_{15}\rho_{20} \\ + k\rho_{16}\rho_{19} + k\rho_{16}\rho_{20} - \rho_3 \rho_m \end{array} \right)_{i^{\text{th}}\text{layer}} \quad (3.58)$$

$$\left(\frac{dp_4}{dh}\right)_{i^{\text{th}}\text{layer}} = \left( \begin{array}{l} -\rho_4 k(\rho_1 + \rho_9 + \rho_{10} + \rho_{13} + \rho_{14} + \rho_{17} + \rho_{18} + \rho_{21} + \rho_{22}) + k\rho_{11}\rho_{23} + k\rho_{11}\rho_{24} \\ + k\rho_{12}\rho_{23} + k\rho_{12}\rho_{24} - \rho_4 \rho_m \end{array} \right)_{i^{\text{th}}\text{layer}} \quad (3.59)$$

$$\left(\frac{dp_5}{dh}\right)_{i^{\text{th}}\text{layer}} = \left( \begin{array}{l} -\rho_5 k(\rho_8 + \rho_{11} + \rho_{12} + \rho_{15} + \rho_{16} + \rho_{17} + \rho_{18} + \rho_{21} + \rho_{22}) + k\rho_9\rho_{19} + k\rho_9\rho_{20} \\ + k\rho_{10}\rho_{19} + k\rho_{10}\rho_{20} - \rho_5 \rho_m \end{array} \right)_{i^{\text{th}}\text{layer}} \quad (3.60)$$

$$\left(\frac{dp_6}{dh}\right)_{i^{\text{th}}\text{layer}} = \left( \begin{array}{l} -\rho_6 k(\rho_7 + \rho_{11} + \rho_{12} + \rho_{15} + \rho_{16} + \rho_{17} + \rho_{18} + \rho_{21} + \rho_{22}) + k\rho_{13}\rho_{23} + k\rho_{13}\rho_{24} \\ + k\rho_{14}\rho_{23} + k\rho_{14}\rho_{24} - \rho_6 \rho_m \end{array} \right)_{i^{\text{th}}\text{layer}} \quad (3.61)$$

$$\left(\frac{dp_7}{dh}\right)_{i^{\text{th}}\text{layer}} = \left( \begin{array}{l} -\rho_7 k(\rho_7 + \rho_9 + \rho_{10} + \rho_{13} + \rho_{14} + \rho_{19} + \rho_{20} + \rho_{23} + \rho_{24}) + k\rho_{11}\rho_{17} + k\rho_{11}\rho_{18} \\ + k\rho_{12}\rho_{17} + k\rho_{12}\rho_{18} - \rho_7 \rho_m \end{array} \right)_{i^{\text{th}}\text{layer}} \quad (3.62)$$

$$\left(\frac{dp_8}{dh}\right)_{i^{\text{th}}\text{layer}} = \left( \begin{array}{l} -\rho_8 k(\rho_5 + \rho_9 + \rho_{10} + \rho_{13} + \rho_{14} + \rho_{19} + \rho_{20} + \rho_{23} + \rho_{24}) + k\rho_{15}\rho_{21} + k\rho_{15}\rho_{22} \\ + k\rho_{16}\rho_{21} + k\rho_{16}\rho_{22} - \rho_8 \rho_m \end{array} \right)_{i^{\text{th}}\text{layer}} \quad (3.63)$$

$$\left( \frac{dp_9}{dh} \right)_{i^{th} \text{ layer}} = \left( \begin{array}{l} -\rho_9 k(\rho_3 + \rho_4 + \rho_7 + \rho_8 + \rho_{12} + \rho_{19} + \rho_{20} + \rho_{21} + \rho_{22}) + k\rho_1\rho_{23} + k\rho_1\rho_{24} \\ + k\rho_2\rho_{23} + k\rho_2\rho_{24} - \rho_9\rho_m \end{array} \right)_{i^{th} \text{ layer}} \quad (3.64)$$

$$\left( \frac{dp_{10}}{dh} \right)_{i^{th} \text{ layer}} = \left( \begin{array}{l} -\rho_{10} k(\rho_3 + \rho_4 + \rho_7 + \rho_8 + \rho_{11} + \rho_{19} + \rho_{20} + \rho_{21} + \rho_{22}) + k\rho_5\rho_{17} + k\rho_5\rho_{18} \\ + k\rho_6\rho_{17} + k\rho_6\rho_{18} - \rho_{10}\rho_m \end{array} \right)_{i^{th} \text{ layer}} \quad (3.65)$$

$$\left( \frac{dp_{11}}{dh} \right)_{i^{th} \text{ layer}} = \left( \begin{array}{l} -\rho_{11} k(\rho_1 + \rho_2 + \rho_5 + \rho_6 + \rho_{11} + \rho_{17} + \rho_{18} + \rho_{23} + \rho_{24}) + k\rho_3\rho_{21} + k\rho_3\rho_{22} \\ + k\rho_4\rho_{21} + k\rho_4\rho_{22} - \rho_{11}\rho_m \end{array} \right)_{i^{th} \text{ layer}} \quad (3.66)$$

$$\left( \frac{dp_{12}}{dh} \right)_{i^{th} \text{ layer}} = \left( \begin{array}{l} -\rho_{12} k(\rho_1 + \rho_2 + \rho_5 + \rho_6 + \rho_9 + \rho_{17} + \rho_{18} + \rho_{23} + \rho_{24}) + k\rho_7\rho_{19} + k\rho_7\rho_{20} \\ + k\rho_8\rho_{19} + k\rho_8\rho_{20} - \rho_{12}\rho_m \end{array} \right)_{i^{th} \text{ layer}} \quad (3.67)$$

$$\left( \frac{dp_{13}}{dh} \right)_{i^{th} \text{ layer}} = \left( \begin{array}{l} -\rho_{13} k(\rho_3 + \rho_4 + \rho_7 + \rho_8 + \rho_{13} + \rho_{17} + \rho_{18} + \rho_{23} + \rho_{24}) + k\rho_5\rho_{21} + k\rho_5\rho_{22} \\ + k\rho_6\rho_{21} + k\rho_6\rho_{22} - \rho_{13}\rho_m \end{array} \right)_{i^{th} \text{ layer}} \quad (3.68)$$

$$\left( \frac{dp_{14}}{dh} \right)_{i^{th} \text{ layer}} = \left( \begin{array}{l} -\rho_{14} k(\rho_3 + \rho_4 + \rho_7 + \rho_8 + \rho_{14} + \rho_{17} + \rho_{18} + \rho_{23} + \rho_{24}) + k\rho_1\rho_{19} + k\rho_1\rho_{20} \\ + k\rho_2\rho_{19} + k\rho_2\rho_{20} - \rho_{14}\rho_m \end{array} \right)_{i^{th} \text{ layer}} \quad (3.69)$$

$$\left( \frac{dp_{15}}{dh} \right)_{i^{th} \text{ layer}} = \left( \begin{array}{l} -\rho_{15} k(\rho_1 + \rho_2 + \rho_5 + \rho_6 + \rho_{15} + \rho_{19} + \rho_{20} + \rho_{21} + \rho_{22}) + k\rho_7\rho_{23} + k\rho_7\rho_{24} \\ + k\rho_8\rho_{23} + k\rho_8\rho_{24} - \rho_{15}\rho_m \end{array} \right)_{i^{th} \text{ layer}} \quad (3.70)$$

$$\left( \frac{dp_{16}}{dh} \right)_{i^{th} \text{ layer}} = \left( \begin{array}{l} -\rho_{16} k(\rho_1 + \rho_2 + \rho_5 + \rho_6 + \rho_{13} + \rho_{19} + \rho_{20} + \rho_{21} + \rho_{22}) + k\rho_3\rho_{17} + k\rho_3\rho_{18} \\ + k\rho_4\rho_{17} + k\rho_4\rho_{18} - \rho_{16}\rho_m \end{array} \right)_{i^{th} \text{ layer}} \quad (3.71)$$

$$\left( \frac{dp_{17}}{dh} \right)_{i^{th} \text{ layer}} = \left( \begin{array}{l} -\rho_{17} k(\rho_3 + \rho_4 + \rho_5 + \rho_6 + \rho_{11} + \rho_{12} + \rho_{13} + \rho_{14} + \rho_{20}) + k\rho_1\rho_{15} + k\rho_1\rho_{15} \\ + k\rho_2\rho_{15} + k\rho_2\rho_{16} - \rho_{17}\rho_m \end{array} \right)_{i^{th} \text{ layer}} \quad (3.72)$$

$$\left( \frac{dp_{18}}{dh} \right)_{i^{th} \text{ layer}} = \left( \begin{array}{l} -\rho_{18} k(\rho_3 + \rho_4 + \rho_5 + \rho_6 + \rho_{11} + \rho_{12} + \rho_{13} + \rho_{14} + \rho_{19}) + k\rho_7\rho_9 + k\rho_7\rho_{10} \\ + k\rho_8\rho_9 + k\rho_8\rho_{10} - \rho_{18}\rho_m \end{array} \right)_{i^{th} \text{ layer}} \quad (3.73)$$

$$\left( \frac{dp_{19}}{dh} \right)_{i^{th} \text{ layer}} = \left( \begin{array}{l} -\rho_{19} k(\rho_1 + \rho_2 + \rho_7 + \rho_8 + \rho_9 + \rho_{10} + \rho_{15} + \rho_{16} + \rho_{18}) + k\rho_3\rho_{13} + k\rho_3\rho_{14} \\ + k\rho_4\rho_{13} + k\rho_4\rho_{14} - \rho_{19}\rho_m \end{array} \right)_{i^{th} \text{ layer}} \quad (3.74)$$

$$\left( \frac{dp_{20}}{dh} \right)_{i^{th} \text{ layer}} = \left( \begin{array}{l} -\rho_{20} k(\rho_1 + \rho_2 + \rho_7 + \rho_8 + \rho_9 + \rho_{10} + \rho_{15} + \rho_{16} + \rho_{17}) + k\rho_5\rho_{11} + k\rho_5\rho_{12} \\ + k\rho_6\rho_{11} + k\rho_6\rho_{12} - \rho_{20}\rho_m \end{array} \right)_{i^{th} \text{ layer}} \quad (3.75)$$

$$\left( \frac{dp_{21}}{dh} \right)_{i^{th} \text{ layer}} = \left( \begin{array}{l} -\rho_{21} k(\rho_3 + \rho_4 + \rho_5 + \rho_6 + \rho_9 + \rho_{10} + \rho_{15} + \rho_{16} + \rho_{24}) + k\rho_1\rho_{11} + k\rho_1\rho_{12} \\ + k\rho_2\rho_{11} + k\rho_2\rho_{12} - \rho_{21}\rho_m \end{array} \right)_{i^{th} \text{ layer}} \quad (3.76)$$



$$\left(\frac{dp_{22}}{dh}\right)_{i^{\text{th}}\text{layer}} = \left( \begin{array}{l} -\rho_{22}k(\rho_3 + \rho_4 + \rho_5 + \rho_6 + \rho_9 + \rho_{10} + \rho_{15} + \rho_{16} + \rho_{23}) + k\rho_7\rho_{13} + k\rho_7\rho_{14} \\ + k\rho_8\rho_{13} + k\rho_8\rho_{14} - \rho_{22}\rho_m \end{array} \right)_{i^{\text{th}}\text{layer}} \quad (3.77)$$

$$\left(\frac{dp_{23}}{dh}\right)_{i^{\text{th}}\text{layer}} = \left( \begin{array}{l} -\rho_{23}k(\rho_1 + \rho_2 + \rho_7 + \rho_8 + \rho_{11} + \rho_{12} + \rho_{13} + \rho_{14} + \rho_{23}) + k\rho_3\rho_9 + k\rho_3\rho_{10} \\ + k\rho_4\rho_9 + k\rho_4\rho_{10} - \rho_{23}\rho_m \end{array} \right)_{i^{\text{th}}\text{layer}} \quad (3.78)$$

$$\left(\frac{dp_{24}}{dh}\right)_{i^{\text{th}}\text{layer}} = \left( \begin{array}{l} -\rho_{24}k(\rho_1 + \rho_2 + \rho_7 + \rho_8 + \rho_{11} + \rho_{12} + \rho_{13} + \rho_{14} + \rho_{21}) + k\rho_5\rho_{15} + k\rho_5\rho_{16} \\ + k\rho_6\rho_{15} + k\rho_6\rho_{16} - \rho_{24}\rho_m \end{array} \right)_{i^{\text{th}}\text{layer}} \quad (3.79)$$

**Table 3.2:** Reaction table for TDs in growing InGaAs heteroepitaxy. Reactions that are not possible due to  $b^2$ -criterion or for geometric reasons are indicated with a “-” while reactions that are possible are indicated with their designated number. Annihilation reactions are denoted with “0”

$p_y$	$p_x$	b	1	2	3	4	5	6	7	8	9	10	11	12	13	14	15	16	17	18	19	20	21	22	23	24
			[2-13]	[213]	[2-13]	[213]	[-213]	[-213]	[-213]	[-213]	[123]	[-123]	[123]	[-123]	[-123]	[-123]	[-123]	[-123]	[-123]	[-123]	[-123]	[-123]	[-123]	[-123]	[-123]	[-123]
			$a/2[101]$	$a/2[-10-1]$	$a/2[-101]$	$a/2[10-1]$	$a/2[011]$	$a/2[0-1-1]$	$a/2[0-11]$	$a/2[01-1]$	$a/2[110]$	$a/2[-1-10]$	$a/2[1-10]$	$a/2[-110]$												
1	[2-13]	$a/2[101]$	-	-	-	0	-	-	-	-	-	-	21	21	-	-	17	17	-	-	14	14	-	-	9	9
2	[213]	$a/2[101]$	-	-	0	-	-	-	-	-	-	-	21	21	-	-	17	17	-	-	14	14	-	-	9	9
3	[2-13]	$a/2[-10-1]$	-	0	-	-	-	-	-	-	-	-	23	23	-	-	19	19	-	-	16	16	-	-	11	11
4	[213]	$a/2[-10-1]$	0	-	-	-	-	-	-	-	-	-	23	23	-	-	19	19	-	-	16	16	-	-	11	11
5	[-213]	$a/2[-101]$	-	-	-	-	-	-	-	0	-	-	20	20	-	-	24	24	10	10	-	-	13	13	-	-
6	[-2-13]	$a/2[-101]$	-	-	-	-	-	-	0	-	-	-	20	20	-	-	24	24	10	10	-	-	13	13	-	-
7	[-213]	$a/2[10-1]$	-	-	-	-	-	0	-	-	18	18	-	-	22	22	-	-	-	-	12	12	-	-	15	15
8	[-2-13]	$a/2[10-1]$	-	-	-	-	0	-	-	-	18	18	-	-	22	22	-	-	-	-	12	12	-	-	15	15
9	[123]	$a/2[011]$	-	-	23	23	-	-	18	18	-	-	0	-	-	-	-	-	-	-	5	2	2	-	-	-
10	[-123]	$a/2[011]$	-	-	23	23	-	-	18	18	-	-	0	-	-	-	-	-	-	-	5	2	2	-	-	-
11	[123]	$a/2[0-1-1]$	21	21	-	-	20	20	-	-	-	0	-	-	-	-	-	-	7	7	-	-	-	-	4	4
12	[-123]	$a/2[0-1-1]$	21	21	-	-	20	20	-	-	0	-	-	-	-	-	-	-	7	7	-	-	-	-	4	4
13	[-1-23]	$a/2[0-11]$	-	-	19	19	-	-	22	22	-	-	-	-	-	-	0	-	1	1	-	-	-	-	6	6
14	[1-23]	$a/2[0-11]$	-	-	19	19	-	-	22	22	-	-	-	-	-	-	0	-	1	1	-	-	-	-	6	6
15	[-1-23]	$a/2[01-1]$	17	17	-	-	24	24	-	-	-	-	-	-	-	0	-	-	-	-	3	3	8	8	-	-
16	[1-23]	$a/2[01-1]$	17	17	-	-	24	24	-	-	-	-	-	-	0	-	-	-	-	-	3	3	8	8	-	-
17	[1-12]	$a/2[110]$	-	-	16	16	10	10	-	-	-	-	7	7	1	1	-	-	-	-	-	0	-	-	-	-
18	[-112]	$a/2[110]$	-	-	16	16	10	10	-	-	-	-	7	7	1	1	-	-	-	-	-	0	-	-	-	-
19	[1-12]	$a/2[-1-10]$	24	24	-	-	-	-	12	12	5	5	-	-	-	-	3	3	-	0	-	-	-	-	-	-
20	[-112]	$a/2[-1-10]$	24	24	-	-	-	-	12	12	5	5	-	-	-	-	3	3	0	-	-	-	-	-	-	-
21	[112]	$a/2[1-10]$	-	-	11	11	13	13	-	-	2	2	-	-	-	-	8	8	-	-	-	-	-	-	-	0
22	[-1-12]	$a/2[1-10]$	-	-	11	11	13	13	-	-	2	2	-	-	-	-	8	8	-	-	-	-	-	-	-	0
23	[112]	$a/2[-110]$	9	9	-	-	-	-	15	15	-	-	4	4	6	6	-	-	-	-	-	-	-	0	-	-
24	[-1-12]	$a/2[-110]$	9	9	-	-	-	-	15	15	-	-	4	4	6	6	-	-	-	-	-	-	0	-	-	-



## References:

- [1] J. W. Matthews, and A. E. Blakeslee, "Defects in epitaxial multilayers: 1. Misfit dislocation," *Journal of Crystal Growth*, Vol. 27, pp. 118-125 (1974).
- [2] R. Liu, J. Mei, S. Srinivasan, H. Omiya, F. A. Ponce, D. Cherns, Y. Narukawa, and T. Mukai, "Misfit dislocation generation in InGaN epilayers on free-standing GaN," *Jpn. J. Applied Physics*, Vol. 45, pp. L549-L551 (2006).
- [3] B. Bertoli, E. N. Suarez, J. E. Ayers, and F. C. Jain, "Misfit dislocation density and strain relaxation in graded semiconductor heterostructures with arbitrary composition profile," *Journal of Applied Physics*, Vol. 106, p. 073519 (2009).
- [4] D. Sidoti, S. Xhurxhi, T. Kujofsa, S. Cheruku, J. Reed, B. Bertoli, P. B. Rago, E. N. Suarez, F.C. Jain, and J. E. Ayers, "Critical layer thickness in exponentially graded heteroepitaxial layers," *Journal of Electronic Materials*, Vol. 39, Issue 8, pp. 1140-1145 (2010).
- [5] G. Macpherson, R. Beanland, and J. P. Goodhew, "A novel design method for the suppression of edge dislocation formation in step-graded InGaAs/GaAs layers," *Philosophical Magazine A*, Vol. 73, Issue 5, pp. 1439-1450 (1996).
- [6] Y. Nishidate and G. P. Nikishkov, "Generalized plane strain deformation of multilayer structures with initial strains," *Journal of Applied Physics* Vol. 100, pp. 113518-4 (2006).
- [7] D. Holec, P. M. F. J. Costa, M. J. Kappers, and C. J. Humphreys, "Critical thickness calculations for InGaN/GaN," *Journal of Crystal Growth*, Vol. 303, pp. 314-317 (2007).
- [8] D. Holec, and C. J. Humphreys, "Calculation of equilibrium critical thickness for non-polar wuzrite InGaN/GaN systems," *Material Science Forum*, Vol. 567-568, pp. 209-212 (2008).
- [9] J. W. Steeds, "Introduction to anisotropic elasticity theory of dislocations," Clarendon Press, Oxford, 1973.
- [10] S. M. Hu, "Misfit dislocation and critical thickness of heteroepitaxy," *Journal of Applied Physics*, Vol. 69, Issue 11, pp. 7901-7903 (1991).
- [11] J. P. Hirth, and J. Lothe, "Theory of dislocations," McGraw-Hill, New York, Chapter 3 (1968).

- [12] R. W. Lardner, "Mathematical theory of dislocations and fracture," Toronto University Press, Toronto, pp. 79 (1974).
- [13] J. D. Eshelby, in Dislocations, edited by F. R. N. Nabarro, North Holland, New York, Vol. 1, Ch 3 (1979).
- [14] A. E. Romanov, W. Pompe, G. Beltz, and J. S. Speck, "Modeling of threading dislocation density reduction in heteroepitaxial layer: Part I. Geometry and Crystallography," Phys. Stat. Sol. (b), Vol. 198, pp. 599-613 (1996).
- [15] A. E. Romanov, W. Pompe, G. Beltz, J. S. Speck, and S. Mathis, "Threading dislocation reduction in strained layers," Journal of Applied Physics, Vol. 85, Issue 1, pp. 182-192 (1999).
- [16] J. S. Speck, M. A. Brewer, G. Beltz, A. E. Romanov, and W. Pompe, "Scaling laws for the reduction of threading dislocation densities in homogenous buffer layer," Journal of Applied Physics, Vol. 80, Issue 7, pp. 3808-3816 (1996).
- [17] A. E. Romanov, W. Pompe, G. Beltz, and J. S. Speck, "Modeling of threading dislocation density reduction in heteroepitaxial layer: Part II. Effective dislocation kinetics," Phys. Stat. Sol. (b), Vol. 199, pp. 33-49 (1997).
- [18] R. E. Romanov, W. Pompe, G. E. Beltz, and J. S. Speck, "An approach to threading dislocations 'reaction kinetics'," Applied Physics Letter, Vol. 69, Issue 22, pp. 3342-3344 (1996).
- [19] N. A. El-Masty, J. C. Tarn, and N. H. Karam, "Interactions of dislocations in GaAs grown on Si substrates with InGaAs-GaAsP strained layer superlattices," Journal of Applied Physics, Vol. 64, Issue 7, pp. 3672-3676 (1988).
- [20] S. K. Mathis, A. E. Romanov, L. F. Chen, G. Beltz, W. Pompe, and J. S. Speck, "Modeling of threading dislocation reduction in growing GaN layers," Phys. Stat. Sol. (a), Vol. 179, pp. 125-145 (2000).



## Chapter IV

### Simulation Results and Discussion

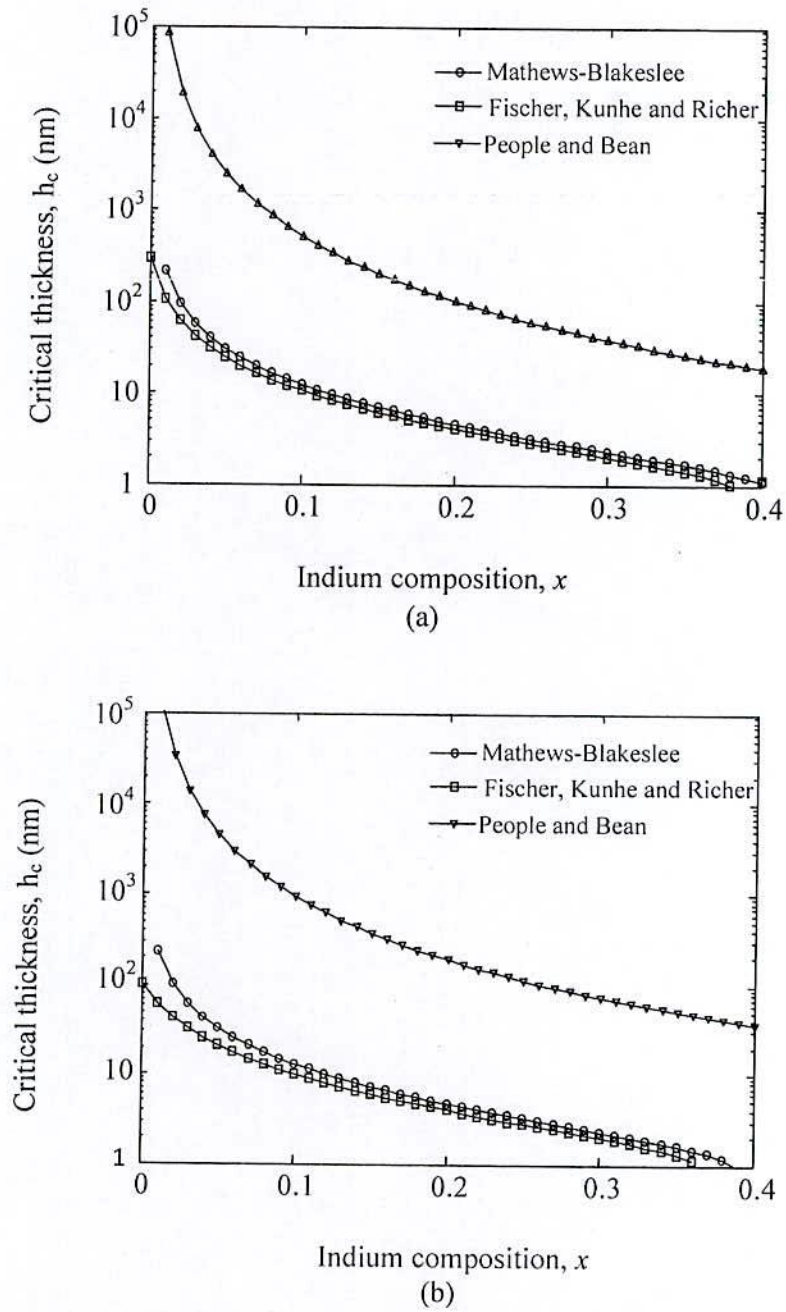
#### 4.1 Introduction

The proposed step-graded interlayer technique is expected to be very promising and superior for improving the material quality in case of InGaN and InGaAs heteroepitaxial film. To fabricate novel devices, it is of crucial importance to study the crystalline quality of the constituent materials. The main objective of this chapter is to investigate the results of the numerical calculation for misfit dislocations (MDs) as well as threading dislocations (TDs) during the heteroepitaxial growth. The results of edge, screw and mixed type MD and TD densities in all possible slips of both step-graded heteroepitaxy have been compared with constant composition layer. The dislocation densities and residual strain profile of these heteroepitaxy observed in experiments has been compared with the result found from the numerical simulation.

#### 4.2 Critical Thickness of InGaN/GaN and InGaAs/GaAs System

The evaluation of critical thickness ( $h_c$ ) is an important issue to estimate the MD generation with the increase of thickness for any heteroepitaxy. According to the different models discussed in chapter 2, the critical thickness for MD formation in wurtzite InGaN and cubic InGaAs heteroepitaxy has been calculated. The results have been as shown in Fig. 4.1(a) and (b). It can be seen from the figures that critical thickness decreases with the increase of In composition and so the misfit strain for all models. The calculations were done for the  $1/3\langle 11-23 \rangle\{1-101\}$  of InGaN and  $1/2\langle 110 \rangle\{111\}$  of InGaAs slip system using the inner cut-off radius  $r_0 = b/2$ . It is clear from the figures that the model of People and Bean gives extremely high estimates of  $h_c$  compared to others which can be ruled out as inappropriate for III-nitrides and arsenide. The Fisher's model gives reasonable estimations for the  $h_c$  as compared with experimental data. The curve presented in line with circle in these graphs corresponds to the simplest isotropic formulation of the energy balance (EB) model. The EB model in this form strongly underestimates the possible values of the  $h_c$ . Therefore, MB force balance model has been used to calculate the  $h_c$  in each step-graded interlayer. A multiple critical thickness at different interfaces have been calculated in case of step-graded structure. Due to inverse relationship a gradual decrease of in plane strain with thickness [1] introduces larger critical thickness for the

upper layers of the step-graded structures. To calculate  $h_c$  at each interface the in plane strain after each interlayer thickness have been considered according to Eq. (3.2).

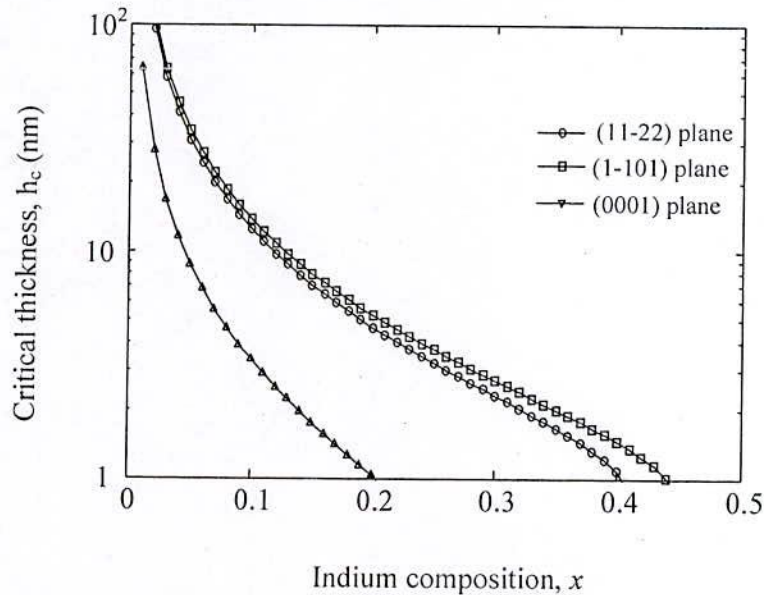


**Figure 4.1:** Comparison of critical thickness from various models for (a)  $In_xGa_{1-x}N/GaN$  and (b)  $In_xGa_{1-x}As/GaAs$  systems.



### 4.2.1 Critical Thickness at Different Slips

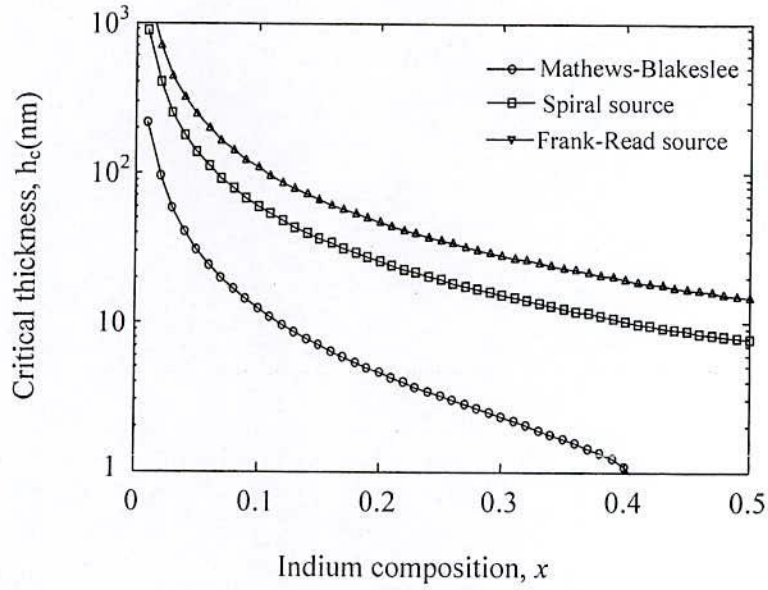
The critical thicknesses for different possible slip system of  $\text{In}_x\text{Ga}_{1-x}\text{N}/\text{GaN}$  are shown in Fig. 4.2. It can be seen from the plot that neither the  $1/3\langle 1120 \rangle(0001)$  nor the prismatic slip systems predict any critical thickness values for high  $\text{In}$  composition. Differences between the two prismatic slip systems  $1/3\langle 11-23 \rangle(11-22)$  and  $1/3\langle 11-23 \rangle(1-101)$  are not very large. The basal slip shows the lowest value of critical thickness. On the other hand the critical thicknesses in cubic  $\text{In}_x\text{Ga}_{1-x}\text{As}/\text{GaAs}$  heteroepitaxy are identical in all possible slip systems.



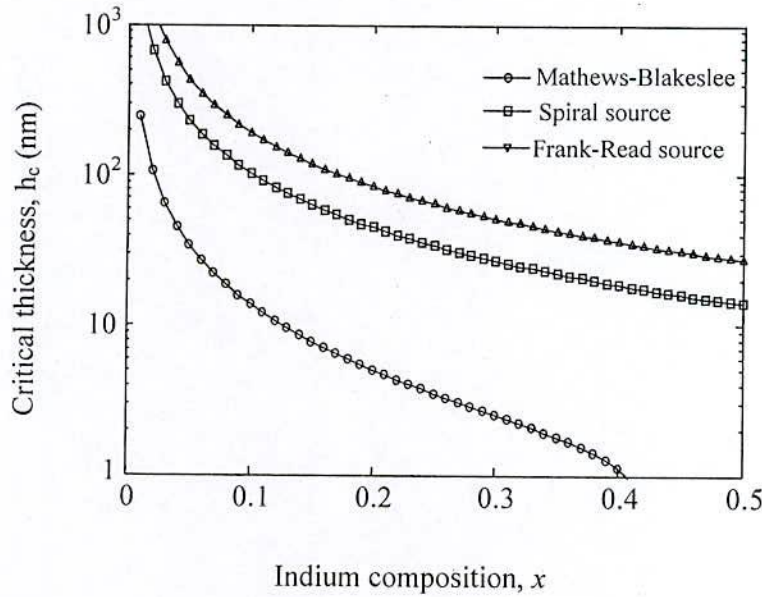
**Figure 4.2:** The critical thickness in different slip systems of  $\text{In}_x\text{Ga}_{1-x}\text{N}/\text{GaN}$  heteroepitaxy

### 4.3 Dislocation Sources in Step-graded Heteroepitaxy

As the dislocation propagation from the preexisting substrate is negligibly small the dominant mechanism for their generation in a thick, low strained epilayer is multiplication [2]. The evaluation of critical layer thickness for different multiplication mechanism of dislocation is also an important issue to proper design of the interlayer thickness in step-graded structure. The critical layer thicknesses for the individual operation of Frank-Read and spiral sources of multiplication have been calculated for wuzrite  $\text{In}_x\text{Ga}_{1-x}\text{N}/\text{GaN}$  and cubic  $\text{In}_x\text{Ga}_{1-x}\text{As}/\text{GaAs}$  systems and shown in Fig. 4.3 and Fig. 4.4 respectively. These thicknesses also show an inverse relationship with  $\text{In}$  composition. Therefore a gradual decrease in misfit strain in the step-graded structure introduces larger critical thickness of these sources in the upper layers. In case of step-graded  $\text{InGaN}$  and  $\text{InGaAs}$  interlayers a step increase of  $\text{In}$  composition offers larger critical



**Figure 4.3:** The critical thicknesses for different sources of dislocations in InGaN heteroepitaxy



**Figure 4.4:** The critical thicknesses for different sources of dislocations in InGaAs heteroepitaxy

thicknesses of these dislocation sources. From the figures it is clear that these values are typically six to seven times larger than that of the Mathews-Blakeslee critical layer thickness. A further observation found that the Frank-Read and spiral sources start the generation after 108 and 60 nm respectively for a composition difference of 10% in each InGaN interlayer of the step-graded structure. Whereas these distances are 20 and 10 nm for 40% composition



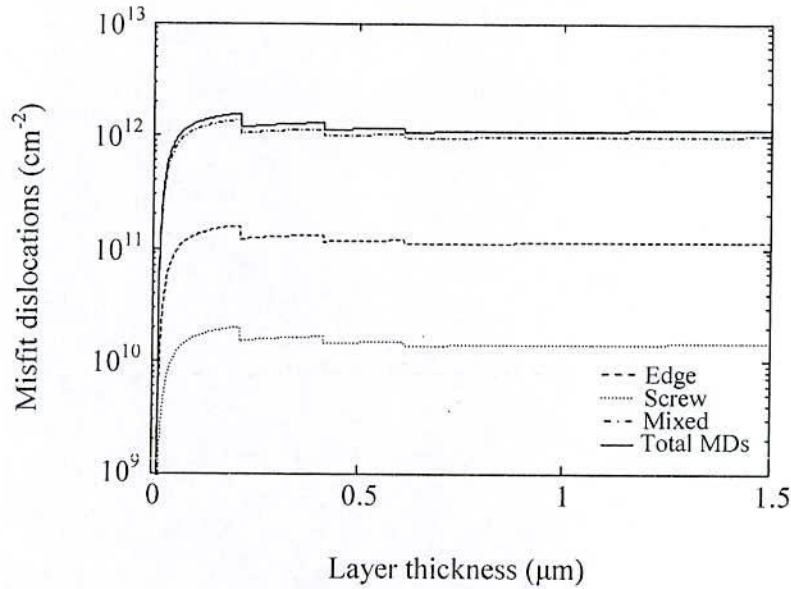
difference in without graded layer. On the other hand, in case of InGaAs step-graded structure the critical thicknesses of Frank-Read and spiral sources are 191 and 103 nm respectively for 10% increase of indium at each step. Whereas these distances are only 36 and 19 nm respectively for without graded InGaN layer. Thus, in a 1.5  $\mu\text{m}$  step-graded structure with 3 interlayer each thickness of 200 nm with In composition difference 0.1 will reduce their possibility of multiplication in both heteroepitaxy. Therefore, comparatively lower numbers of MDs from these sources are expected in the proposed step-graded  $\text{In}_{0.4}\text{Ga}_{0.6}\text{N}/\text{GaN}$  and  $\text{In}_{0.4}\text{Ga}_{0.6}\text{As}/\text{GaAs}$  heteroepitaxy using 3 interlayers.

#### 4.4 MDs in Step-graded InGaN and InGaAs

The calculated critical thicknesses of the step-graded  $\text{In}_{0.4}\text{Ga}_{0.6}\text{N}$  and  $\text{In}_{0.4}\text{Ga}_{0.6}\text{As}$  layer on a rigid GaN and GaAs substrate are reported in the previous section. At these film thicknesses the appearance of MDs are, for the first time, energetically favorable and start to relax the misfit strain. However, there is no reason to assume that all MDs will appear suddenly when the film thickness reaches  $h_c$ . Instead, Hu introduced a simple calculation for determining MD density with increasing film thickness  $h$  [3]. His model is based on balancing the elastic energy from partially relaxed misfit strain and the energy of the non-interacting MD arrays that cause misfit strain relaxation. Here the model of Hu is used to calculate MD at each interlayer and the upper epilayer.

##### 4.4.1 MDs Generation in Wuzrite InGaN

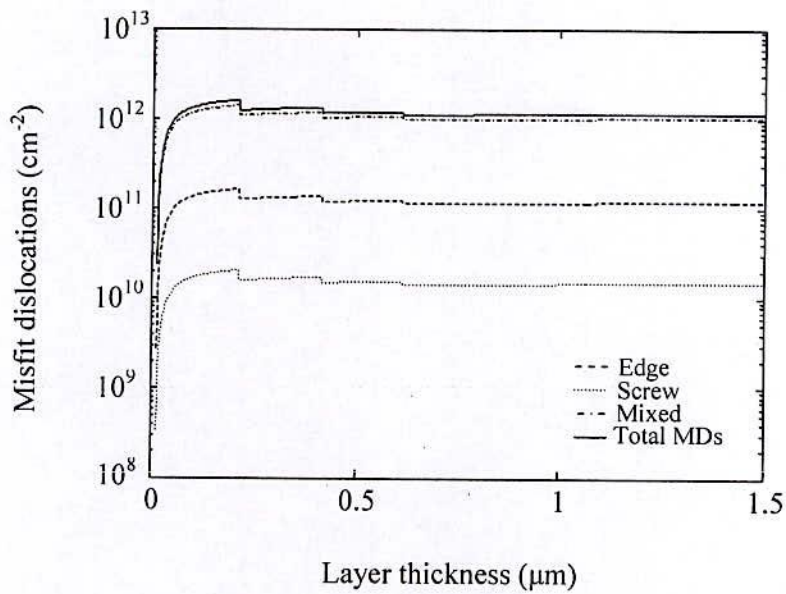
The misfit dislocations are calculated in step-graded  $\text{In}_{0.4}\text{Ga}_{0.6}\text{N}/\text{GaN}$  heteroepitaxy using 3 interlayers considering 200 nm of each layer. Figure 4.5 shows the total MDs generation in  $1/3\langle 11-23 \rangle (11-22)$  slip as a function of layer thickness. This slip generates edge, screw and mixed dislocation depending on the angle between the burger vector and dislocation line direction. This figure also presents these three types of MDs separately in the step-graded  $\text{In}_{0.4}\text{Ga}_{0.6}\text{N}$ . The mixed MDs are considered as  $60^\circ$  types. There is a significant difference observed among the results with most of the MDs are of mixed types. It has been clear from the figure that the step wise decrease in MDs densities of all types at each interlayer with extremely low dislocation density in the epilayer can be achieved. It can be seen from the figure that the edge, screw and mixed type MDs are of  $1.14 \times 10^{11}$ ,  $1.4 \times 10^{10}$  and  $9.9 \times 10^{11} \text{ cm}^{-2}$  respectively in the epilayer of the (11-22) plane InGaN step-graded structure. Similarly the MDs of different types can be evaluated in other possible slips considering their parameters as listed in Table 2.1.



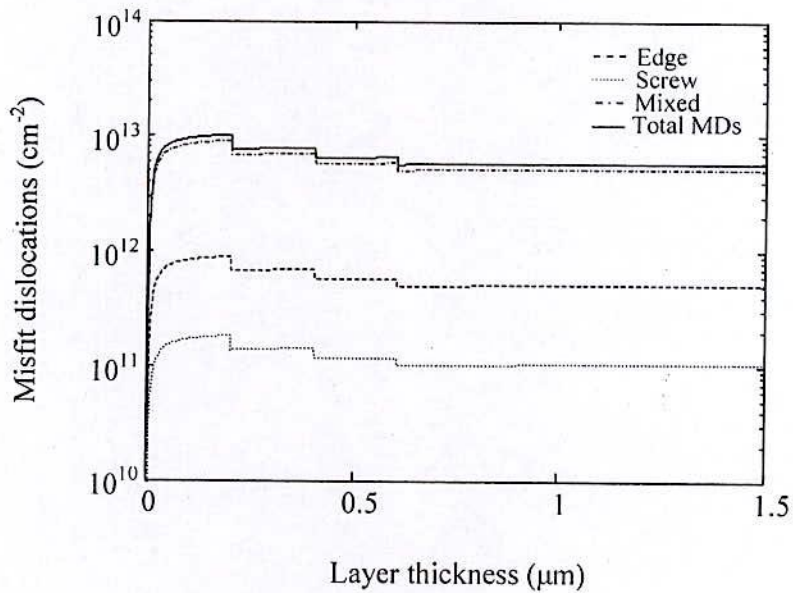
**Figure 4.5:** The different types of misfit dislocations on  $1/3\langle 11-23 \rangle(11-22)$  slip of a step-graded InGaN ( $\text{In}_{0.4}\text{Ga}_{0.6}\text{N}/\text{In}_{0.3}\text{Ga}_{0.7}\text{N}/\text{In}_{0.2}\text{Ga}_{0.8}\text{N}/\text{In}_{0.1}\text{Ga}_{0.9}\text{N}/\text{GaN}$  heteroepitaxy) layer

The Fig. 4.6(a) and (b) show the edge, screw and mixed type MDs in the  $1/3\langle 11-23 \rangle(1-101)$  and  $1/3\langle 11-20 \rangle(0001)$  slips respectively in epilayer of the InGaN heteroepitaxy. Now, the effects of step grading on the different types of MDs can be analyzed. From the above we can see that the MDs of all types generated in  $1/3\langle 11-20 \rangle(0001)$  slip are much higher than that of the other prismatic slips. This is because the hexagonal c-plane is isotropic and therefore burgers vector for all dislocation lines with different angles  $\phi$  are equivalent. It is also clear in all figures that the mixed and edge type MDs have higher densities than screw type. This is due to the lower energy configuration for mixed and edge type whereas screw type requires highest energy. It can be seen from the figure that the edge, screw and mixed type MDs are of  $1.18 \times 10^{11}$ ,  $1.5 \times 10^{10}$  and  $1 \times 10^{12}$   $\text{cm}^{-2}$  respectively on the (1-101) plane whereas these values are  $5.1 \times 10^{11}$ ,  $1.4 \times 10^{11}$  and  $6.9 \times 10^{12}$   $\text{cm}^{-2}$  respectively in the epilayer of the (0001) plane InGaN step-graded structure. The Fig. 4.7 shows a comparison of total generated edge type MDs in all possible planes of the step-graded and without graded structure. The total edge type MDs at the InGaN epilayer are found to be  $7.3 \times 10^{11}$  and  $1.72 \times 10^{12}$   $\text{cm}^{-2}$  for step-graded and without graded structure respectively. The significant difference of dislocation density indicates that the step-graded interlayers successfully decrease the dislocation between GaN and InGaN interface and between the interlayers. The improvements of total mixed type MDs have also been calculated for the step-graded and without graded structure and shown in Fig. 4.8. It has again confirms a significant improvement of epilayer quality due to use of step-graded interlayers.



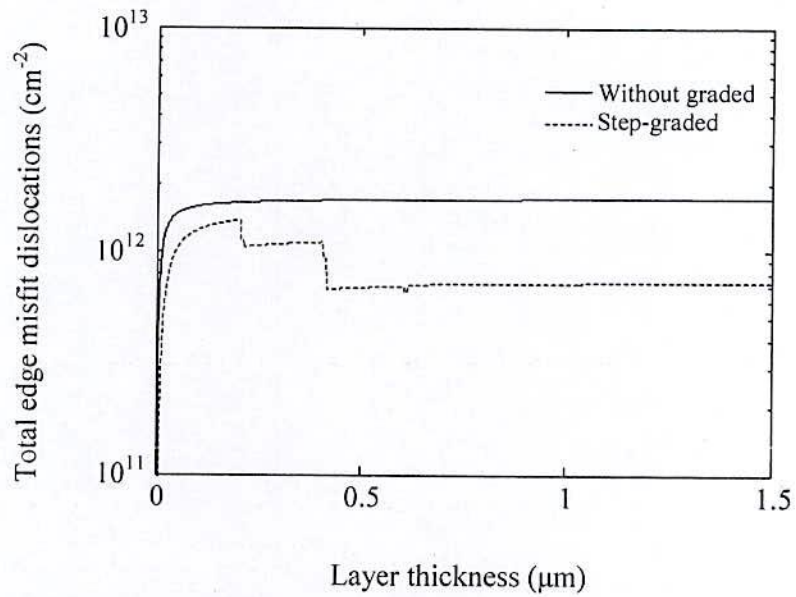


(a)

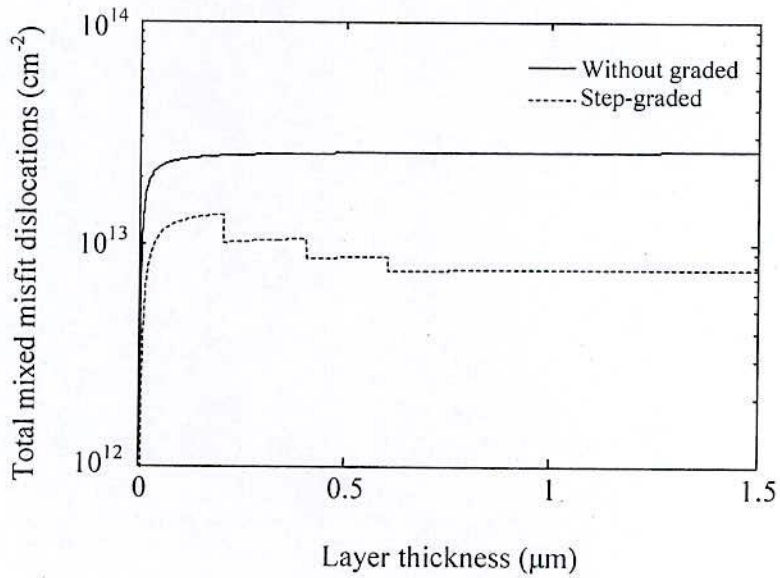


(b)

**Figure 4.6:** The different types of misfit dislocations of a step-graded InGaN ( $\text{In}_{0.4}\text{Ga}_{0.6}\text{N}/\text{In}_{0.3}\text{Ga}_{0.7}\text{N}/\text{In}_{0.2}\text{Ga}_{0.8}\text{N}/\text{In}_{0.1}\text{Ga}_{0.9}\text{N}/\text{GaN}$  heteroepitaxy) layer - (a) on  $1/3\langle 11\bar{2}3 \rangle$  (1-101) slip and (b) on  $1/3\langle 11\bar{2}0 \rangle$  (0001) slip



**Figure 4.7:** Comparison of total edge type misfit dislocations in step-graded and without graded InGaN/GaN heteroepitaxy using 3 interlayers



**Figure 4.8:** Comparison of total mixed type misfit dislocations in step-graded and without graded InGaN/GaN heteroepitaxy using 3 interlayers

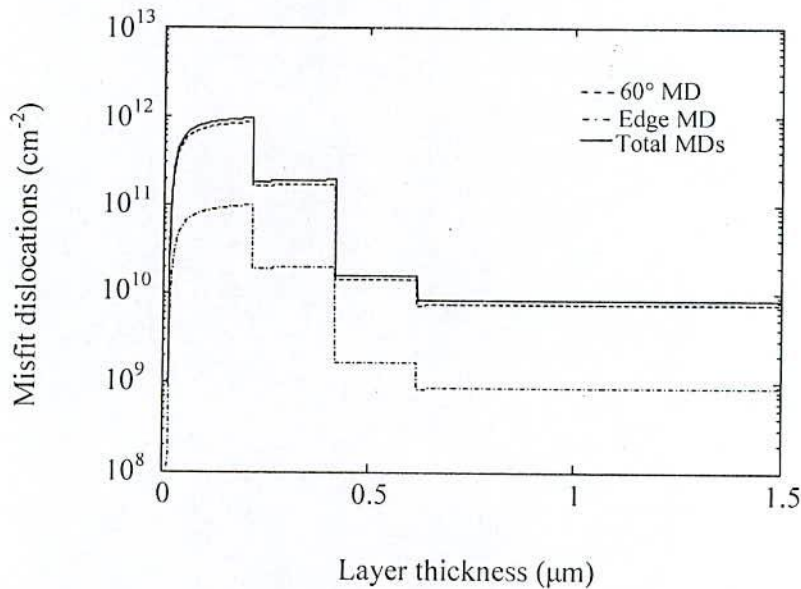
The gradual decrease of in plane strain with thickness is primarily responsible for this improvement in dislocation density. With no interlayer the difference in mismatch between



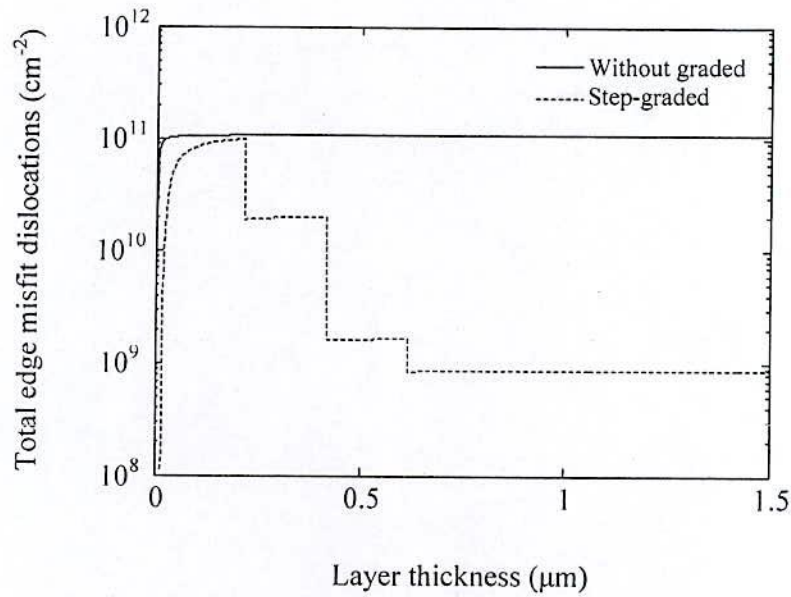
epilayer and substrate causes a large misfit and thermal strain between them. The large compressive stress also yields in the InGaN because of large thermal expansion coefficient for GaN ( $5.5 \times 10^{-6} \text{K}^{-1}$ ) than for InN ( $4.0 \times 10^{-6} \text{K}^{-1}$ ), resulting in an introduction of misfit lattice dislocations in the epilayer. On the other hand, with increasing the InGaN interlayer in a step-graded structure composition increases slowly step-wise. Thus the lattice mismatch as well as thermal expansion coefficient of the step graded interlayer would be expected to be gradual change from GaN to  $\text{In}_{0.4}\text{Ga}_{0.6}\text{N}$ . Furthermore the misfit strain at the new interlayer could be compensated by the residual strain of opposite polarity from the previous layer. Therefore, the stress may be decreased or accommodated within a graded interlayer resulting in lower misfit dislocation.

#### 4.4.2 MDs Generation in Cubic InGaAs

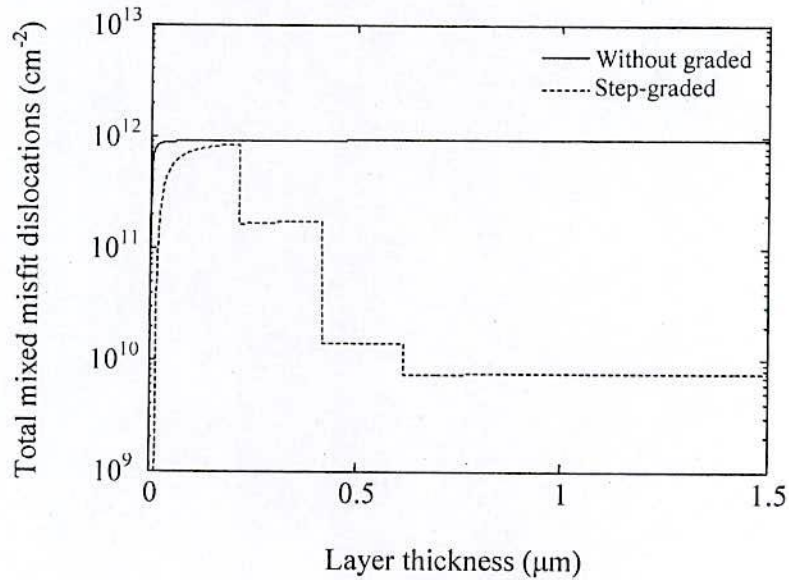
The misfit dislocation in a step-graded InGaAs heteroepitaxy has been evaluated analytically using the energy balance model developed in chapter 3. The calculations have been done for a  $1.5 \mu\text{m}$  step-graded structure with 3 InGaAs interlayer each of  $200 \text{nm}$  thickness and 10% In composition increase at each interlayer. The results have been presented in Fig. 4.9. Most of the MDs generated in cubic InGaAs heteroepitaxy are of mixed ( $60^\circ$  type) dislocations with few edge dislocations. It can be seen from the figure that the edge type MDs of  $9.8 \times 10^{10}$ ,  $2.0 \times 10^{10}$ ,



**Figure 4.9:** The different types of misfit dislocations in step-graded InGaAs ( $\text{In}_{0.4}\text{Ga}_{0.6}\text{As}/\text{In}_{0.3}\text{Ga}_{0.7}\text{As}/\text{In}_{0.2}\text{Ga}_{0.8}\text{As}/\text{In}_{0.1}\text{Ga}_{0.9}\text{As}/\text{GaAs}$  heteroepitaxy) layer



**Figure 4.10:** Comparison of total edge type misfit dislocations in step-graded and without graded  $\text{In}_x\text{Ga}_{1-x}\text{As}/\text{GaAs}$  heteroepitaxy using 3 interlayers



**Figure 4.11:** Total mixed type MD generated in step-graded and without graded  $\text{In}_x\text{Ga}_{1-x}\text{As}/\text{GaAs}$  heteroepitaxy using 3 interlayers

$1.7 \times 10^9$  and  $8.8 \times 10^8 \text{ cm}^{-2}$  are calculated at first, second, third interlayer and epilayer respectively for the step-graded structure. Whereas these values are found to be  $8.5 \times 10^{11}$ ,  $1.73 \times 10^{11}$ ,



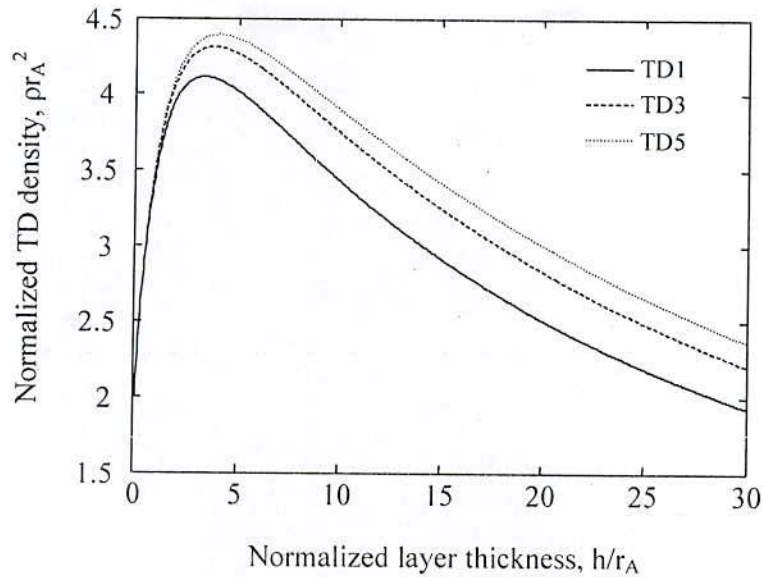
$1.4 \times 10^{10}$  and  $7.6 \times 10^9 \text{ cm}^{-2}$  for mixed type MD. These again confirm the generation of a large number of mixed type MDs. The improvement of epilayer using step graded interlayers can be evaluated using the Fig. 4.10 and 4.11. These figures present a comparison of total edge and mixed type MDs in step-graded and without graded structure. Due to step grading the edge type MDs decreases from  $1.1 \times 10^{11}$  to  $8.8 \times 10^8 \text{ cm}^{-2}$  and mixed type from  $9.2 \times 10^{11}$  to  $7.6 \times 10^9 \text{ cm}^{-2}$ . These found good agreement with experimental results [4, 5].

#### 4.5 TDs Reduction Using Step-graded Interlayer

Reduction of the threading dislocation density is one of the main challenges in GaN and GaAs-based materials research. Many efforts have been going on for detail modeling of different approach to low TD densities. Romanov et al. introduced a model based on “reactions” of inclined dislocations in strained heteroepitaxial layers [6, 7]. An intentionally introduced strained layer can control the interaction by inclination and hence promotes the reaction among the TDs. We have used the model for each interlayer and epilayer with some modification and observed the overall TD density reduction. The possible annihilation and fusion reaction between TDs and blocking by MDs are responsible for decreasing with thickness.

##### 4.5.1 TDs in Wuzrite InGaN

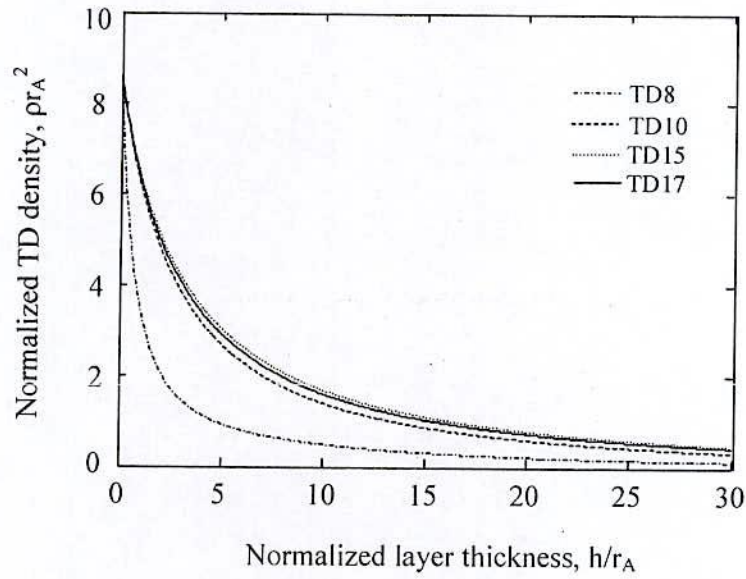
The threading dislocation densities in the step-graded InGaN heteroepitaxy have been evaluated from the numerical simulation of the reaction model developed in chapter 3. The model comprises the possible interaction between all pair of TDs, blocking of a TDs by MDs on its gliding path during the growth of each interlayer. In case of wuzrite  $\text{In}_{0.4}\text{Ga}_{0.6}\text{N}$  a total of 20 first orders, nonlinear differential equations according to all possible burger vectors have been solved using Euler method. The structure comprises of a  $1.5 \mu\text{m}$  InGaN using 3 interlayers each of 200 nm thickness and 10% In composition difference for each. To execute the solution, the MDs are considered as the main source of TDs of specific types to set the initial boundary conditions. The reaction kinetic coefficients between each pair of TDs have been determined for each interlayer considering the annihilation and fusion reaction radius of  $500 \text{ \AA}$ . Commonly three types of TDs are considered in the model. The burger vectors of number 1 to 6 as indicated in Table 3.1 represent the TD with edge character. The mixed characters are associated with burger vector number 7 to 18 and the rest TD with number 19 and 20 are of screw character. The solution presents the variation of TD densities with increasing film thickness. Fig. 4.12 shows the density reduction of TDI, 3 and 5 (edge type) in the step-graded InGaN. It can be reported from the



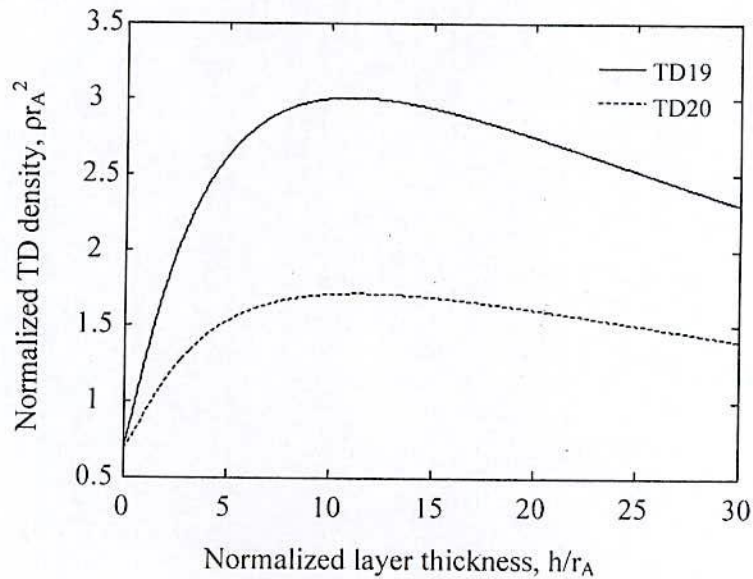
**Figure 4.12:** The variation of edge type TD density with specific number in step-graded  $\text{In}_x\text{Ga}_{1-x}\text{N}/\text{GaN}$  system

figure that, initially the edge type TDs increase rapidly and then begin to decrease with increasing film thickness. The initial increase is due to their lower initial values and their generation from reaction of other types is higher. Fig. 4.13 (a) and (b) present the variation of mixed and screw type TD densities with specific number respectively as a function of film thickness for the step-graded structure. The mixed type TD decrease monotonically with increasing film thickness and these decreases are more quickly than any other type of TD. This is because though the screw dislocations are considered very low initial values they can be the product of other reaction and allowed to participate in reaction with other TDs. As a result, both the screw-mixed reaction producing vertical edge dislocation and the edge-mixed reaction producing vertical screw dislocations. Therefore the mixed TD density becomes so low as to prevent the further interaction among TDs, with the end result of saturation in TD density. The nature of screw type TDs are different from the others. Though the both TDs increase with thickness, the TD19 has higher rate than TD20. The improvement in TD density in the top surface of the epilayer has been understood from the comparison of Fig. 4.14 (a) and (b). These figures show the decrease of average edge, mixed and screw TD densities of the step-graded and without graded  $\text{In}_{0.4}\text{Ga}_{0.6}\text{N}$  heteroepitaxy respectively. The total edge, screw and mixed type TDs densities for the step graded structures are found to be  $8.68 \times 10^{10}$ ,  $7.4 \times 10^{10}$  and  $1.32 \times 10^{10}$   $\text{cm}^{-2}$  respectively at the top surface of the epilayer. Whereas these values are  $4.6 \times 10^{11}$ ,  $3.78 \times 10^{11}$  and  $7.52 \times 10^{10}$   $\text{cm}^{-2}$  respectively for the without graded structure. Finally, the Fig. 4.15 shows the





(a)

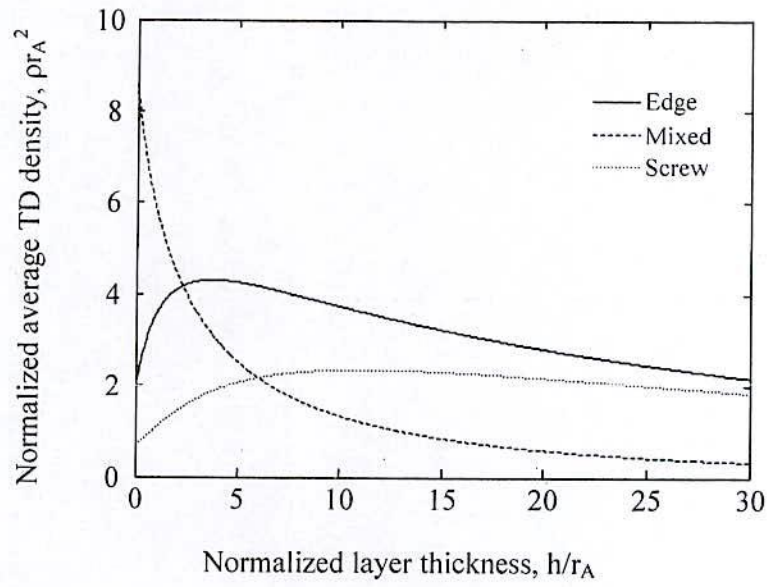


(b)

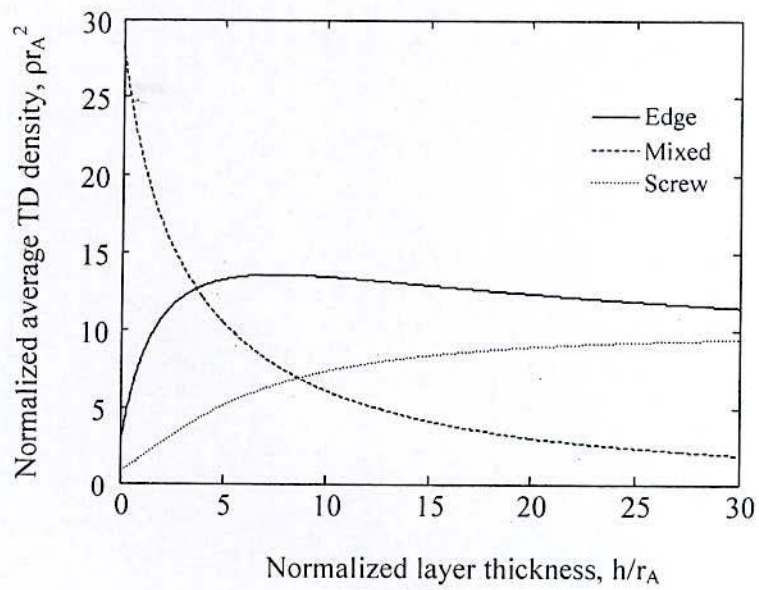
**Figure 4.13:** The variation of – (a) mixed type and (b) screw type TD density with specific number in step-graded  $In_xGa_{1-x}N/GaN$  system

variation total TD density of the step-graded structure. In the step-graded structure the total TD density decreases from  $4.65 \times 10^{12}$  to  $8.27 \times 10^{11} \text{ cm}^{-2}$ . The TD density in the upper surface of step-graded structure is found to be extremely lower (less than one-fifth) than that of the without graded structure.





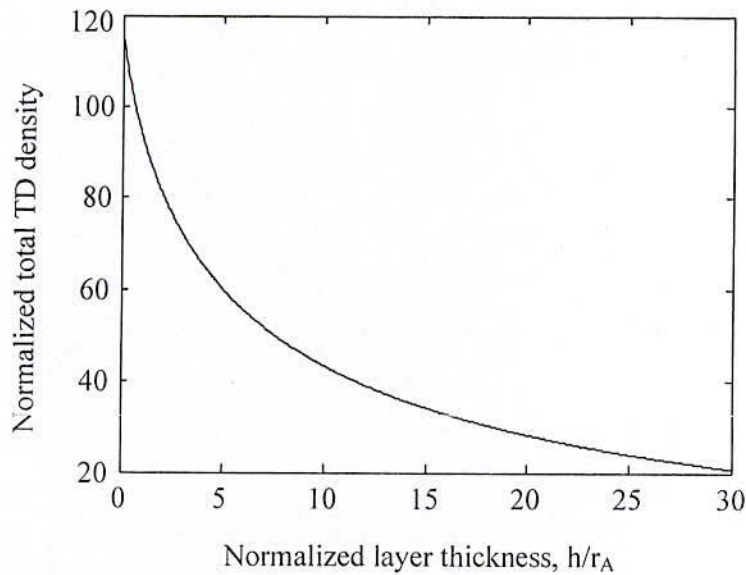
(a)



(b)

**Figure 4.14:** The average edge, screw and mixed type TDs for- (a) step-graded and (b) without graded  $\text{In}_x\text{Ga}_{1-x}\text{N}/\text{GaN}$  system

There are several reasons behind this improvement in epilayer quality of the step-grade structure. Since the dislocations from the substrate are extremely much lower than the dislocation generated from other sources, the MDs are considered as the main source of TDs. In



**Figure 4.15:** The variation of overall TD density with step-graded InGaN thickness

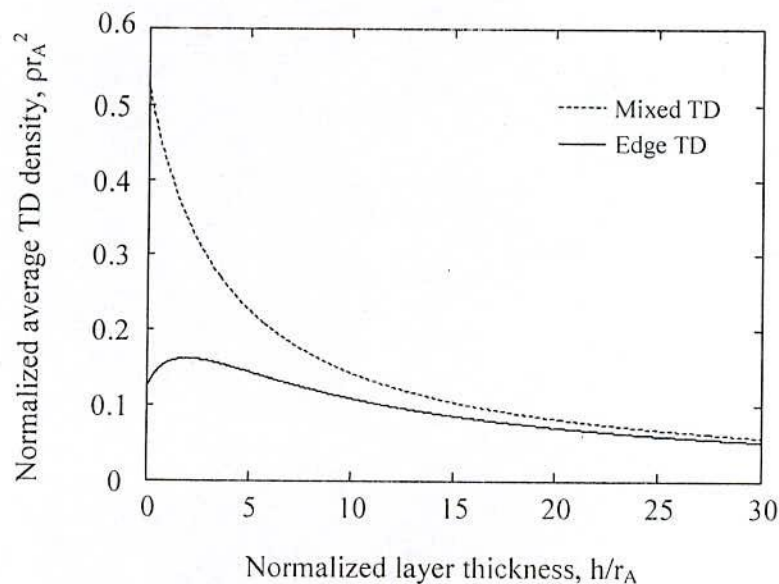
case of without graded structure the most of the MDs are generated near the film-substrate interface due to large mismatch and lower critical thickness. Therefore the TDs that glided in the upper layers could not be blocked by the MDs. On the other hand, the MDs generations are spread out throughout the entire layer instead of concentrate in a single interface. As a result the, the TD glided out from the first interlayer could be blocked by MD generated in the second interlayer, TD from second layer may be blocked by MDs in upper layer and so on. Therefore the TD reduction in step-graded structure can be enhanced by the MD blocking.

Beside this, as the strain inside the thin film drives threading dislocations to incline at each interface and react with each other, the introduction of an intentionally strained layer can be used to facilitate the TD reduction process. This is the basic TD reduction mechanism of step-graded layer. Bending of dislocations in without graded structure only occurs very close to the  $\text{In}_x\text{Ga}_{1-x}\text{N}/\text{GaN}$  interface, whereas dislocation bending can be noticed at each interface between InGaN interlayers of different composition in step-graded structure. Moreover, due to large misfit dislocation density a strong interaction force among them prohibit the glide motion of the dislocation and further relaxation. Therefore, it requires further dislocation nucleation to relax the strain resulting higher TD densities in epilayer. On the other hand lower MD densities offers weak interaction force with easy gliding of TDs. A well designed graded layer should relax the misfit strain mostly through the glide motion of existing threading dislocations instead of nucleation of new dislocation [8].

Furthermore, the number of growing dislocations at a certain time is given by the sum of the number of preexisting dislocations in the substrate, the number of thermally activated dislocation sources, the number of dislocations generated by multiplication mechanisms, and the loss of dislocations due to interactions. Among them the last term plays a significant role. In order to obtain low dislocation density the most dangerous interaction that has to be avoided is the multiplication of dislocations. As observed in various experimental works the most nucleation sites for TDs are MDs which are extremely lower in step-graded structure than the without graded.

#### 4.5.2 TDs in Cubic InGaAs

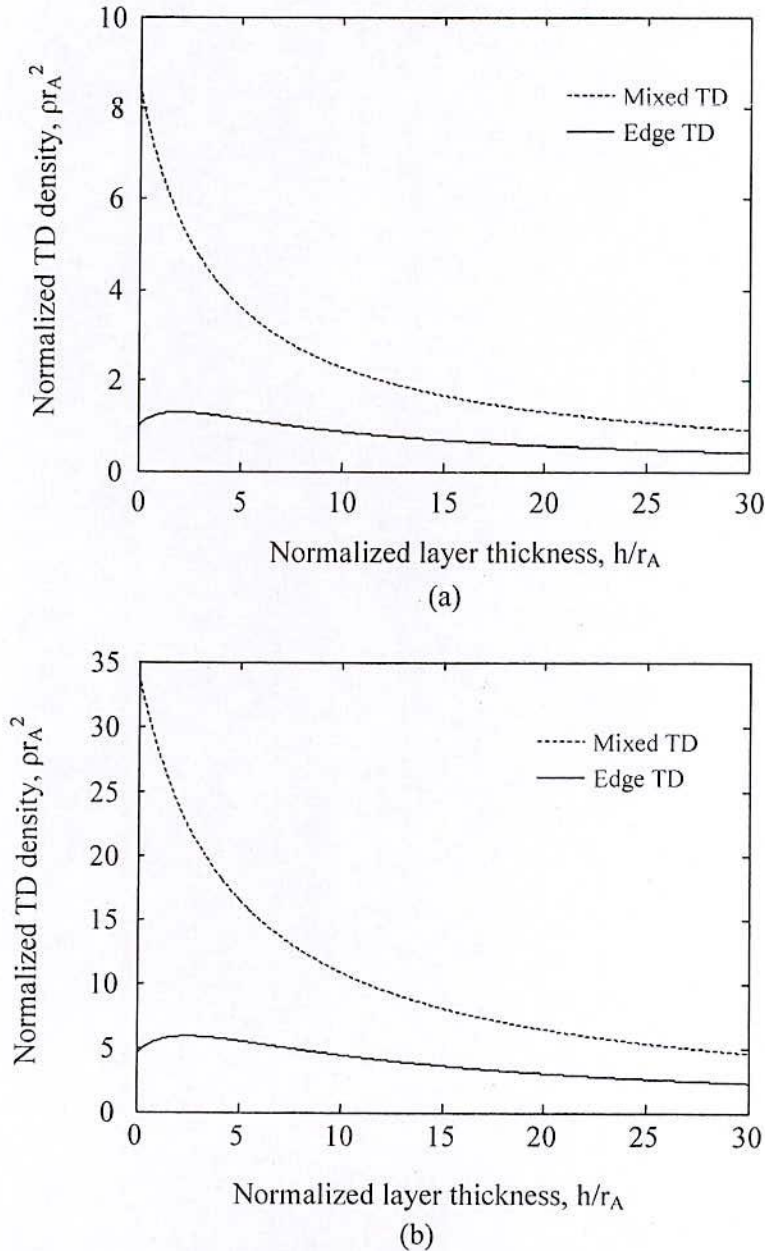
A similar methodology has been applied to develop the reaction model for the step-graded cubic InGaAs/GaAs heteroepitaxy with some modifications where most of the mixed TDs are of mixed ( $60^\circ$  type) type in  $1/2\langle 110 \rangle\{111\}$  slip system with few edge type TDs. A total of 24 similar equations formed according to all possible burger vectors have been solved using the Euler method. The simulation of the step-graded InGaAs interlayer has been done for similar structure as InGaN heteroepitaxy. The burger vectors from 1 to 16 are of mixed type gliding along the inclined  $\{111\}$  plane and 17 to 24 are of edge TDs with burger vector parallel to the (001) plane. The solution shows the diminishing densities of TD densities with increasing film thickness. The mixed TDs decrease monotonically with increasing film thickness at higher rate



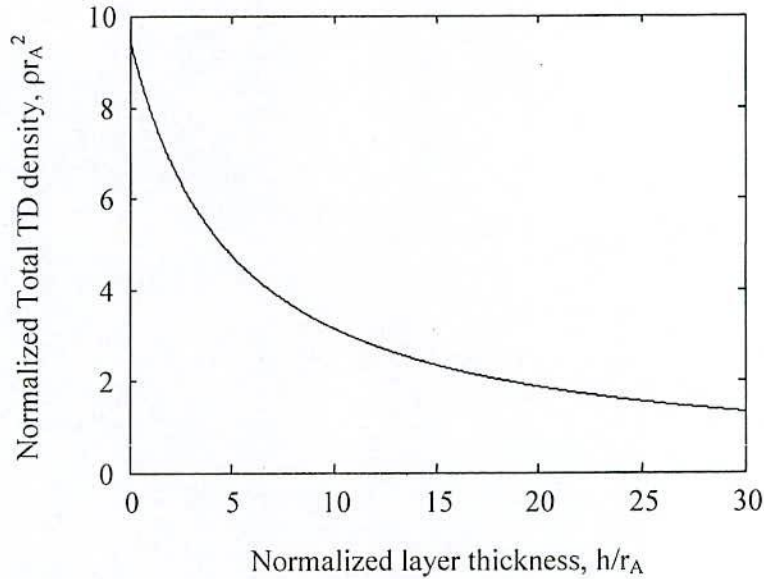
**Figure 4.16:** The variation of average TD density in step-graded  $\text{In}_x\text{Ga}_{1-x}\text{As}/\text{GaAs}$  system



than the edge TDs. The Fig. 4.16 shows the decrease of average mixed and edge type TD densities from  $2.12 \times 10^{10}$  to  $2.28 \times 10^9 \text{ cm}^{-2}$  and  $4.9 \times 10^9$  to  $2.05 \times 10^9 \text{ cm}^{-2}$  respectively after a  $1.5 \mu\text{m}$  step-graded InGaAs heteroepitaxy. The higher rate of decreasing mixed type TDs is due to the more relative motion of these TDs even without any glide motion and higher initial densities. The coherent variation of TD density is due to the dealing of family 1 through 24 equivalently and geometrical symmetry of cubic InGaAs. Furthermore, the blocking of TD due to interaction



**Figure 4.17:** The total edge and mixed type TD density in - (a) step-graded and (b) without graded  $\text{In}_x\text{Ga}_{1-x}\text{As}/\text{GaAs}$  system

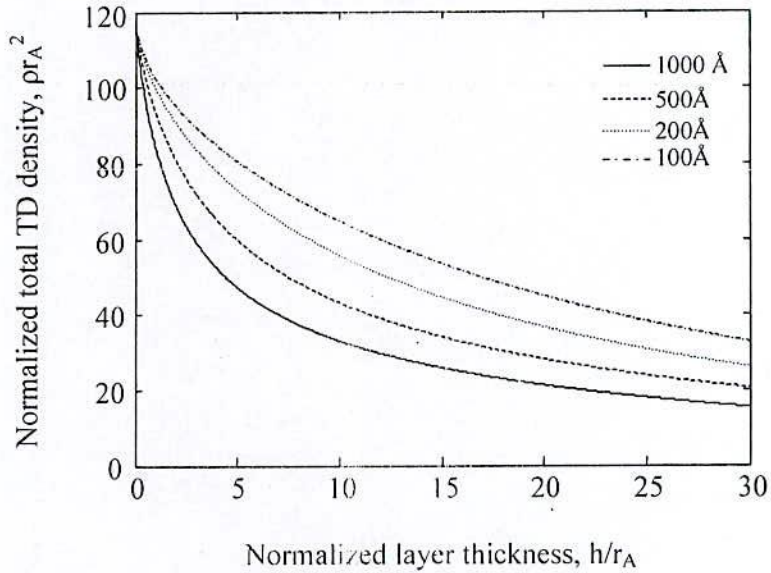


**Figure 4.18:** The variation of overall TD density with step-graded  $\text{In}_x\text{Ga}_{1-x}\text{As}$  thickness

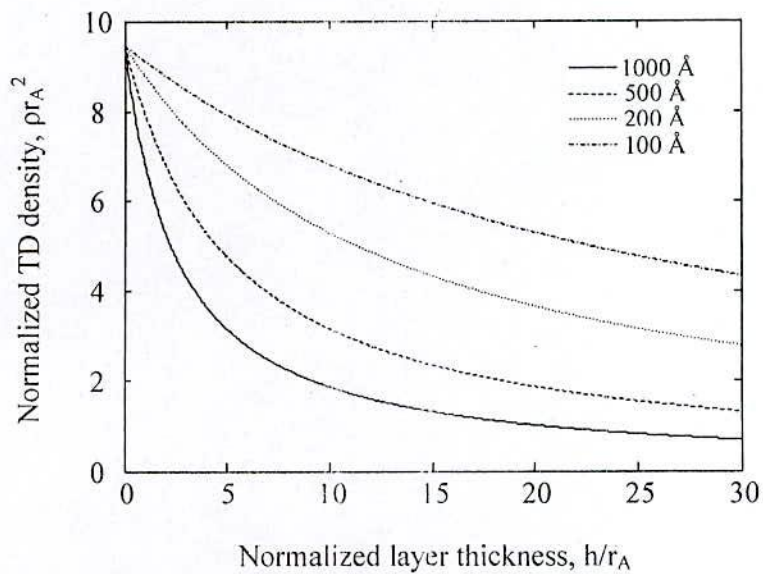
with MD on its gliding plane is same for all family of dislocation. However if the symmetry of initial condition is broken then there is a transition thickness necessary for all the families to converge to the same value for increasing  $h$ . The Fig. 4.17 (a) and (b) present total variation of different type of TD densities in the step-graded and without graded structure. The TD densities of both type have extremely lower values at the top of the epilayer in the step-graded structure than that of the without graded layer. The TD density of  $3.65 \times 10^{10}$  and  $1.64 \times 10^{10} \text{ cm}^{-2}$  for mixed and edge character respectively have been calculated in the top surface for step-graded. Whereas these values are found to be  $1.84 \times 10^{11}$  and  $9.12 \times 10^{10} \text{ cm}^{-2}$  respectively for without graded structure. The step inclination of TD at each interface promotes the reaction between them in case of step-graded layers. This decrease in TD in case of InGaAs of more than that of InGaN because of more relative motion of TD in the absence of glide, more annihilation and fusion reaction. The behavior of overall TD density for the step-graded structure is presented in Fig. 4.18. A total TD density decreases from  $3.76 \times 10^{11}$  to  $5.28 \times 10^{10} \text{ cm}^{-2}$  after a  $1.5 \mu\text{m}$  step-graded  $\text{In}_x\text{Ga}_{1-x}\text{As}/\text{GaAs}$  heteroepitaxy using 3 interlayers. This improvement in epilayer quality is due to the step inclination of TDs, lower dislocation sources, easy gliding motion of TDs and higher blocking by MDs have been discussed in the previous section.

#### 4.6 Effect of Annihilation Radius

In determination of TD density with increase of film thickness in step-graded InGaN and InGaAs interlayers, the annihilation radius,  $r_A$  is an effective rate constant. The total TD density variation is calculated for four different values of  $r_A$ . The total TD densities for annihilation



**Figure 4.19:** The effects of annihilation radius on total TD density of InGaN/GaN heteroepitaxy



**Figure 4.20:** The effects of annihilation radius on total TD density of InGaAs/GaAs



radius of 1000, 500, 200 and 100Å are shown in Fig. 4.19 and 4.20 for step-graded InGaN and InGaAs heteroepitaxy respectively. The results indicate that the initial rate of TD reduction is faster for higher annihilation radii and becomes saturates early. On the other hand, in case of lower annihilation radius, saturation happens at higher thickness due to slower reaction between TDs. The dislocation density at annihilation radii 500Å has good agreement with the values found experimentally in literature. Therefore, these values have been considered for all calculations in the reaction model. It can be found from the comparison of the figures that the TDs in InGaN are relatively less reactive than in InGaAs with same reaction radius. Lower reactivity means that a higher applied force is required to move TDs in InGaN.

### References:

- [1] Y. Nishidate and G. P. Nikishkov, "Generalized plane strain deformation of multilayer structures with initial strains," *Journal of Applied Physics*, Vol. 100, pp. 113518-4 (2006).
- [2] F. K. LeGoues, and B. S. Meyerson, "Mechanism and conditions for anomalous strain relaxation in graded thin-films and superlattices," *Journal of Applied Physics*, Vol. 71, Issue 9, pp. 4230-4243 (1992).
- [3] S. M. Hu, "Misfit dislocation and critical thickness of heteroepitaxy," *Journal of Applied Physics*, Vol. 69, Issue 11, pp. 7901-7903 (1991).
- [4] K. L. Kavanagh, J. C. P. Chang, J. Chen, J. M. Fernandez, and H. H. Wieder, "Lattice tilt and dislocations in compositionally step-graded buffer layers for mismatched InGaAs/GaAs heterointerfaces," *J. Vac. Sci. Technol. B*, Vol. 10, No. 4, pp.1820-1823 (1992).
- [5] A. E. Romanov, W. Pompe, G. Beltz, and J. S. Speck, "Modeling of threading dislocation density reduction in heteroepitaxial layer: Part I. Geometry and Crystallography," *Phys. Stat. Sol. (b)*, Vol. 198, pp. 599-613 (1996).
- [6] P. Kidd, D.J. Dunstan, H.G. Colson, M. A. Louren, A. Saceddn, F. Gonzhlez-Sanz, L. Gonzfilez, Y. Gonzfilez, R. Garch, D. Gonzfilez, F.J. Pacheco, and P.J. Goodhew, "Comparison of the crystalline quality of step-graded and continuously graded InGaAs buffer layers," *Journal of Crystal Growth*, Vol. 169, pp. 649-659(1996).
- [7] A. E. Romanov, W. Pompe, G. Beltz, and J. S. Speck, "Modeling of threading dislocation density reduction in heteroepitaxial layer: Part II. Effective dislocation kinetics," *Phys. Stat. Sol. (b)*, Vol. 199, pp. 33-49 (1997).

- [8] Md. R. Islam, M. A. Hossain, A. Hashimoto, and A. Yamamoto, "Strain Relaxation and Improvement of Epi-Layer Quality Using Step-graded Layers for MOVPE  $\text{In}_x\text{Ga}_{1-x}\text{N}$  ( $x \sim 0.4$ )," Proc. in International Conference on Informatics, Electronics & Vision (ICIEV12), 18-19 May, 2012, Dhaka, Bangladesh.

## Chapter VII

### Conclusions and Future Work

#### 7.1 Conclusions

The fundamental challenge involved in InGaN and InGaAs heteroepitaxy is maintaining material crystalline quality at higher In composition; it is imperative to incorporate indium in the alloys to sufficiently lower its band gap for PV applications. A proper management of magnitude and rate of misfit strain is the key requirement to control the misfit and threading dislocation during these heteroepitaxial growths. The gradual decrease of in plane strain, use of residual strain, step inclination of TDs and TDs blocking by MDs makes the step-graded interlayer technique very promising and superior for high performance electronic and optoelectronic devices employing InGaN and InGaAs alloys. In this dissertation, the step-graded interlayer technique for wuzrite as well as cubic heteroepitaxy has been investigated through theoretical studies, mathematical modeling and numerical simulations. An energy balance model based on elastic energy calculation of dislocation and misfit strain in each interlayer has been utilized to find the MD generation in the step-graded structure. The residual strain from the previous layer has been taken into account to consider the exact values of misfit strain. Beside these, reaction models have been developed according to their crystal geometry and all possible burger vectors to observe the nature of TDs in the step-graded structures. The model holds a couple of ordinary differential equations considering the possible annihilation and fusion reaction between TDs as well as blocking by MDs on its gliding path for the heteroepitaxy.

The multilayer epitaxial structures with 40% In compositions for  $\text{In}_x\text{Ga}_{1-x}\text{N}$  and  $\text{In}_x\text{Ga}_{1-x}\text{As}$  have been considered using step-graded structures. Different types of MDs have been calculated in all possible slip systems for these heteroepitaxy. It has been demonstrated that the insertion of step-graded interlayers significantly reduces the MDs for InGaN as well as InGaAs heteroepitaxy. The total edge type MDs from all planes has been decreased from  $1.72 \times 10^{12}$  to  $7.3 \times 10^{11} \text{ cm}^{-2}$  for a  $1.5 \mu\text{m}$  step-graded  $\text{In}_{0.4}\text{Ga}_{0.6}\text{N}$  due to use of 3 interlayers with 10% In composition difference. In case of step-graded  $\text{In}_{0.4}\text{Ga}_{0.6}\text{As}$  heteroepitaxy with similar structure, this density decreased from  $1.1 \times 10^{11}$  to  $8.8 \times 10^8 \text{ cm}^{-2}$ . On the other hand the total mixed type MDs has found to been reduced from  $2.3 \times 10^{13}$  to  $7.8 \times 10^{12} \text{ cm}^{-2}$  and  $9.2 \times 10^{11}$  to  $7.6 \times 10^9 \text{ cm}^{-2}$  by using 3 InGaN and InGaAs interlayers respectively. These reduced densities of dislocation in the upper layers are consistent with the experimentally observed results.



In addition, the solutions TDs reaction models using the Euler method have been confirmed their diminishing densities with increasing thickness. The most nucleation sites for TDs are misfit dislocations which are extremely lower in step-graded structure results significant improvement in the epilayer quality. Since the mixed type TDs have higher initial densities and relative motion to each other even in the absence of glide they have higher rate of reduction than others for both heteroepitaxy. Though the edge and screw type TDs increase initially for lower densities start to decrease with a slower rate after some thickness. The density of mixed type TDs decreases rapidly with average value from  $3.43 \times 10^{11}$  to  $1.32 \times 10^{10} \text{ cm}^{-2}$  for  $1.5 \text{ }\mu\text{m}$  step-graded  $\text{In}_{0.4}\text{Ga}_{0.6}\text{N}$  using 3 interlayers. As a result, the overall TD density decreases monotonically from  $4.65 \times 10^{12}$  to  $8.27 \times 10^{11} \text{ cm}^{-2}$  for the step-graded structure. On the other hand, the TDs in cubic InGaAs heteroepitaxy are found to be higher reactive than the wuzrite InGaN. The average edge and mixed type TDs decrease from  $4.9 \times 10^9$  to  $2.05 \times 10^9 \text{ cm}^{-2}$  and  $2.1 \times 10^{10}$  to  $2.28 \times 10^9 \text{ cm}^{-2}$  after a  $1.5 \text{ }\mu\text{m}$  step-graded  $\text{In}_{0.4}\text{Ga}_{0.6}\text{As}$  using 3 interlayers. Therefore, the overall TD density has been found to be decreased from  $3.76 \times 10^{11}$  to  $5.28 \times 10^{10} \text{ cm}^{-2}$ . The effect of annihilation radius on the diminishing densities of TDs have been demonstrated the more reduction nature with higher annihilation radius. These results again confirmed the more reactive nature of TDs in cubic heteroepitaxy.

The above realizations indicate the potentiality of step-graded interlayer technique for InGaN and InGaAs heteroepitaxy. This simulation methodology can be used for other wuzrite as well as cubic material step-graded interlayer heteroepitaxy for future generation high performance electronic and optoelectronic devices.

## 7.2 Future Work

This dissertation presented a theoretical analysis of dislocation behavior and numerical simulations for step-graded wuzrite InGaN and cubic InGaAs heteroepitaxy. This work covers a wide range of problems. There are many areas where future works can be done. The works for future study are discussed as follows.

The critical thickness calculations are of a great interest for experimentalists. In order to improve the current models, it would be interesting to account for the dislocation generation mechanism in the multiple quantum wells and thus to provide a theory critical thickness. Another possible direction would be to try to incorporate into the model other possible strain-relieving mechanisms such as the V-pits. The modeling of threading dislocation density reduction as described here was only a small step towards a model capable of quantitative predictions. Future work may include further studies on the effects of different parameters of the model as well as

new geometries (including different facets, different growth rates of the facets). In addition, using the knowledge gained with the 2D model, an importance advance can be achieved by extending this model to 3D. Another significant improvement toward realism would be to consider significant optimization of the code used for simulations of the reaction models. the actual dislocation–dislocation interactions. This would involve the implementation of other numerical methods with higher accuracy such as Runge-Kutta. However, a model capable of *quantitative* predictions is expected as an outcome.

## Appendix A

**Values of Different Parameters of InGaN and InGaAs heteroepitaxy**

InGaN		InGaAs	
$a_{\text{GaN}}$	3.1893Å	$a_{\text{GaAs}}$	5.6534Å
$a_{\text{InN}}$	3.538Å	$a_{\text{InAs}}$	6.0584Å
$c_{\text{GaN}}$	5.1851Å	$v_{\text{GaAs}}$	0.31
$c_{\text{InN}}$	5.702Å	$V_{\text{InAs}}$	0.35
$v_{\text{InN}}$	0.42	$a_{\text{InGaAs}}$	$x*a_{\text{InAs}}+(1-x)*a_{\text{GaAs}}$
$v_{\text{GaN}}$	0.35	$v_{\text{InGaAs}}$	$x*v_{\text{InAs}}+(1-x)*v_{\text{GaAs}}$
$a_{\text{InGaN}}$	$x*a_{\text{InN}}+(1-x)*a_{\text{GaN}}$	$b$	$\sqrt{2}a_{\text{InGaAs}}$
$c_{\text{InGaN}}$	$x*c_{\text{InN}}+(1-x)*c_{\text{GaN}}$	$\theta_{\text{edge}}$	90°
$v_{\text{InGaN}}$	$x*v_{\text{InN}}+(1-x)*v_{\text{GaN}}$	$\theta_{\text{screw}}$	0°
$b_{(11-22)}$	$\sqrt{a_{\text{InGaN}}^2+c_{\text{InGaN}}^2}$	$\theta_{\text{mixed}}$	60°
$b_{(1-101)}$	$\sqrt{a_{\text{InGaN}}^2+c_{\text{InGaN}}^2}$	$\varphi_{(111)}$	60°
$b_{(0001)}$	$\sqrt{3}a_{\text{InGaN}}$	$r_0$	$b$
$\theta_{\text{edge}}$	90°	$v$	0.3
$\theta_{\text{screw}}$	0°	$r_A$	500Å
$\theta_{\text{mixed}}$	60°	$r_F$	500Å
$\varphi_{(11-22)}$	$\arctan \frac{a_{\text{InGaN}}}{c_{\text{InGaN}}}$		
$\varphi_{(1-101)}$	$\arctan \frac{\sqrt{3}a_{\text{InGaN}}}{2c_{\text{InGaN}}}$		
$\varphi_{(0001)}$	90°		
$r_0$	$b/2$		
$r_A$	500Å		
$r_F$	500Å		



## Related Publications

### Journals

1. **Md. Arafat Hossain** and Md. Rafiqul Islam “A Theoretical Calculation of Misfit Dislocation and Strain Relaxation in Step-graded  $\text{In}_x\text{Ga}_{1-x}\text{N}/\text{GaN}$  Layers” *Advanced Materials Research*, Vols. 403-408, pp 456-460 (2012)

### Conferences/Proceedings

1. Md. Rafiqul Islam, **Md. Arafat Hossain**, A. Hashimoto and A. Yamamoto “Strain Relaxation and Improvement of Epi-Layer Quality Using Step-graded Layers for MOVPE  $\text{In}_x\text{Ga}_{1-x}\text{N}$  ( $x \sim 0.4$ )” *International Conference on Informatics, Electronics & Vision (ICIEV12)*, 18-19 May, 2012, Dhaka, Bangladesh.